Winter 2007

MYO1C Binds to PiP2 With High Affinity Through a Putative Ph Domain

David Hokanson
University of Pennsylvania

MYO1C Binds to PiP2 With High Affinity Through a Putative Ph Domain

Abstract

Myo1c is a member of the myosin superfamily that links the dynamic actin cytoskeleton to the membrane, and plays roles in mechano-signal transduction and membrane trafficking. We located and characterized two distinct membrane binding sites within the regulatory and tail domains of this myosin. We found that the tail domain binds tightly and specifically to PIP2 in a non-cooperative manner. It binds with slightly higher affinity to Ins(1,4,5)P3 as well as other inositol phosphates which may act as inhibitors to membrane binding in the cell. By sequence and secondary structure analysis, we identified this phosphatidylinositol binding site in the tail to be a putative pleckstrin homology (PH) domain. Point mutations of residues known to be essential for phosphatidylinositol binding in previously characterized PH domains inhibit myo1c binding to PIP2 in vitro and eradicate correct localization and membrane binding in vivo. The extended sequence of this binding site is conserved within many other myosin-Is across species, suggesting they also contain a putative PH domain. We also characterized a previously identified membrane binding site within the IQ motifs in the regulatory domain. This region is not phosphatidylinositol specific, but binds anionic phospholipids in a Ca2+ dependent manner; nevertheless, this site is not essential for in vivo membrane binding. As a result, we have determined that myo1c contains two lipid binding sites, a polybasic region that binds to high levels of PS in a Ca2+ dependent manner and a putative PH domain that binds tightly and specifically to phosphatidylinositols.

Degree Type

Dissertation

Degree Name

Doctor of Philosophy (PhD)

Graduate Group

Biochemistry & Molecular Biophysics

First Advisor

E. Michael Ostap

Subject Categories

Medical Biochemistry

MYO1C BINDS TO PIP_2 WITH HIGH AFFINITY THROUGH A PUTATIVE PH DOMAIN

David Hokanson

A DISSERTATION

in

Biochemistry and Molecular Biophysics

Presented to the Faculties of the University of Pennsylvania

in Partial Fulfillment of the Requirements for the Degree of Doctor of Philosophy

2007

_____

Dr. E. Michael Ostap

Supervisor of Dissertation

_____

Dr. Josh Wand

Graduate Group Chairperson

ABSTRACT

MYO1C BINDS TO PIP_2 WITH HIGH AFFINITY THROUGH A PUTATIVE PH DOMAIN

David Hokanson

Dr. E. Michael Ostap

Myo1c is a member of the myosin superfamily that links the dynamic actin cytoskeleton to the membrane, and plays roles in mechano-signal transduction and membrane trafficking. We located and characterized two distinct membrane binding sites within the regulatory and tail domains of this myosin. We found that the tail domain binds tightly and specifically to PIP_2 in a non-cooperative manner. It binds with slightly higher affinity to $Ins(1,4,5)P_3$ as well as other inositol phosphates which may act as inhibitors to membrane binding in the cell. By sequence and secondary structure analysis, we identified this phosphatidylinositol binding site in the tail to be a putative pleckstrin homology (PH) domain. Point mutations of residues known to be essential for phosphatidylinositol binding in previously characterized PH domains inhibit myo1c binding to PIP_2 *in vitro* and eradicate correct localization and membrane binding *in vivo*. The extended sequence of this binding site is conserved within many other myosin-Is across species, suggesting they also contain a putative PH domain. We also characterized a previously identified membrane binding site within the IQ motifs in the regulatory domain. This region is not phosphatidylinositol specific, but binds anionic phospholipids in a Ca^{2+} dependent manner; nevertheless, this site is not essential for *in vivo* membrane binding. As a result, we have determined that myo1c contains two lipid binding sites, a polybasic region that binds to high levels of PS in a Ca^{2+} dependent manner and a putative PH domain that binds tightly and specifically to phosphatidylinositols.

Preface

When I was looking for a graduate school, while finishing my undergrad degrees at Ohio University, I didn't know what to expect. I was in complete disbelief after I took my GRE that schools were actually going to pay ME to go to school instead of the other way around. Initially, I selected just two schools to apply to based on the protein folding research that was being done by the faculty, and avoiding any of the pompous Ivy-league schools. I was fortunately unaware at the time that the University of Pennsylvania was, in fact, an Ivy-league school, or I would never have applied. My girlfriend at the time hid this from me, and for that I am grateful. When I discovered the truth a fortnight before my interview, I almost cancelled, but instead I reserved my prejudice and came anyway. I was shocked at how collaborative and non-cutthroat Penn was. It seemed to have all the success and prestige I envisioned an Ivy-league school to have, but was also laid back and friendly. My interview went well and I knew this was where I would end up for the next five to seven years of my life.

Mercifully, it has only taken me five years to finish my thesis; although, I have never been in a hurry to leave Philly or Penn. The best decision I could have made was working for Dr. Mike Ostap. I was Mike's first graduate student, yet it seemed as though he had mentored hundreds before me. I truly believe that much of my happiness here at Penn is due to having a great mentor and lab environment. For anyone that has watched the NBC show, "Scrubs", Mike is my Dr. Cox. He picks on me constantly and never quite gives me that pat on the back I yearn for, but inspires me to work even harder to get it. To me, Mike is much more than just a brilliant boss who has all the

answers and is rarely wrong, he is a truly inspiring human being. I can't think of a better man to look up to professionally.

There are many people at Penn that I owe some part of my sanity to, including the faculty on my committee and in the PMI, fellow graduate students, and Ruth and Angie in the department offices. After my prelim, I was worried about picking such well-established faculty to serve on my thesis committee for fear that they would make my life hell. However, with each committee meeting I learned that their vast knowledge and expertise in my field were indispensable and made my work more forthright, not more grueling. Also, I've made some great friends here and without them, finishing graduate school would have been a much more menacing feat. Thank you fellow BMB students.

The Ostap lab is smaller than most labs, and I think that was beneficial to me as a beginning graduate student. I would like to thank current and past members of the lab, in particular, Nanyung, Tianming, Joe, and Jennine. Nanyung was a postdoc when I started in the lab and played a hand in training me to do many of the things I now take for granted (I just wish some of her cloning magic wore off on me). Tianming, what isn't there to say about Tianming. He is an invaluable member of the lab to me and everyone else. Never complaining, always willing to help, and an absolute master of what he does everyday. Thank you Tianming for constantly keeping the lab stocked with protein and helping in every way you can. Joe has given me the much needed comic relief I've needed to get through the frustrating days over the years. You've

always been there to ask the stupid questions I'm too embarrassed to ask Mike. Jennine has been a very welcomed new addition to the lab. I'm thrilled there is someone to take over my project at least in part when I depart. I have enjoyed trying to play the role of a mentor and it is humanitarian of you to always laugh at my jokes.

And lastly I would like to thank my family and extended family, my friends. Dad, you always said you would buy me a car if I followed in your footsteps and graduated from med school. Well, I'm graduating from the University of Pennsylvania School of Medicine, it's a technicality I know, but I'll take what I can get. Thank you for always believing in me and supporting me through undergrad and the rough times since. Liz, I'm so glad we are still as close as ever. Your support at the beginning and now has always meant so much to me. I am ecstatic that you are ecstatic for me. Oh and I guess thanks for the help with Illustrator too. Bryan, you've always been a great friend here at Penn: may we continue to brew great beer and times together for many years. And of course a big thank you to my beautiful girlfriend Sarah (Dorkface). I know I'm probably more difficult than you've ever imagined, but I hope it has been worth it for you because it certainly has been for me. Your English major background has been a big help with the editing, but it doesn't come close to the mental and emotional clutch you have been…when I let you. Thank you to everyone, I love you all. "All right, brain, I don't like you and you don't like me, so let's just do this and I'll get back to killing you with beer." Homer Simpson.

Contents

Figures

Equations

Tables

1 Introduction

1.1 Objective

The myosin super-family is very diverse and expands well beyond the typical myosin II stereotype found in muscle. Most characterized myosins are able to bind actin filaments through their motor domain, possess ATPase activity, and are able to generate force. Humans express 40 different myosin genes that differ in the kinetics of their motor domains, and the cargo binding of their tail domains. Eight of these myosins are class-I isoforms. It has been known since 1989 that myosin-I isoforms associate with anionic lipids, yet the specificity and lipid binding site(s) were not known. The overall purpose of this dissertation was to characterize the interaction of a myosin-I motor with the plasma membrane. The focus of this thesis is myo1c, a single headed, membrane associated isoform that is found in most eukaryotic cells and is involved in membrane dynamics, cytoskeletal structure, and mechano-signal transduction. Little was known of the mechanism by which myo1c bound to the membrane or what kinds of forces it could generate once anchored to the fluid bilayer. Knowing the specificity and mechanism of how a myosin-I interacts with lipids was essential for understanding the possible functions of an actin-based motor bound to the plasma membrane. Therefore, my aim was to characterize the protein-lipid interactions in much greater detail.

1.2 Summary

Myo1c is a member of the myosin superfamily that links the dynamic actin cytoskeleton to the membrane, and plays roles in mechano-signal transduction and

membrane trafficking. We located and characterized two distinct membrane binding sites within the regulatory and tail domains of this myosin. We found that the tail domain binds tightly and specifically to PIP_2 in a non-cooperative manner. It binds with slightly higher affinity to Ins(1,4,5)P_3 as well as other inositol phosphates which may act as inhibitors to membrane binding in the cell. By sequence and secondary structure analysis, we identified this phosphatidylinositol binding site in the tail to be a putative pleckstrin homology (PH) domain. Point mutations of residues known to be essential for phosphatidylinositol binding in previously characterized PH domains inhibit myo1c binding to PIP_2 *in vitro* and eradicate correct localization and membrane binding *in vivo*. The extended sequence of this binding site is conserved within many other myosin-Is across species, suggesting they also contain a putative PH domain. We also characterized a previously identified membrane binding site within the IQ motifs in the regulatory domain. This region is not phosphatidylinositol specific, but binds anionic phospholipids in a Ca^{2+} dependent manner; nevertheless, this site is not essential for *in vivo* membrane binding. As a result, we have determined that myo1c contains two lipid binding sites, a polybasic region that binds to high levels of PS in a Ca^{2+} dependent manner and a putative PH domain that binds tightly and specifically to phosphatidylinositols.

1.3 Background

1.3.1 Myosin

Myosins are molecular motors that convert the chemical energy from ATP to a mechanical force along actin filaments in the cell. Conventional myosin, myosin-II, was the first molecular motor to be discovered and has been studied for many decades due to its fundamental role in muscle contraction. Myosin-II is a two-headed molecule that oligomerizes into bipolar filaments, which slide relative to actin filaments to create a contraction in muscle cells. In 1973, the first unconventional myosin, *Acanthamoeba* myosin-I, was discovered (Pollard and Korn 1973). There are now 24 classes of myosins identified (Figure 1) (Foth, Goedecke et al. 2006) with humans expressing 40 different myosin genes. Mutations in myosin genes lead to a variety of diseases including myopathies, hearing loss, and blindness. Myosins are involved in a large number of cellular processes, such as muscle contraction, cell motility, cytokinesis, phagocytosis, growth cone extension, maintenance of cell shape, mechano-signal transduction, endocytosis, exocytosis, and organelle/particle trafficking.

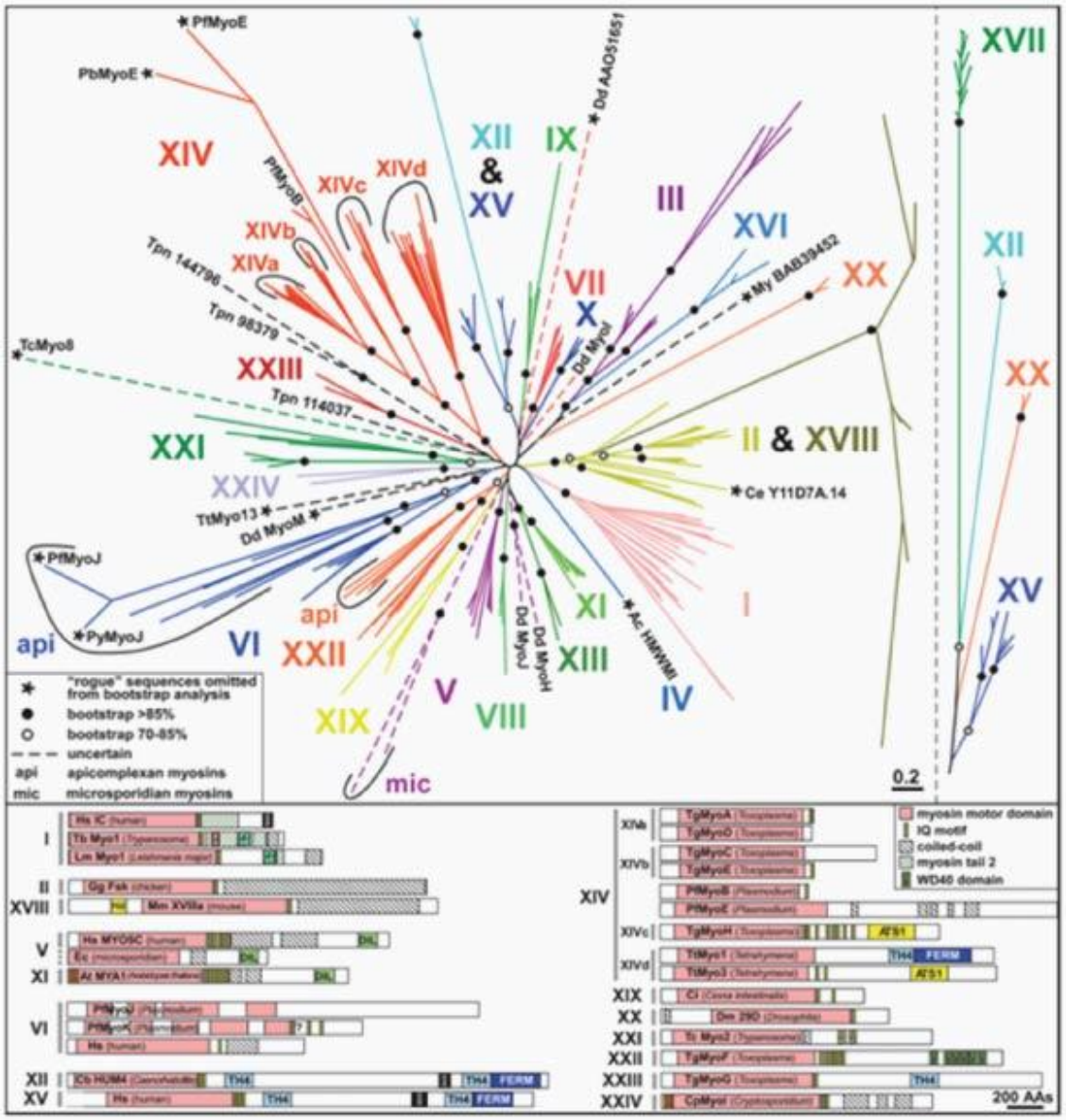

Figure 1 Myosin Family Tree

Figure 1: The most recent phylogenetic tree of the myosin super family from (Foth, Goedecke et al. 2006). It was created from a representative distance matrix-based phylogeny (PROTDIST_NEIGHBOR) of myosin head domains. Listed are the 24 classes of myosin motors that have been identified. Note that the largest family consists of members of the myosin-I family.

1.3.1.1 Myosin Domain Structure

All characterized members of the myosin super family contain a head, neck and tail domain (Figure 2). The head domain is an 80 kDa catalytic motor, which binds to actin and hydrolyzes ATP to induce a powerstroke. The degree of conservation varies among families and isoforms, and results in observed enzymatic differences in the ATPase cycle of the myosin. The neck domain is an extended α-helical light chain-binding region consisting of one or more IQ motifs, which have a 23 residue consensus sequence IQXXXRGXXXRK. These IQ motifs bind to light chains, such as calmodulin (CaM), or other EF-hand proteins that stiffen the α-helix and regulate the myosin in a Ca^{2+} dependent manner (Zhu, Beckingham et al. 1998). The neck domain serves as a lever arm that transduces small conformational changes in the motor domain to larger displacements. The tail domain is varied among the different myosin isoforms and in many cases determines the localization and function of the myosin. The tail domain exhibits class-specific properties such as filament forming, dimerizing, cargo binding, or kinase activity (Mooseker and Cheney 1995). This thesis will focus on the regulatory and tail domain of myo1c, a class I myosin.

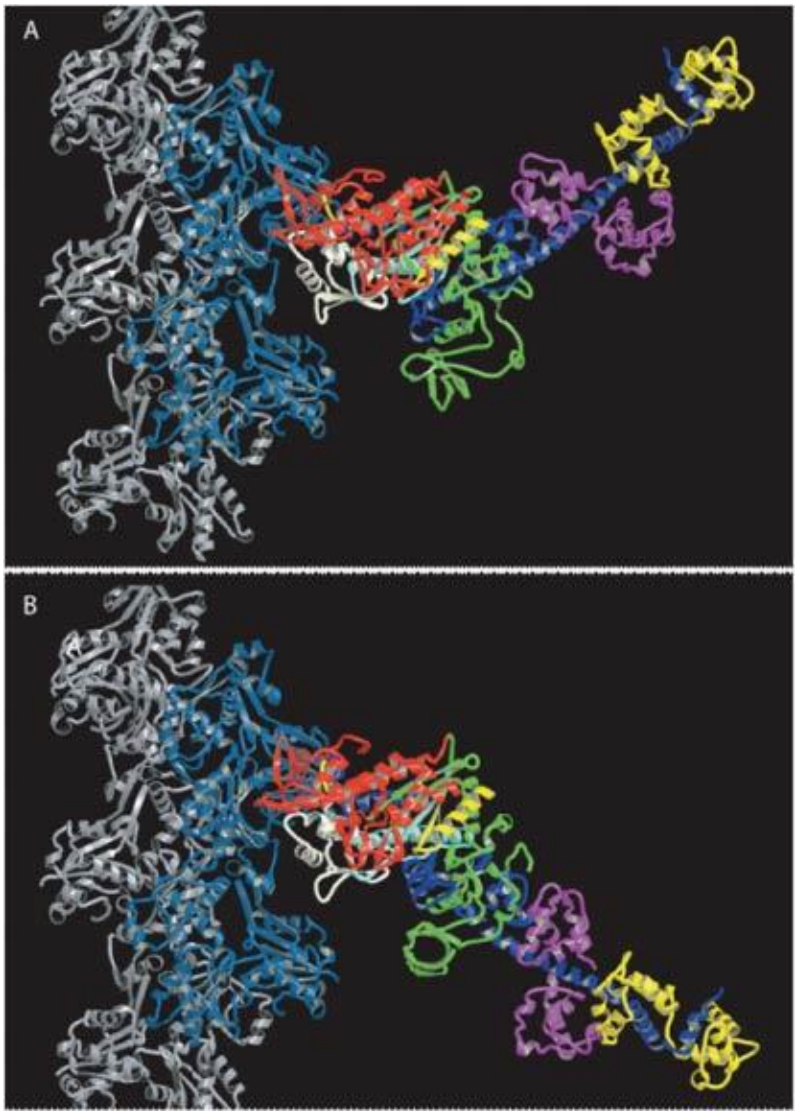

Figure 2 Myosin Structure

Figure 2: Model of myosin-II bound to actin from (Holmes, Schroder et al. 2004). Crystal structure of myosin–II bound to a modeled actin filament, which is shown on the left. Myosin-II is shown in A) pre-powerstroke, and B) post-powerstroke conformations. The 80 kDa head domain is shown in red, cyan, yellow and green, and the regulatory domain is shown in blue with light chains (purple and yellow) bound. The tail domain is not present in this structure.

1.3.1.2 Myosin ATPase Cycle

Myosin motors bind and hydrolyze ATP to convert chemical energy to a mechanical force used to translocate actin filaments (Figure 3). Myosin in a nucleotide-free state remains tightly bound to actin in what is referred to as the rigor state. Upon ATP binding, myosin enters a weak actin binding state and dissociates from the filament. ATP is hydrolyzed and the myosin lever arm is cocked into a pre-powerstroke conformation. Upon binding to actin, phosphate (P_i) is released and the lever arm is moved forward during the powerstroke as myosin enters the strong binding state. ADP is released, which results in a second sub-step for some isoforms, and the myosin returns to the rigor state. A new ATP molecule is now able to bind to the myosin motor to repeat the cycle. Although all myosins follow this cycle, the kinetics and regulation of these steps can differ greatly between myosin families and even isoforms. The rate limiting step for myosin-I motors is P_i release, which means that myosin-Is most often exist in the weakly bound state. However, they have been proposed to enter a state of isometric contraction that prevents ADP release under stall forces, which may increase their lifetime bound to actin (Batters, Arthur et al. 2004). This proposed function of myosin-Is to act as a tension sensor will be further discussed throughout.

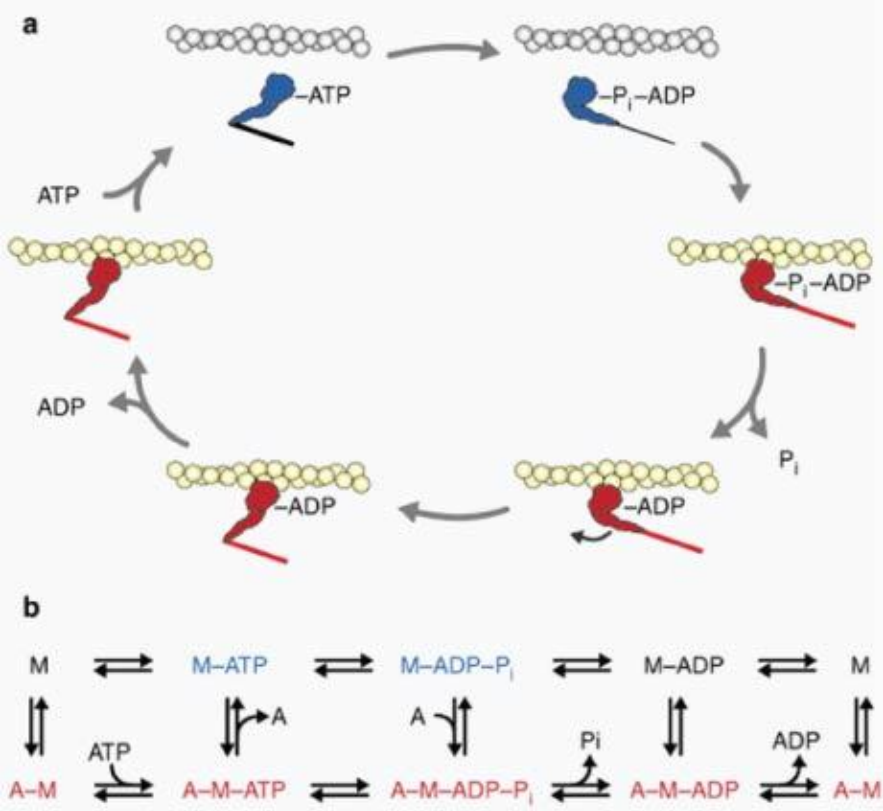

Figure 3 Myosin ATPase cycle

Figure 3: The ATPase cycle of a myosin motor is shown as A) a cartoon model, and B) a kinetic scheme from (Murphy, Rock et al. 2001). Strong actin bound states are shown in red, whereas weak actin bound states are shown in blue. Note, the powerstroke is depicted as occurring after P_i release; however, this point remains to be settled (Dantzig, Goldman et al. 1992; Takagi, Homsher et al. 2006).

1.3.1.3 Ca^{2+} Regulation of Light Chains

Most characterized myosins contain one or more IQ motifs in their regulatory domain that bind to EF-containing light chains in a Ca^{2+} dependent manner. These light chains are thought to structurally stabilize the regulatory domain, which is a long α-helix that would be flaccid without light chains bound. In the case of many myosins, this light chain is CaM, which contains two lobes, each containing two EF hand motifs that can each bind to two Ca^{2+} ions (Figure 4). CaM undergoes a conformational change when Ca^{2+} binds, which in most cases lowers the affinity of CaM for the IQ motifs, and can even lead to dissociation of the CaM. For myosin-Is, this is proposed to reveal positively charged residues within the IQ motifs, which can then bind through electrostatic interactions to the negatively charged phospholipids in the plasma membrane (Swanljung-Collins and Collins 1992; Tang, Lin et al. 2002; Hirono, Denis et al. 2004); although, this property has not been shown to be physiologically relevant.

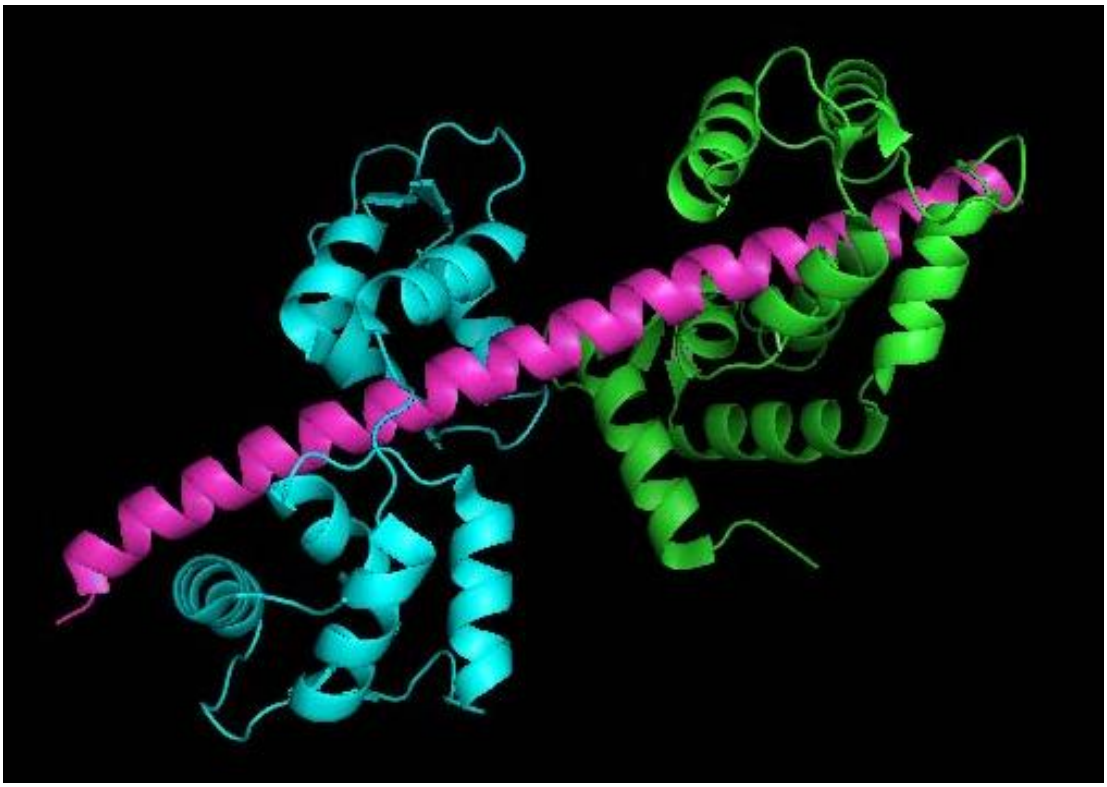

Figure 4 CaM Bound to IQ Peptide

Figure 4: Structure of two apo-CaM light chains bound to a portion of the regulatory domain consisting of 6 adjacent IQ motives of myosin-V. Two CaM light chains, cyan and green, are shown bound a section of the regulatory domain, magenta, containing two adjacent IQ motifs (PDB 2IX7).

1.3.2 Myosin-I

Myosin-Is comprise the largest unconventional myosin family in humans (Berg, Powell et al. 2001) where they function in membrane dynamics, cell structure, endocytosis, and mechanical signal transduction (Ruppert, Godel et al. 1995; Tang and Ostap 2001; Bose, Guilherme et al. 2002; Holt, Gillespie et al. 2002; Tyska, Mackey et al. 2005; Sokac, Schietroma et al. 2006). They are single-headed myosins that do not dimerize or form filaments. The IQ motifs in the regulatory domain of all vertebrate myosin-Is each bind to a CaM. The tail domains of myosin-Is are highly basic and bind to anionic lipids in the plasma membrane. Myosin-Is can be further divided into two sub-classes, the short-tail and long-tail isoforms. The long-tail isoforms have two additional protein:protein interaction domains, a src homology 3 (SH3) and a glycine-proline-rich domain. Vertebrates express six short-tail myosin-Is (myo1a, myo1b, myo1c, myo1d, myo1g) and two long-tail isoforms (myo1e, myo1f) (Berg, Powell et al. 2001).

1.3.2.1 Localization of Myosin-I

Subcellular fractionations of vertebrate cells show that a large percentage of myosin-I is associated with the membrane and the cytoskeletal fractions (Ruppert, Godel et al. 1995; Bose, Guilherme et al. 2002; Cho, Kim et al. 2005), and immunofluorescence and live cell microscopy suggest that myosin-I is dynamically localized to the cell membrane. Thus, a key property of myosin-I isoforms appears to

be their ability to bind in a regulated manner to cellular membranes (Coluccio 1997; Tang and Ostap 2001).

1.3.2.2 History of Myosin-I Membrane Association

The association of myosin-I with anionic lipids has been studied since the late 1980s. In 1989, Pollard showed that *Acanthamoeba* myosin-I bound to both extracted membranes and to vesicles of pure lipids (Adams and Pollard 1989) and Korn found that *Acanthamoeba* myosin-I localized to the plasma membrane (Miyata, Bowers et al. 1989). A year later, Mooseker discovered that a vertebrate myosin-I, myo1a, bound to anionic lipid vesicles through its tail domain (Hayden, Wolenski et al. 1990), which Pollard also found to be true of *Acanthamoeba* myosin-I (Doberstein and Pollard 1992). Since then, many laboratories have shown through *in vivo* experiments that myosin-I isoforms associate with anionic phospholipids (Hirono, Denis et al. 2004; Huang, Lifshitz et al. 2004). Kinetic studies of myo1c showed that association rates with acidic large unilamellar vesicles (LUVs) were diffusion limited, whereas the dissociation rates depended on the ratio of PS to myo1c-tail and was slower than the myo1c ATPase rate (Tang, Lin et al. 2002).

Since myosin-Is are able to bind to both the cell membrane and actin, this leads to many possible mechanical functions. A dynamic link between the actin cytoskeleton and membrane can be formed. This could deform the membrane, form barriers, or form micro-domains around proteins in the membrane with the cytoskeleton acting much like

a fence around cattle, supplying support and rigidity. Myosin-Is could also bind to endocytic vesicles and transport them along an actin track, or aid in retrograde flow. One of the molecular roles that has become more characterized in recent years is the role of myo1c as a mechanical signal transducer in hair cells (Batters, et al. 2004).

Although there are many hypotheses in the scientific community, there is still little evidence as to what myosin-Is can functionally do while bound to the membrane. Therefore, the goal of this thesis was to characterize the interactions of a particular myosin-I isoform, myo1c, with the plasma membrane, thus leading to a better understanding of its molecular roles as a link between the plasma membrane and the cytoskeleton.

1.3.3 Myo1c

Myo1c has been shown to play roles in lamellipodial retraction, endosomal processing, glucose transportation, and mechanical signal transduction. It is widely expressed in vertebrate cell types and is largely localized to the plasma membrane and cytoskeleton (Ruppert, Godel et al. 1995; Bose, Guilherme et al. 2002; Cho, Kim et al. 2005). This is especially true at specialized dynamic membrane structures such as lamellipodia, microvilli, endocytic structures and inner-ear hair cell stereocilia. Myo1c has also been shown to be enriched in micro domains through proteonimics analysis (Saeki, Miura et al. 2003). However, the functions and regulation of myo1c while bound to the plasma membrane are still unknown.

1.3.3.1 Possible Functions of Myo1c

Myo1c being able to bind to both the cell membrane and actin leads to many possible mechanical functions. These functions include tethering the cytoskeleton to the membrane, translocating actin in the plane of the membrane, deforming or rearranging membrane structures, and acting as a tension sensor. Although many of the biological roles of myo1c are poorly understood, the one role that has become better characterized in recent years is the role of myo1c as a mechanical signal transducer in hair cells of the inner ear.

1.3.3.2 Myo1c Catalytic Activity

In order to hypothesize about the possible functions of myo1c while bound to the membrane, it is important to first review its biochemical properties. Myo1c hydrolyzes ATP at a rate of 0.1 – 1 s^{-1} and has a low duty ratio of 0.05 under no load (Gillespie, Gillespie et al. 1999). This means that myosin will be in a strong actin binding state only 5% of the time. Actin activates the ATPase rate by 2 – 10 fold, and the actin motility rate has been measured at 100 nm/s (Batters, Arthur et al. 2004). Ca^{2+} appears to affect the motility of myo1c by altering its mechanical activity; moreover, some laboratories have found that Ca^{2+} increases actin activated ATPase activity (Barylko, Wagner et al. 1992; Batters, Arthur et al. 2004). These effects are most likely

due to Ca^{2+} binding to and changing the conformation of CaM light chains bound to the IQ motifs in the regulatory domain.

The powerstroke of myo1c seems to occur in two phases. The first substep of ~3 nm correlates with the release of P_i, whereas the second substep of ~1 nm corresponds to ADP release (Batters, Arthur et al. 2004). This is supported by electron microscopy data showing a large difference in the position of the neck domain between ADP-bound and nucleotide free states (Batters, Arthur et al. 2004). The kinetics of myo1c seem to be load dependent (Batters, Arthur et al. 2004). Since nucleotide release and mechanical states are coupled, one explanation for the motor domain being unable to release ADP is myo1c arrest after the first substep, staying strongly bound to ADP and maintaining tension. This would cause the myo1c to remain bound in an isometric contraction until either the load is released and it is able to proceed through its catalytic cycle, or the load increases and myo1c is forced back into a ADP.P_i-like state in which it will detach from actin (Batters, Arthur et al. 2004). However, the role of myo1c as a tension sensor still needs to be demonstrated.

1.3.4 Biological Roles

Myo1c has been implicated through biochemical and cell biological techniques to be involved in many different cellular processes. Many laboratories have shown the importance of myo1c function at areas in the cell where the cytoskeleton and membrane interact. However, aside from its role as a mechano-signal transducer in hair cells, no precise functional data has been demonstrated for myo1c at the plasma membrane.

Characterizing how myo1c interacts with the membrane will give insight to its role in the following biological processes.

1.3.4.1 Compensatory Endocytosis

Egg activation in *Xenopus* and several other vertebrates is induced upon fertilization by an increase in intracellular Ca^{2+}. This initiates several events, one of which is cortical granule exocytosis which is required to block polysperm. Cortical granule containing vesicles lie just beneath the plasma membrane until fertilization. Upon activation, they fuse with the membrane and exocytosis commences. To prevent the membrane from growing due to the fusion of cortical granule vesicles, compensatory endocytosis takes place just after vesicle fusion. This process involves an actin coat forming around the fused vesicles and compressing it to retrieve the vesicle (Sokac, Schietroma et al. 2006).

Myo1c is upregulated by polyadenylation during meiotic maturation in *Xenopus* eggs. Upon fertilization, myo1c is recruited to the cortical granule containing vesicle preceding actin coat assembly. Inhibition of myo1c leads to an uncoupling of the actin coats from the exocytosing cortical granules, resulting in failure of compensatory endocytosis. There is also an increase in polymerization of actin at the membrane throughout the cell. These findings suggest that myo1c couples the barbed ends of actin to the membrane, mediating force production from the polymerizing actin during compensatory endocytosis, rather than directly producing force through a powerstroke (Sokac, Schietroma et al. 2006). This requires a specific localization of myo1c to sites

of endocytosis as well as a strong link to the plasma membrane to support the actin coat and forces of polymerization.

1.3.4.2 Glucose Exocytosis

Insulin stimulates the uptake of glucose in muscle and adipocytes by inducing the translocation and exocytosis of vesicles containing the glucose transporter protein, GLUT4. This process is required for maintaining normal blood glucose levels. GLUT4 translocation requires the actin cytoskeleton. Rapid and directed movement along filaments implicates the involvement of myosin motors, most likely myosin-V (Bose, Guilherme et al. 2002). Phosphatidylinositol-4,5-bisphosphate (PIP_2) has also been shown to stimulate the glucose transport activity of GLUT4 at the plasma membrane (Funaki, DiFransico et al. 2006). These results suggest that PIP_2 acts as a second messenger to activate release of GLUT4 through the remodeling of the actin cytoskeleton.

Cells lacking myo1c have a reduced glucose uptake (Bose, Guilherme et al. 2002). Over-expression reverses the effect of inhibiting phosphoinositol-3 kinase (PI3K), which inhibits GLUT4-containing vesicles and causes them to accumulate right below the plasma membrane. Over-expression also induced membrane ruffling in adipocytes which is normally induced by insulin. GLUT4-containing vesicles have been shown to colocalize with myo1c only at the membrane, suggesting that myo1c is not involved in translocating vesicles to the membrane, but rather in anchoring them to the membrane, fusing them to the membrane, or exocytosis (Bose, Guilherme et al.

2002). Glucose exocytosis clearly requires both PIP_2 and myo1c to be present at the membrane for proper function.

1.3.4.3 Neuronal Growth Cone Extension

Neurons extend growth cones from the tips of growing axons to form a precise pattern in the nervous system. They have the ability to maneuver through the developing nervous system which is enabled by both actin and microtubule-based mechanisms. Protrusion of the lamellipodia and filopodia at the cell periphery is known to be actin-based. Several myosin motors have been implicated in this process (Wang, Wolenski et al. 1996; Wylie, Wu et al. 1998). Inhibition of myosin-V causes retraction of filopodia, whereas inhibition of myosin-II causes reduction in the size of the lamellipodia.

Inactivation of myo1c in chick dorsal root ganglion results in lamellipodial extension by actin polymerization (Diefenbach, Latham et al. 2002). When this rearward movement of actin is inhibited, the lamellipodia extends forward unchecked. Using chromophore assisted laser inactivation, areas of the lamellipodia where myo1c was inactivated would polymerize and extend, causing the neuron to steer in that direction (Wang, Liu et al. 2003). This suggests that myo1c has an effect on actin polymerization, or possibly acts to translocate actin filaments rearward. The localization and regulation of myo1c at areas of lamellipodial extension remain unclear.

1.3.4.4 Hair Cells

The most knowledge on a molecular role of myo1c is its role in the stereocilia of hair cells as a mechano-sensing transducer. Hair cells contain bundles of 30 – 300 actin–filled stereocilia arranged in a tiered arrangement (Figure 5). Auditory or vestibular stimuli, caused by sound or head movements, cause the individual stereocilia to move with respect to one another, which results in the opening and closing of transduction channels. When the channels open, cations, K^+ and Ca^{2+}, rush into the stereocilia, which depolarizes the cell and causes a neurotransmitter to be released. The channels then close causing the cell to hyper-polarize and cease the release of the neurotransmitter (Gillespie 2004). The channels are opened by tension placed on them by an extracellular tip link composed of a filament of cadherin 23 that is connected to the tip of an adjacent stereocilia (Siemens, Lillo et al. 2004).

Hair cells are able to adapt after being initially displaced to retain the same intrinsic sensitivity but operate over a higher range of movements. This suggested that there was a change in the mechanical arrangement within the bundles during adaptation. For this to occur, the tip link from one bundle must be able to slide down the stereocilium of a neighboring stereocilium to reduce the tension felt by the channel and allow it to close. During periods of no simulation, the channel would have to relocate back to its original position to restore tension. This model seemed like a perfect fit for myosin-I (Howard and Hudspeth 1987). Two forms of adaptation have been described to occur in hair cells concurrently under distinct mechanisms. A fast adaptation of a few milliseconds for channel closing suggests that Ca^{2+} entering through the channel

signals them to shut. A slow adaptation of 20 ms is thought to be myosin-I based (Holt, Gillespie et al. 2002).

In the hair cells of developing mice, although stereocilia have formed, no sensory activity is present until embryonic day 16. This correlates precisely with the formation of tip links and the expression of myo1c (Geleoc and Holt 2003). Three components have been found to be essential for adaptation and transduction in hair cells, PIP_2, cadherin 23, and myo1c (Hirono, Denis et al. 2004; Siemens, Lillo et al. 2004). Myo1c has been shown to bind to both cadherin 23 and PIP_2 (Phillips, Tong et al. 2006). These interactions allow myo1c to link the transduction apparatus to the bundled actin filaments. Under resting conditions, stereocilia are upright with resting tension from the tip links on the transduction channels. Myo1c bound to actin and the transduction complex remains in an isometric contraction, keeping the channel closed. When stereocilia move in relation to each other, tension is produced and the tip link pulls open the transduction channel as myo1c is forced into an ADP.Pi-like state, releases from actin, and slides down the actin bundle. During the adaptation discussed above, myo1c motors, now at the beginning of their catalytic cycle, rebind and climb the actin bundle under zero load until tension is restored, thus closing the channel (Batters, Arthur et al. 2004). Therefore, myo1c is responsible for allowing the channels to open under tension, and then closing them by restoring tension (Gillespie 2004). From data showing that the tip link complex can withstand up to 80 pN of force before

breaking, it has been estimated that up to 50 myosin motors are required per tip link (Hudspeth and Gillespie 1994).

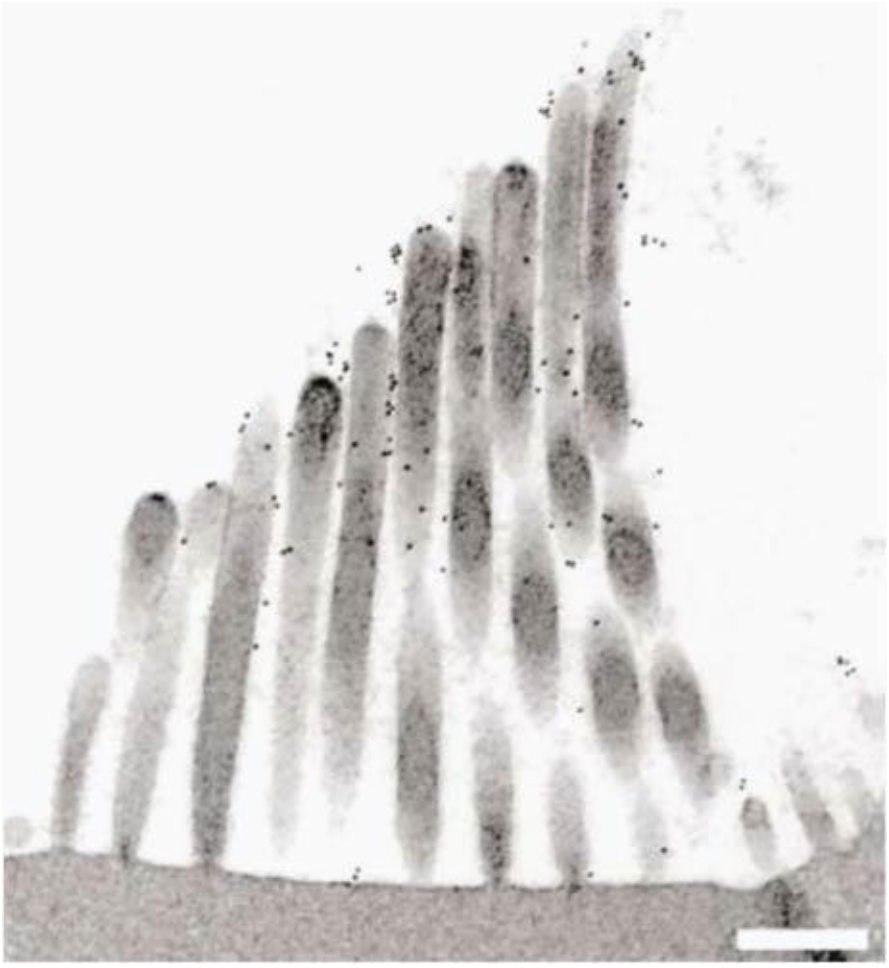

Figure 5 Hair cell

Figure 5: Figure is from (Hirono, Denis et al. 2004). Immunogold electron microscopy of hair cell in intact saccular epithelium using a monoclonal antibody for PIP_2, 2C11, without subtilisin treatment and with fixative-saline permeabilization. Scale bar, 500 nm.

1.3.5 Myo1c Binding Partners

The tail domains of myosin are generally known as the cargo binding domains. Many efforts have been made to identify proteins that bind to the tail domain of myo1c with little success. Proteins that bind to the regulatory or tail domain of myo1c could be important for its sub-cellular localization and non-redundant functions from other myosin-I isoforms. Binding partners could incorporate myo1c into larger protein complexes needed to form at the plasma membrane, or could require myo1c for proper positioning at the membrane. They could also regulate lipid binding or affect the kinetics of membrane association or dissociation. To date, only three proteins have been found: cadherin 23, NEMO, and PHR1.

1.3.5.1 Cadherin 23

Cadherin 23 is a component of the tip link complex in hair cells. The cytoplasmic domain of cadherin 23 was shown to colocalize and immunoprecipate with myo1c when coexpressed in HEK cells (Siemens, Lillo et al. 2004). This interaction functions to link the adaptive motor to the transduction channel in stereocilia. More on this function will be discussed later.

1.3.5.2 NEMO

Nuclear factor κB essential modulator (NEMO) is a subunit of the IκB kinase complex which attenuates insulin action by phosphorylating the insulin receptor substrate. NEMO was found to accumulate at membrane ruffles preceding an

interaction with the insulin receptor substrate. Location of NEMO is dependent on insulin, actin and myo1c. Over-expression of myo1c enhanced the interaction between NEMO and insulin receptor substrate, while expression of a dominate negative tail domain of myo1c inhibited insulin receptor substrate phosphorylation. NEMO and myo1c were shown to interact through both endogenous and recombinant immunoprecipation from cell extracts (Nakamori, Emoto et al. 2006). It is thought that myo1c helps localize NEMO at the plasma membrane so that it can form a complex to the insulin receptor in order to pacify insulin action through phosphorylation.

1.3.5.2 PHR1

PHR1 is an integral membrane protein found in photoreceptor cells, olfactory receptor neurons, and hair cells. It has four different splice isoforms that can be expressed, and contains a PH domain that lacks the signature motif containing basic residues required for phosphatidylinositol binding. PHR1 interacts with the tail domains of myo1c and myoVIIa through this PH domain as evidenced by immunoprecipitation and a yeast two hybrid interaction (myo1c only) (Etournay, El-Amraoui et al. 2005). Although its role in hair cells is unclear, it has potential functions in post golgi protein trafficking and possibly the mechano-transduction slow adaptation process through its interaction with myo1c.

1.3.6 The Plasma Membrane

To characterize the interaction of myo1c with the membrane, it is important to consider the role of different lipids that make up the inner leaflet. The plasma membrane in most cells is made up of transmembrane proteins and a variety of phospholipids which include phosphatidyl choline (PC), phosphatidyl serine (PS), phosphatidyl ethanolamine (PE), phosphatidyl inositol (PI), and phosphatidic acid (PA). PC and PE are neutral Zwitterions, whereas PS, PA, and PI carry a negative charge. PI can be phosphorylated in the cell by phospholipid kinases to produce PIP, PIP_2 and PIP_3, which carry multiple negative charges on a single headgroup. These PIs are locally concentrated in regions of the cell and act as signaling second messengers and substrates for proteins that localize to the plasma membrane. There are no naturally basic phospholipids, and because of this, the levels of PS and PIs in the inner leaflet can confer a substantial negative charge (DiNitto, Cronin et al. 2003).

The three phospholipids that were used in this dissertation are PC, PS, and PIP_2 (Figure 6). The vesicles in our experiments were comprised of PC, which is neutral, and was used as a background. PS was used as the standard negatively charged phospholipid in the inner leaflet of the plasma membrane. It has an effective charge of negative one and is found in vivo at ~20-30%. PIP_2 is used as the primary multivalent phospholipid. Its concentration at the plasma membrane is 100-fold greater than other poly-phosphatidylinositols, and it is the anchor for many membrane bound proteins, as well as a source for second messengers diacylglycerol (DAG) and inositol-1,4,5-trisphosphate ($Ins(1,4,5)P_3$).

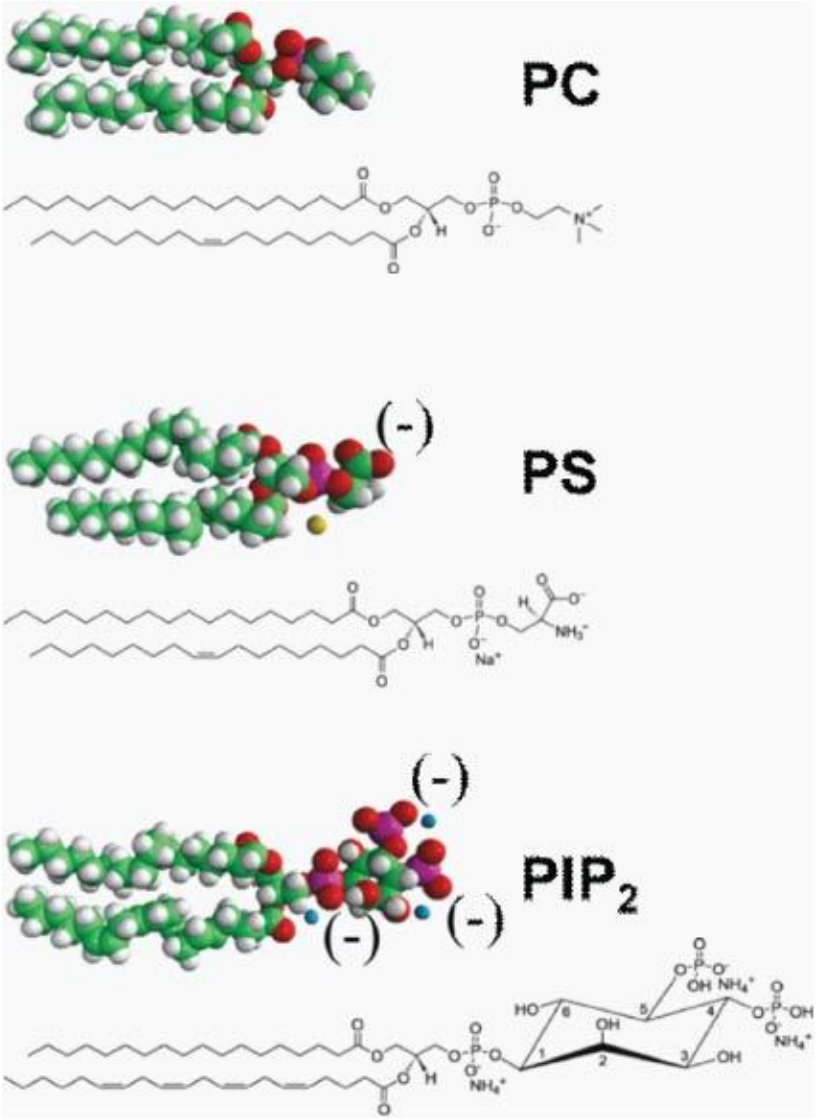

Figure 6 Phospholipids

Figure 6: Structures of the phospholipids used in this dissertation, from avantilipids.com. Space filling models are shown above chemical structures. Negative charges are identified by (-).

1.3.7 PIP_2

PIP_2 is the major poly-phosphatidylinositol in mammalian cells. Its physical properties, organization and role in signaling are involved in many cell processes that occur at the membrane. The biochemical and biophysical properties of this essential phospholipid and its interactions with proteins at the plasma membrane will be briefly reviewed here. For a full review, refer to (McLaughlin, Wang et al. 2002).

1.3.7.1 Structure and Charge

PIP_2 contains a DAG tail that is linked to the phosphate at the 1 position of an inositol ring that is also phosphorylated at the 4 and 5 positions. The pK values are 6.7 and 7.7 respectively. The protonation states vary depending on the binding of proteins as well as the pH and ionic strength of the environment. Consequently, the net charge of PIP_2 can range from -3 to -4 due to the protonation states of these phosphate groups.

1.3.7.2 Biological Roles of PIP_2

PIP_2 was initially studied as the source of two second messengers in the cell, DAG and $Ins(1,4,5)P_3$, which go on to activate PKC and release Ca^{2+} from the endoplasmic reticulum respectively. It is now known that PIP_2 is important for the membrane localization of proteins. The attachment of these proteins to PIP_2 is essential to their role in cytoskeleton dynamics, exocytosis, endocytosis, membrane trafficking,

and the activation of enzymes (Yin and Janmey 2003). Many laboratories have proposed that the existence of high local concentrations of PIP_2 within the cell are responsible for some of these functions. PIP_2 and other phosphaphatidylinositides are in fact distributed non-uniformly in the plasma membrane. Moreover, PIP_2 has been found to be abundant in certain regions of the plasma membrane, including stereocilia, membrane ruffles, macropinocytes, and nascent phagosomes (McLaughlin, Wang et al. 2002; Huang, Lifshitz et al. 2004).

1.3.7.3 PIP_2 Concentration

PIP_2 is anabolized and catabolized by a number of different kinases, phosphatases, and lipases, and can also be sequestered by a plethora of PIP_2 binding proteins in the cell (Figure 7). It comprises >99% of the doubly phosphorylated phosphatidylinositols in a mammalian cell, yet it makes up only ~1% of the phospholipids in the inner leaflet of the plasma membrane. Assuming a typical cell with a radius of 10 µm has an effective total lipid concentration of 1 mM, the effective concentration of PIP_2 would be ~10 µM (McLaughlin, Wang et al. 2002). However, this would not be the concentration of PIP_2 available since there are many proteins in the cell that bind to and sequester PIP_2.

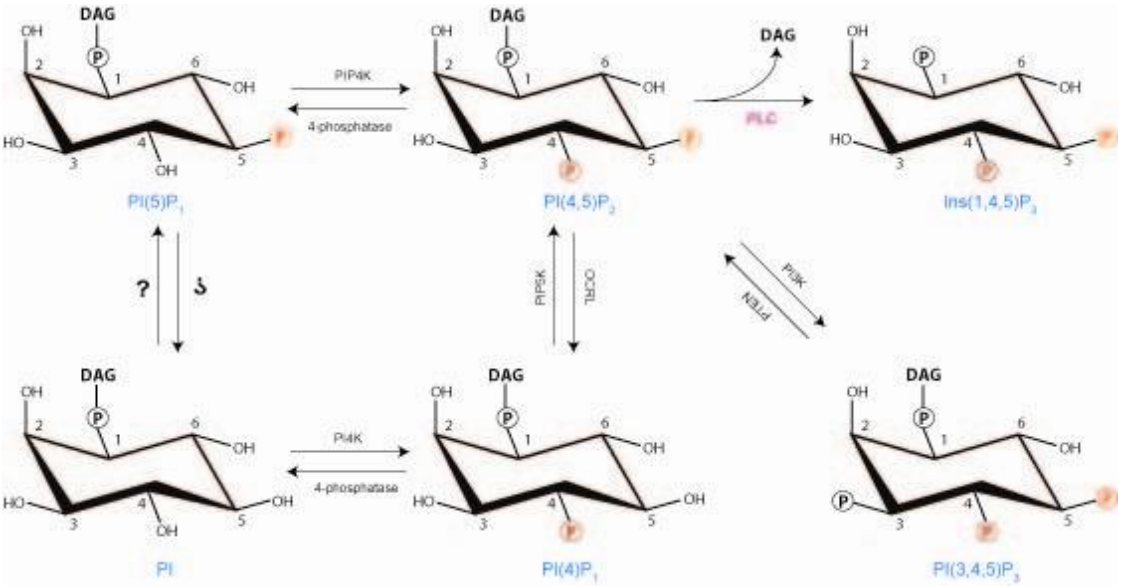

Figure 7 PIP_2 metabolism

Figure 7: A schematic of PIP_2 metabolism adapted from (Rusten and Stenmark 2006). Inositol rings of biological phosphoinositols are drawn with DAG attached to the P_i at the "1" position. Arrows between structures are labeled with appropriate kinases and phosphatases.

1.3.8 Membrane Binding Domains

There are numerous strategies that proteins have developed to bind to the membrane (DiNitto, Cronin et al. 2003). They range from the very specific binding interaction of phospholipase C delta pleckstrin homology (PLCδ-PH) domain with PIP_2 to the non-specific interaction of myristoylated alanine rich C kinase substrate (MARCKS). To understand the localization and how myo1c functions at the membrane, it is essential to first understand how it is associated with the membrane. These two extremes of binding will be discussed below.

1.3.8.1 MARCKS

MARCKS contains a polybasic effector domain (ED) which binds to the plasma membrane (Figure 8). The ED of MARCKS has been well studied, and contains 13 basic residues, five phenylalanines, and a myristoylated N-terminus. MARCKS has no set structure when it is bound or unbound to the membrane (Arbuzova, Schmitz et al. 2002). MARCKS also binds to CaM and actin; these interactions, along with phosphorylation, inhibit it from binding to the membrane. Myristoylation, hydrophobic insertions, and electrostatic interactions all contribute to membrane binding, and make MARCKS an eminent example for non-specific membrane association.

Electrostatic interactions mainly contribute to MARCKS binding to the membrane. This is accomplished by the polybasic region of the ED having an electrostatic attraction with the negatively charged inner leaflet of the plasma

membrane. The negative charge is made up from PS and phosphatidyl inositols, the most abundant of which is PIP_2. These negatively charged lipids anchor the cluster of basic residues in the ED to the membrane. Partition coefficients increase linearly in binding studies done with increasing the percent of acidic lipid (Arbuzova, Wang et al. 2000; Lemmon and Ferguson 2001).

These electrostatic interactions were found to be very non-specific. The individual residues and lipids were inconsequential, as long as the residues were positively charged arginines or lysines, and the lipids were negative. Studies done with R/K mutants and K/R mutants showed no effects on membrane binding (Wang, Gambhir et al. 2002). It has also been shown that peptides with stretches of arginine or lysine bind just as well to a negative membrane as a protein made up with the same number of basic residues (Wang, Gambhir et al. 2002). The only time this differs is when the protein has a rigid structure, and is able to make the same amount of contacts with fewer basic residues per total residues. It has also been shown that MARCKS has no preference for PS or phosphatidyl glycine (PG), which has the same negative charge. However, MARCKS does bind preferentially to PIP_2, as the partition coefficient is the same with 20% PS as it is with only 1% PIP_2 (Wang, Arbuzova et al. 2001). This preference for PIP_2 over singularly charged phospholipids enables the polybasic ED of MARCKS to laterally sequester PIP_2 into micro domains. Through fluorescence experiments with physiological concentrations of 33% PS, MARCKS has been shown to bring together numerous PIP_2 molecules (Wang, Gambhir et al. 2002).

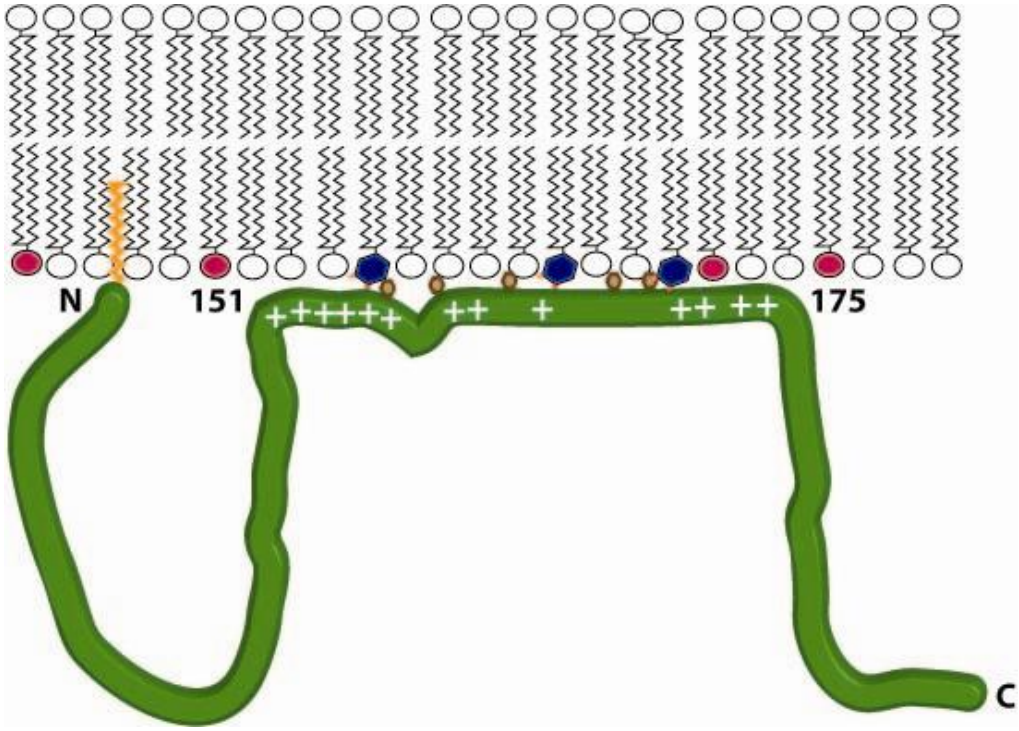

Figure 8 MARKS peptide

Figure 8: A representation of MARCKS binding to the plasma membrane, adapted from (Gambhir, Hangyas-Mihalyne et al. 2004). MARCKS is shown as a green snake. The position of positively charged residues are denoted by white crosses. N-terminal myristoylation is represented by an orange squiggly tongue. Brown hexagons are hydrophobic residues that insert into the membrane. Lipids shown are: PC, white; PS, fuschia; PIP_2, blue.

1.3.8.2 Pleckstrin Homology (PH) Domains

PH domains are the 11th most common domain found in the human proteome (Lemmon 2007). There are more than 250 proteins that contain one or more PH domains. They were first identified in numerous membrane associated proteins with sequence homology to pleckstrin, a protein kinase C (PKC) substrate. PH domains are made up of ~120 residues and contain a β-sandwich consisting of 7 β-strands. This β-core is capped at one open end by a C-terminal α-helix, leaving three hypervariable loops at the other end to interact with binding partners (Figure 9). It was originally thought that all PH domains bound to phosphatidylinositols in cell membranes, although with varying affinities and specificities. It is now known that some PH domains do not bind to phosphatidylinositols, but instead to proteins (Lemmon 2007). An example of this is PHR1, which binds to the tail domains of myo1c and myoVIIa (Etournay, El-Amraoui et al. 2005).

Many PH domains contain a specific binding pocket for the phosphorylated inositol rings of phosphatidyl inositols. These pockets are made up of multiple hypervariable loops that form hydrogen bonds to the phosphates on the inositol rings of phosphatidyl inositols (Figure 10) (Lemmon and Ferguson 2001). The first of these loops between β-strand 1 and β-strand 2 is where the PH domain signature motif lies. Slight variations in the non conserved residues found on these loops give rise to the binding specificity to particular phosphatidyl inositols (Cronin, DiNitto et al. 2004). The binding pockets of poly-phosphoinoitol binding (PPB) PH domains can bind stereo-specifically to a specific phosphatidyl inositol, while others bind promiscuously

to many phosphatidyl inositols. The crystal structures of many PH domains have been solved with the inositol phosphates bound in between the hypervariable loops.

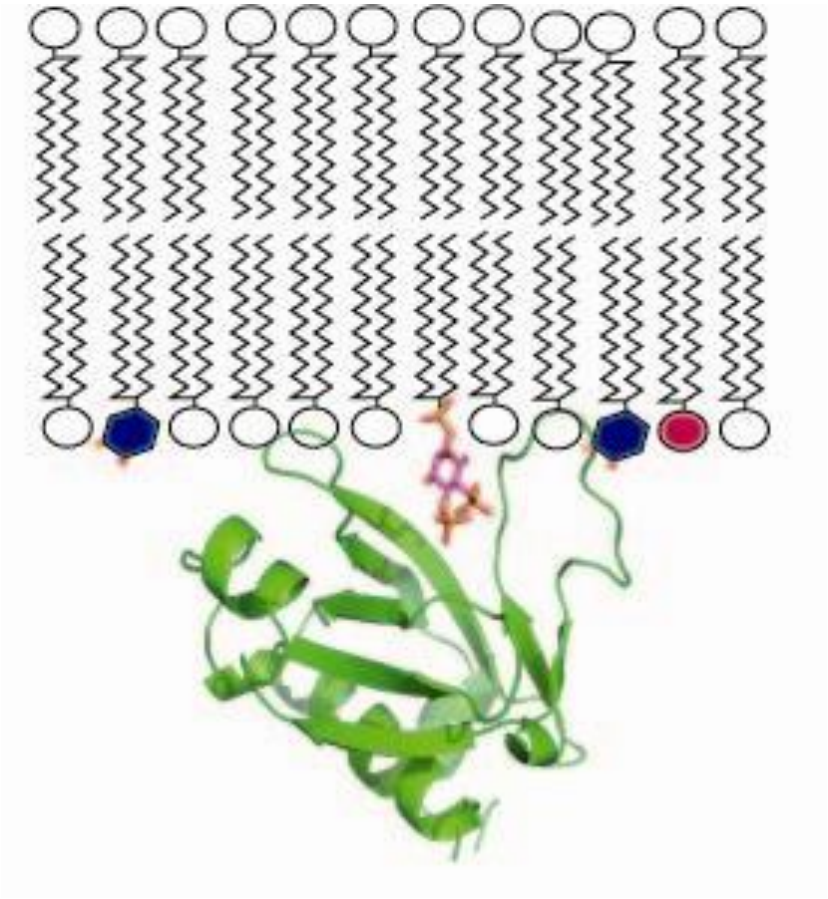

Figure 9 PLCδPH domain

Figure 9: A crystal structure of PLCδ-PH domain bound to Ins(1,4,5)P_3 imposed in a model plasma membrane. The inositol from the crystal structure represents the blue head domain of PIP_2. The structure of PLCδ-PH was drawn with Pymol.

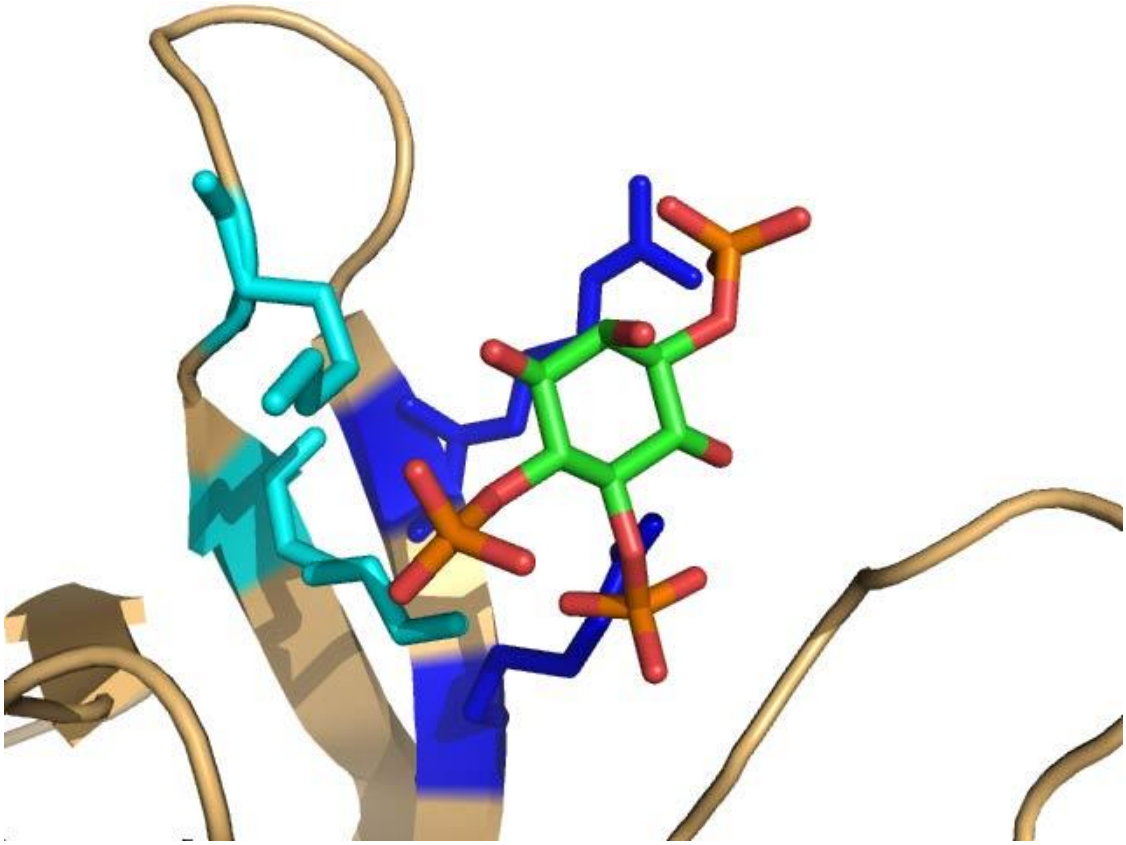

Figure 10 PH domain H-bonds

Figure 10: A close up of the crystal structure from Figure 9 drawn with Pymol. Details are shown of hydrogen bonds from arginines and lysines in hypervariable loop one to the phosphates on Ins(1,4,5)P_3.

2 Materials and Methods

This chapter will discuss all of the materials, equipment, and methods used to complete this thesis including: equipment, reagents and buffers, molecular biology, tissue culture, protein detection, protein preparations, assays, analysis of data, and modeling.

2.1 Equipment

Fast phase liquid chromatography (FPLC), ÄKTA Basic UPC (Amersham Biosciences); fluorimeter, (PTI, Birmingham, NJ); UV-visible spectrophotometer, Cary 50 Bio (Varian); microscope setup: Leica DMIRB microscope fitted with a Nikon 1.45 NA objective lens (Axelrod, 2001), 488 nm 43 series argon laser (Melles Griot), C4742-95 digital camera (Hamamatsu), computer controlled filter wheel (Sutter Instruments); centrifuges: TL ultracentrifuge (Optima), L8-M ultracentrifuge (Beckman), RC-5B superspeed centrifuge (Sorvall), J6-HC swinging bucket (Beckman); gel scanner, 8600 imager (Typhoon); scintillation counter, LS 6000 SC (Beckman); film developer, X-OMAT 2000A Processor (Kodak); Orbital Shaker (Forma Scientific).

2.2 Reagents and Buffers

All *in vitro* experiments were performed in HNa100 (10 mM HEPES, pH 7.0, 100 mM NaCl, 1 mM EGTA, 1 mM DTT) unless otherwise stated. Ca^{2+} concentrations were adjusted by adding $CaCl_2$ to HNa100 and are reported as free Ca^{2+} using EGTA as a chelator. Unless stated otherwise, all experiments done with myosin constructs containing at least one IQ motif were performed with 1 μM free CaM.

Phosphatidylserine (PS), phosphatidylcholine (PC), and phosphatidylinositol-4,5-bisphosphate (PIP_2) were purchased from Avanti Polar Lipids (Alabaster, AL); D-*myo*-inositol-1,4,5-trisphosphate ($Ins(1,4,5)P_3$), D-*myo*-inositol-1,3,4,5-tetrakisphosphate ($Ins(1,3,4,5)P_4$), D-*myo*-inositol-1,3,4,6-tetrakisphosphate ($Ins(1,3,4,6)P_4$), and D-*myo*-inositol hexakisphosphate ($InsP_6$) were purchased from Calbiochem (La Jolla, Ca); D-*myo*-inositol-3-monophosphate ($Ins(3)P_1$) D-*myo*-inositol-1,3,4-trisphosphate ($Ins(1,3,4)P_3$), and D-*myo*-inositol-1,2,6-trisphosphate ($Ins(1,2,6)P_3$) were purchased from Cayman Chemical (Ann Arbor, MI); D-*myo*-inositol-1,2,5,6-tetrakisphosphate ($Ins(1,2,5,6)P_4$) and D-*myo*-inositol-1,2,3,5,6-pentakisphosphate ($Ins(1,2,3,5,6)P_5$) were purchased from A.G. Scientific (San Diego, Ca). Tritiated inositol-1,4,5-trisphosphate (^{3}H-$Ins(1,4,5,)P_3$) was purchased from Perkin Elmer. Anti-GFP rabbit serum was purchased by Invitrogen. Secondary antibodies, ECL anti-rabbit IgG and anti-mouse IgG were purchased from Amersham Biosciences.

2.3 Molecular Biology

2.3.1 Constructs

All constructs used are listed along with their domain structure (Figure 11). Myo1c-tail, myo1c (residues 690-1028); myo1c-motor, myo1c (residues 1-767); GFP-myo1c, GFP-tagged full length myo1c; GFP-tail, GFP-tagged myo1c (residues 690-1028); GFP-tail$^{IQ2–3}$, GFP-tagged myo1c (residues 721-1028); GFP-myo1c-tail^{IQ3}, GFP-tagged myo1c (residues 744-1028); GFP-myo1c-tail^{IQ0}, GFP-tagged myo1c (residues

768-1028); GFP-tail-K892A and GFP-tail-R903A, point mutations in GFP-myo1c-tail; GFP-myo1c-K892A and GFP-myo1c-K903A, point mutations in GFP-myo1c.

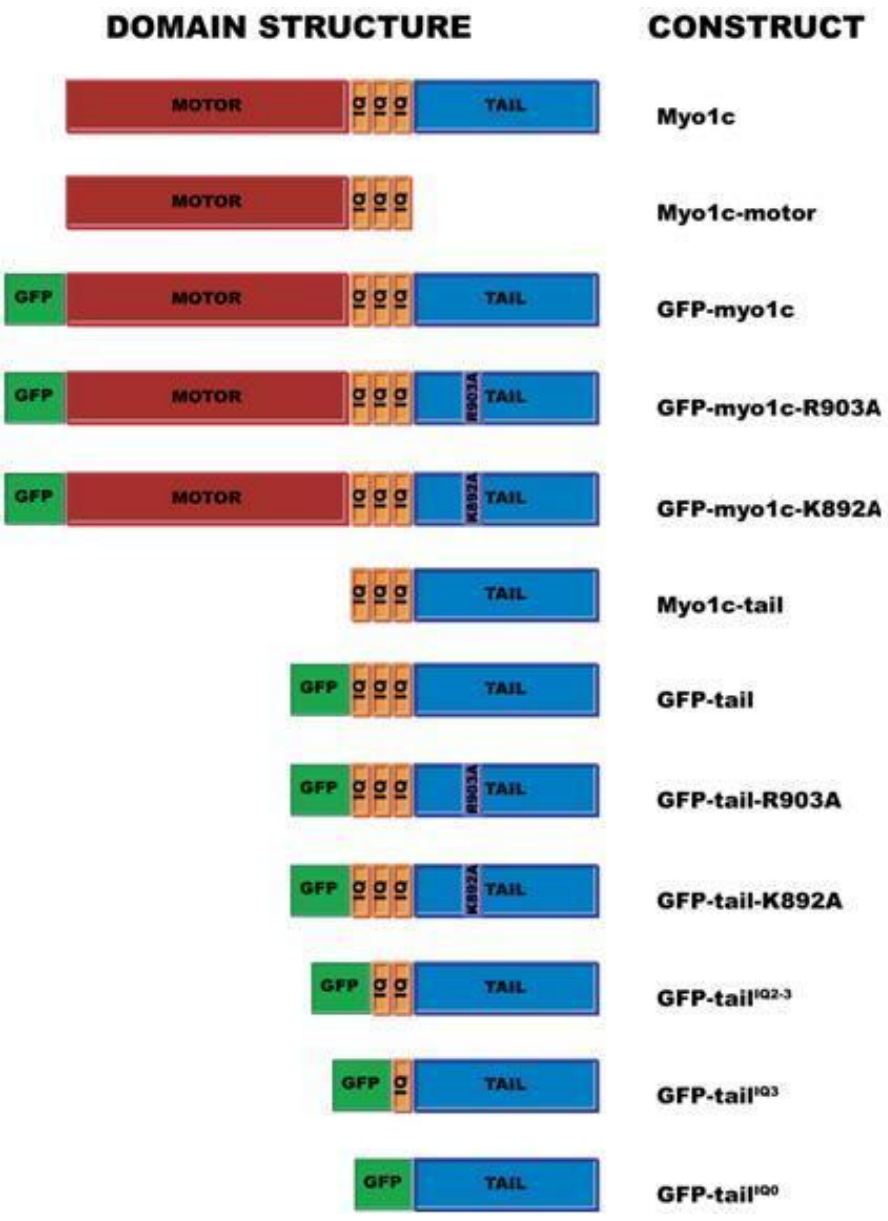

Figure 11 Constructs

Figure 11: Domain structures of myo1c constructs used in this thesis.

2.3.2 DNA Handling

All DNA was amplified in competent DH5α cells. Cells were grown in 2xYT media (171 mM NaCl, 16 g/mL tryptone, 10 g/mL yeast extract) in an orbital shaker overnight at 37 °C, 250 RPM. Transformations were done by adding 0.5 µg DNA to 50 µL DH5α cells in a pre-chilled microcentrifuge tube and incubating on ice for 20 minutes. Reactions were heat pulsed at 42 °C for 45 seconds and placed on ice for 2 minutes. 500 µL of 2xYT was added to each tube and tubes were incubated at 37 °C for 1 hour with shaking at 250 rpm. Cells were placed on appropriate agar plates or transferred to larger cultures containing either 100 µg/mL ampicillin or 30 µg/mL kanamycin. DNA plasmids were purified using Promega Wizard Plus mini and midi kits for 1.5 and 50 mL cultures respectively. DNA concentrations were calculated by measuring absorbance in a UV-Vis spectrophotometer at 260nm, based on one A260 O.D. unit for dsDNA = 50 µg/ml.

2.3.3 Sequencing and Primers

All primers for DNA sequencing and point mutations were designed by hand and ordered through Invitrogen (Life Technologies). DNA sequences were verified by automated dideoxynucleotide sequencing at the University of Pennsylvania DNA sequencing facility.

2.3.4 Mutations

Point mutations in GFP-myo1c-tail (GFP-tail-R903A and GFP-tail-K896A) or full length GFP-myo1c (GFP-myo1c-K892A and GFP-myo1c-R903A) were generated using the Quick-Change Site-Directed Mutagenesis Kit according to the manufacturer's protocol (Stratagene Cloning Systems, La Jolla, California). Forward and reverse primers were designed containing single amino acid mutations to overlap desired sites with melting temperatures over 78 °C. A thermo cycling reaction was performed for 16 cycles, followed by the addition of 10 U of *DpnI* and an hour incubation at 37 °C to digest parent DNA. Each reaction was transformed into XL1-Blue cells and plated on agar plates containing the appropriate antibiotic. Successful plates yielded, on average, 10-100 colonies. All point mutations were verified by automated dideoxynucleotide sequencing.

2.4 Tissue Culture

2.4.1 Cell Types

We used a number of different mammalian cell types for the investigations in this thesis. Normal rat kidney (NRK) epithelial cells were the primary cell type used for our TIRF/FPAP experiments, as well as in many of our fluorescence imaging studies. African green monkey kidney (COS-7) cells, Chinese hamster ovary (CHO) cells, and HeLa cells were used in myo1c localization studies. Human embryonic kidney (293T) cells were used primarily for small scale protein growths.

2.4.2 Growth and Passaging

All cells types were grown in a 37 °C humidified incubator in 5% CO_2. Cells were maintained in growth medium, Dulbecco's Modification of Eagle's Medium (DMEM) containing 10 % Fetal Bovine Serum (FBS), 100 U/ml penicillin, 100 µg/ml streptomycin, and 0.25 µg/ml amphotericin B, in 10-cm round tissue culture plates. Cells were passaged 1:10 using 0.25% trypsin-EDTA when 80-100% confluent, which occurred in 2-4 days, depending on the cell type. Frozen, 1 mL aliquotted stocks in DMEM with 15% FBS and 10% DMSO at 5x the normal passaging concentrations were made for all cell types.

2.4.3 Transfections

NRK and COS-7 cells were transfected using transient electroporation. Approximately five million cells were trypsinized from a 10-cm plate and resuspended in 400 µL cold DMEM. 10 µg DNA was added and cells were transferred to a 0.4-cm electroporation cuvette and incubated on ice for 5 minutes. Cells were electroporated in a Bio Rad Gene Pulser II at 250 V, 950 µF for NRK cells, and 200 V, 950 µF for COS-7 cells. Cells were immediately transferred to 60-mm plates with cover slips in 3 mL growth media and incubated at 37 °C. Media was removed 4-6 hours later and cells were incubated with fresh growth media overnight. To avoid apparent aggregation of GFP-myo1c-tail^{IQ0}, cells electroporated with this construct were grown overnight at 32 °C (Tang and Ostap 2001).

HeLa, CHO, and 293T cells were transfected with Lipofectamine™ 2000. Cells were grown in either 60-mm plates on top of cover slips or 15-cm plates until 95% confluent at time of transfection. For a 60-mm plate, 8 µg DNA in 0.5 mL DMEM was mixed with 10 µL Lipofectamine™ 2000 diluted in 0.5 mL DMEM and incubated for 20 minutes at room temperature. For 15-cm plates, all reagents were scaled up according to surface area. The DNA and Lipofectamine™ 2000 complex was added to the cells and incubated overnight at 37 °C.

2.4.4 Fixing and Mounting Slides

To fix and mount cells for viewing with immunostaining or rhodamine/phalloidin, a 4% paraformaldehyde fixative was added to cells adhered to a cover slip for 15 minutes. Cells were washed with PBS and permeablized in a 0.1% Igepal solution for 10 minutes, then washed with PBS and blocked in a 1% BSA solution with or without 1:1000 dilution of rhodoamine/phalloidin for 30 minutes. Cells were then placed in permeablization buffer with 10 µg/mL primary antibody and incubated for 1 hour, and washed and incubated in 1:500 dilution of secondary antibody in permeablization buffer for 1 hour. Mounting solution was made by combining 120 µL of 0.017 g PPD, 1.5 mL 7.5% $NaHCO_3$, 0.3 mL 0.5 M Na_2CO_3 with 100 µL of 10x PBS + 780 µL 50% glycerol and pipetting 12 µL onto a clean slide. Cover slips were lowered onto slides with mounting solution and sealed on all sides with red nail polish. Before use, all antibodies were spun down at maximum speed in a microcentrifuge tube

centrifuge for 5 minutes at 4°C to remove particulates. All solutions were made up in a PBS solution containing Ca^{2+} and Mg^{2+}.

2.5 Protein Detection

2.5.1 Determining Protein Concentration

All protein concentrations were determined with the Bradford assay using Coomassie Plus (Pierce). Five standards were made containing 0, 2.5, 5, 10, and 20 ng BSA in 95 µL total volume. 5 µL of protein buffer was added to each tube. Samples were then made up by adding 5 µL protein to 95 µL H_2O in duplicate. After adding 1.5 mL of Coomassie Plus, each tube was vortexed for 5 seconds. Absorbance at 595 nm was measured using a UV-visible spectrophotometer. Standards were fit to a linear line and that line was used to determine protein concentration.

2.5.2 Western Blots

For detection of proteins by Western blot analysis, proteins were run on an SDS-PAGE gel and then transferred to a Hybond-C Extra nitrocellulose membrane (Amersham Biosciences) in Towbin buffer (25 mM Tris, 192 mM glycine, 10% methanol, 0.1% SDS) for 1 hour at 100 mV. The membrane was subjected to a series of three 60 minute agitated incubations in blocking buffer, which was comprised of a 5% milk solution in wash buffer (50 mM Tris, 150 mM NaCl, 0.05% Igepal, pH 8.0), primary IgG antibody, and horseradish peroxidase linked ECL secondary-antibody IgG (Amersham Biosciences). All antibodies were diluted in blocking buffer and thorough

washings were done between each incubation. Following incubations, the membrane was incubated in Super Signal West Pico chemiluminescent substrate (Pierce) for 5 minutes and then either placed in a developing cartridge and exposed to Kodak Blue XB-1 film, or imaged using a gel scanner.

2.5.3 SYPRO® Red

For quantitative analysis of nanogram levels of proteins run on gels, we used SYPRO® Red protein gel stain. Proteins were run on an SDS-PAGE gel and agitated with SYPRO diluted 1:5000 in 7.5% acetic acid for 50 minutes. Gels were destained in 7.5% acetic acid for 10 minutes before being imaged on a gel scanner.

2.6 Protein Purification

2.6.1 Mouse Myo1c-Tail

The mouse myo1c-tail (accession # NM_008659) construct (residues 690 – 1028), which consists of an N-terminal HIS_6 tag for purification, three CaM-binding IQ motifs, and the tail domain, was expressed and purified from *Sf9* cells as reported (Tang, Lin et al. 2002). Myo1c-tail with bound CaM was purified from *Sf9* cells that were co-infected with virus-containing recombinant myo1c-tail and CaM. Four liters of cells were suspended in 300 mL of 25 mM Tris, pH 7.5, 20 mM imidazole, 300 mM NaCl, 0.5% Igepal, 0.5 mM EGTA, 1 mM 2-mercaptoethanol, 1 mM PMSF, 0.01 mg/mL aprotinin, and 0.01 mg/mL leupeptin at 4 °C and homogenized with five strokes in a Dounce homogenizer. Cell extract was centrifuged at 100,000 × *g* for 1 h.

The supernatant was sonicated five times for 15 s, incubated with 10 µg/ml RNase A and 5 µg/ml DNase I on ice for 15 min, and loaded on to two 2 mL nickel-nitrilotriacetic acid (Qiagen) columns. The columns were washed with five column volumes of the same buffer without Igepal. Myo1c-tail was eluted with 5 ml of 125 mM imidazole, 300 mM NaCl, 25 mM Tris pH 8.0, 0.5 mM EGTA, 1 mM 2-mercaptoethanol, 0.01 mg/ml aprotinin, 0.01 mg/ml leupeptin, and 5 µM CaM from each column. The elutions were diluted in 30 ml of 10 mM HEPES pH 7.0, 200 mM NaCl, 1 mM EGTA, and 1 mM 2-mercaptoethanol and loaded on to a MonoS column (Amersham Biosciences) equilibrated in 10 mM HEPES, 50 mM NaCl, 1 mM EGTA, and 1 mM DTT. Myo1c-tail was separated and eluted with a linear 50 mM - 1 M NaCl gradient. Myo1c-tail with bound CaM elutes at ~ 400 mM NaCl. Fractions containing myo1c-tail were combined and dialyzed versus 10 mM Tris, pH 8.0, 50 mM NaCl, 1 mM EGTA, and 1 mM DTT and loaded on to MonoQ column (Amersham Biosciences) equilibrated in 10 mM Tris, pH 8.0, 50 mM NaCl, 1mM EGTA, and 1 mM DTT. Myo1c-tail was eluted with a linear 50 mM - 1 M NaCl gradient. Myo1c-tail with bound CaM elutes at ~ 380 mM NaCl. Fractions containing myo1c-tail were combined and concentrated to approximately 1.5 mL using Microsep concentrators (Pall Filtron) or Ultra-15 Centrifugal Filter Units (Amicon). The concentrated protein was dialyzed versus HNa100 overnight. Myo1c-tail concentrations were determined using Coomassie Plus as described above. A typical yield of myo1c-tail with bound CaM from 4 liters of cells was ~1 mg. The purified myo1c-tail contains three bound CaM. A

typical gel showing various stages of the myo1c-tail purification is shown from Tang et al. 2002 (Figure 12).

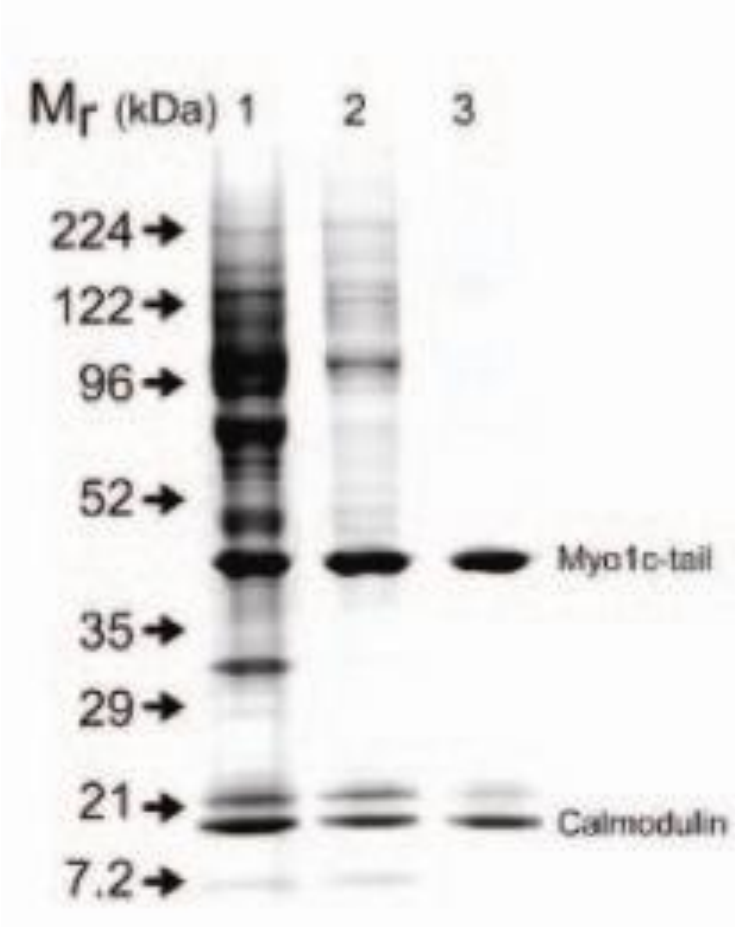

Figure 12 Purification of myo1c-tail

Figure 12: A Coomassie-stained SDS-PAGE gel of the purification of myo1c-tail from (Tang, Lin et al. 2002). Lane 1) nickel-nitrilotriacetic acid column elution. Lanes 2) mono-S elution, and 3) mono-Q elution. Arrows specify location of molecular mass markers. The calculated molecular mass of myo1c-tail is 39 kDa.

2.6.2 Mouse Myo1c-Motor

The myo1c-motor construct (accession # NM_008659) includes the motor domain and 3 IQ motifs (residues 1 - 767). A 15 amino acid sequence for site-specific biotinylation (Schatz 1993) and a FLAG sequence for purification were inserted at the C terminus. Myo1c-motor was expressed and purified from Sf9 cells that were co-infected with virus containing recombinant myo1c-motor and CaM (El Mezgueldi, Tang et al. 2002). Four liters of cells were suspended in 250 mL of 10 mM Tris, pH 7.5, 200 mM NaCl, 4 mM $MgCl_2$, 2 mM ATP, 5 mM DTT, 0.5% Igepal, 1 mM EGTA, 1 mM PMSF, 0.01 mg/ml aprotinin, and 0.01 mg/ml leupeptin at 4 °C and homogenized with five strokes in a Dounce homogenizer. Cell extract was centrifuged at 100,000 × g for 1 h. Supernatant was loaded onto two 1.5 mL FLAG resin columns. The columns were washed with five column volumes of the same buffer without Igepal, then two column volumes of buffer without Igepal or ATP. Myo1c-motor was eluted with 5 ml of 100 mM NaCl, 10 mM Tris, pH 8.0, 1 mM EGTA, 1 mM DTT, 0.01 mg/ml aprotinin, 0.01 mg/ml leupeptin, 0.2 mg/mL FLAG peptide, and 5 µM CaM from each column. Eluted protein was loaded on to a MonoQ column (Amersham Biosciences) equilibrated in 10 mM Tris, pH 8.0, 50 mM NaCl, 1mM EGTA, and 1 mM DTT. Myo1c-motor was eluted with a linear 50 mM - 1 M NaCl gradient. Myo1c-motor with bound CaM eluted at ~ 430 mM NaCl. Fractions containing myo1c-motor were combined and dialyzed versus 50% glycerol, 50% HNa100. Myo1c-motor concentrations were determined using Coomassie Plus as described above. A typical yield of myo1c-motor with bound CaM from 4 L of cells was ~2 mg. The purified

myo1c-motor contained three bound CaM. A typical gel showing various stages of the myo1c-motor purification is shown (Figure 13).

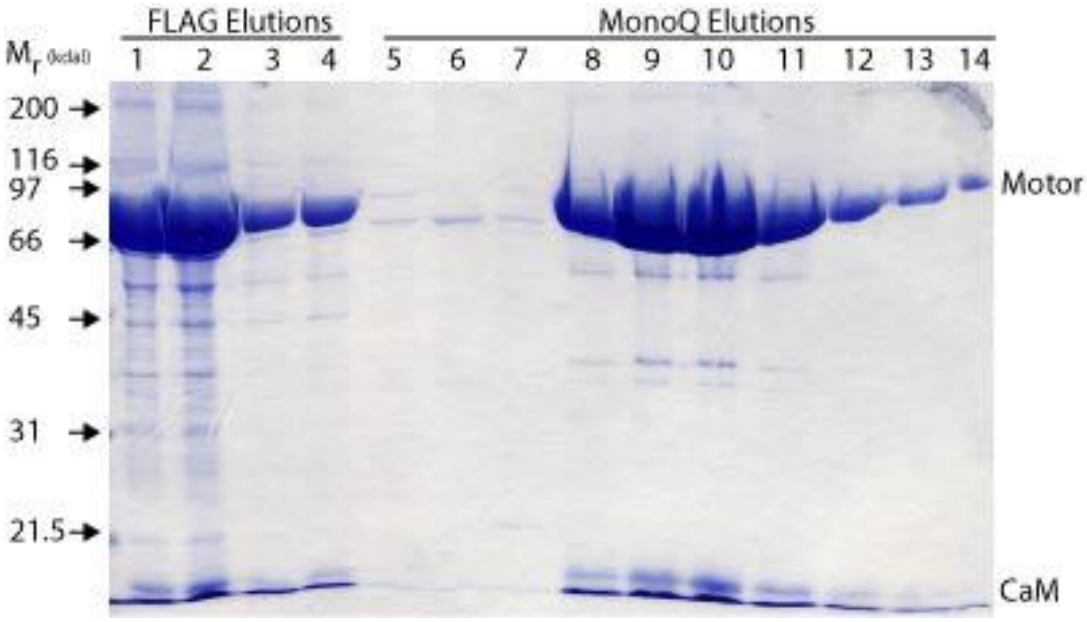

Figure 13 Purification of myo1c-motor

Figure 13: A Coomassie-stained SDS-PAGE gel of the purification of myo1c- motor. Lanes 1-4) Elutions from FLAG resin column. Lanes 5-14) Elutions from Mono-Q column. Arrows specify location of molecular mass markers. The calculated molecular mass of myo1c-motor is 89 kDa.

2.6.3 Calmodulin (CaM)

Recombinant chicken CaM was expressed and purified from bacterial lysates using a phenyl sepharose column in the presence of EDTA, and then $CaCl_2$ (Putkey, Slaughter et al. 1985), and further purified by FPLC using a MonoQ column (Amersham Biosciences). This final MonoQ step was crucial, since we found a bacterial contaminant present in very low abundance (Figure 14) that effectively competed with myo1c-tail for binding to anionic lipids (Hokanson and Ostap 2006).

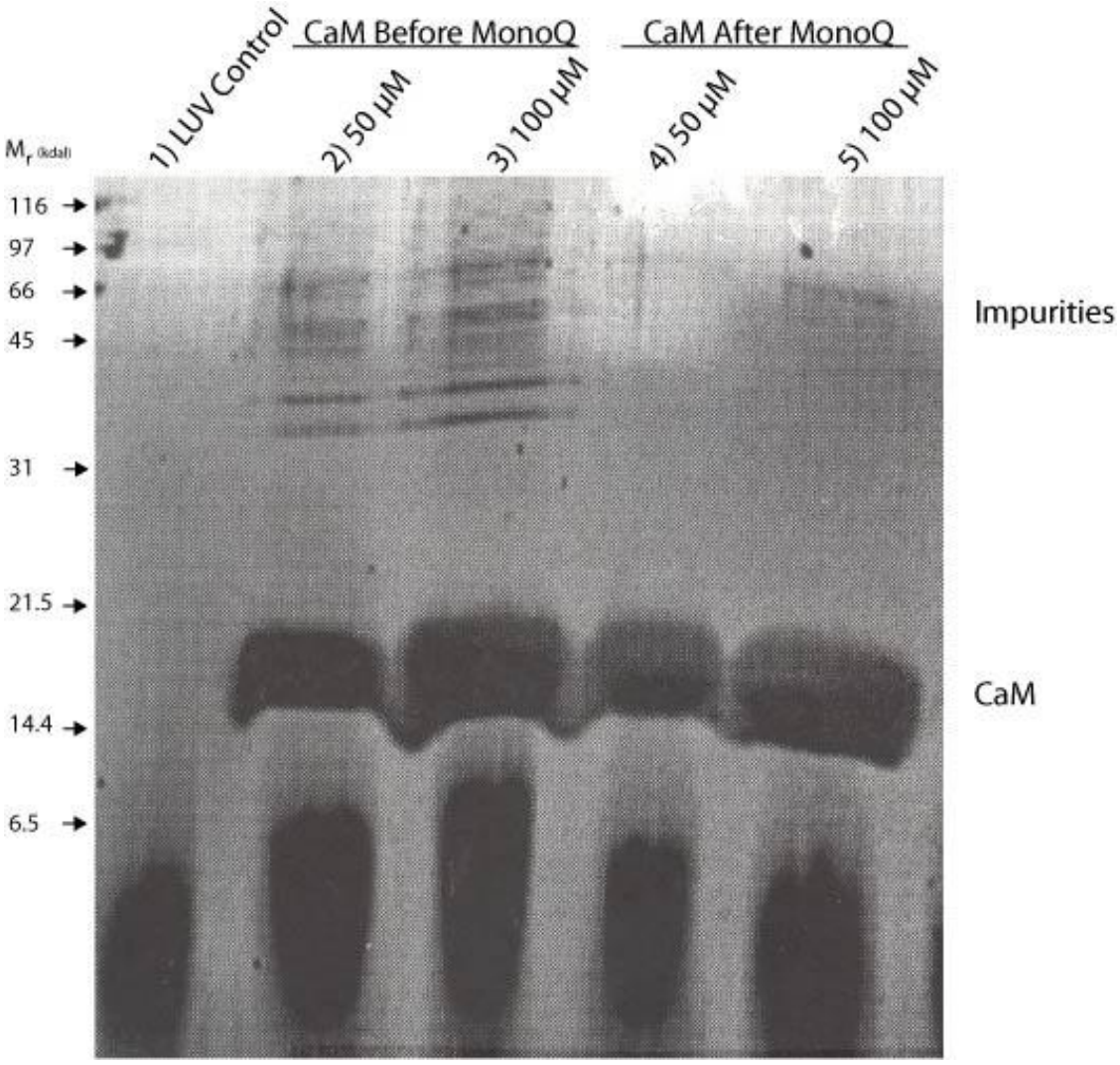

Figure 14 Purification of CaM

Figure 14: A SYPRO red-stained SDS-PAGE gel of pellet samples from a sedimentation assay of CaM with 60% PS LUVs. Lane 1) 60% PS LUVs control. Lanes 2-3) 60% PS LUVs with CaM, 50 and 100 µM. Lanes 4-5) 60% PS LUVs with CaM, 50 and 100 µM, after purification with Mono-Q. Note the high molecular weight contaminants in lanes 2-3. Arrows specify location of molecular mass markers. The calculated molecular mass of CaM is 16 kDa.

2.6.4 Glutathione-S-Transferase (GST)

GST was used to block non-specific interactions and was purified from BL21-pLys cells. BL21-pLys cells were transfected with a pGEX.B23 vector containing GST. Cell cultures of 2.5 L were grown containing 100 µg/mL ampicillin and 34 µg/mL chloramphenacol and induced with 1 mM IPTG for 3 hours after cells reached an OD of 0.7 at 600 nm. Cells were harvested by centrifugation for 20 minutes at 10,500 x g. The pellet was resuspended in 100 mM NaCl and spun at 5000 x g in a 50 mL conical tube for 15 minutes. The pellet was then flash frozen in liquid N_2 and stored at -80 ºC. The frozen cell pellet was resuspended in 50 mL of PBS (1.4 mM NaCl, 27 mM KCl, 101 mM Na_2HPO_4, 18 mM KH_2PO_4), 1 mM DTT, 1 mM PMSF, and 1% triton at 4 °C. The lysate was sonicated for 15 seconds five times and centrifuged for 30 minutes at 27,000 x g. The supernatant was loaded onto a 2.5 mL Glutathione Sepharose 4B matrix column immediately after the spin and washed with five column volumes of PBS with 1 mM DTT. GST was eluted with two column volumes of reduced glutathione buffer (10 mM glutathione, 50 mM Tris, pH 8.0). 2.5 mL of bacterial cells typically yielded ~ 100 mg GST. A typical gel showing various stages of the GST purification is shown (Figure 15).

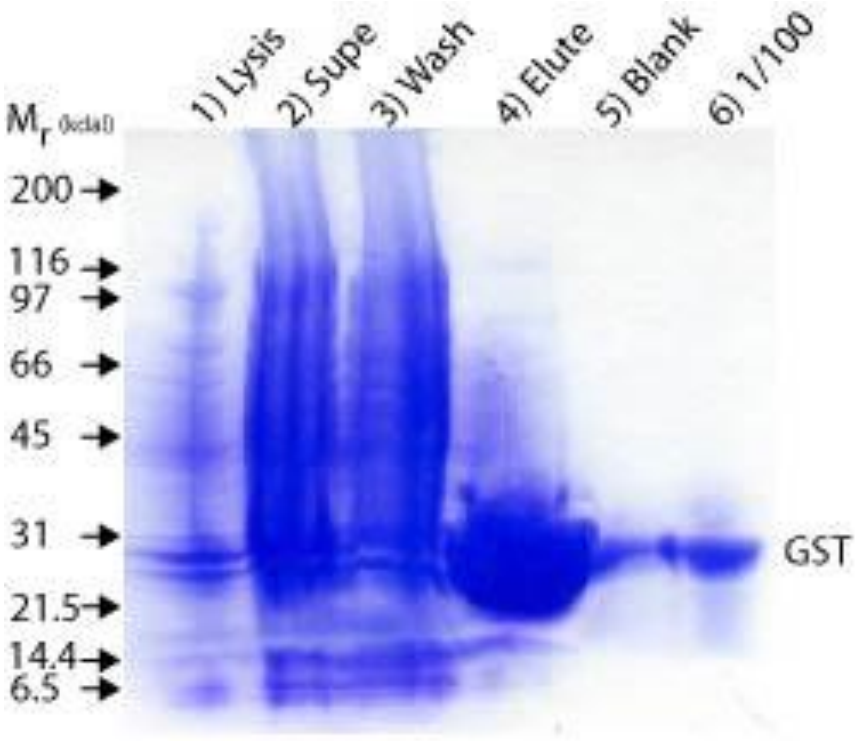

Figure 15 Purification of GST

Figure 15: A Coomassie-stained SDS-PAGE gel of the purification of GST. Lane 1) Lysis from BL21 cells. Lane 2) Supernatant from sedimentation. Lane 3) Wash from glutathione sepharose column. Lane 4) Elution from glutathione sepharose column. Lane 5) Blank. Lane 6) 100 x dilution of elution from glutathione sepharose column. Arrows specify location of molecular mass markers. The calculated molecular mass of GST is 29 kDa.

2.6.5 Fibrinogen

Lyophilized fibrinogen was a gift from Dr. Paul Janmey (University of Pennsylvania) and was rehydrolyzed in HNa100, aliquotted into 1 mL samples, frozen in liquid N_2, and stored at -80 ºC. The final concentration for fibrinogen was ~8 mg/mL with 3% fibronectin present.

2.6.6 Phospholipase-Cδ Pleckstrin Homology Domain (PLCδ-PH)

A bacterial expression plasmid for the PH domain of phospholipase-Cδ (residues 11 – 140; PLCδ-PH) was a gift from Dr. Mark Lemmon (University of Pennsylvania) and was purified as described (Ferguson, Lemmon et al. 1994). BL21 (DE3) RP cells were transfected with a pGEX.B23 vector containing PLCδ-PH. Cells were grown in 4 L cultures containing 100 µg/mL ampicillin and 34 µg/mL chloramphenacol and induced with 1 mM IPTG for 3 hours when cells reached an OD of 0.7 at 600 nm. Cells were harvested by centrifugation for 20 minutes at 10,500 x g, and the pellet was resuspended in 100 mM NaCl and spun at 5000 x g in a 50 mL conical tube for 15 minutes. The pellet was frozen in liquid N_2 and stored at -80 ºC. Upon removal from storage, the pellet was resuspended in 50 mL 100 mM NaCl, 50 mM glucose, 25 mM MES, pH 6.0, 5 mM DTT, and 1 mM PMSF. The lysate was sonicated five times for 15 s and centrifuged for 30 minutes at 27,000 x g. The supernatant was loaded onto a pre-equilibrated 60 mL DEAE cellulose column and washed with two column volumes of 25 mM MES pH 6.0, 50 mM NaCl, 1 mM DTT, and 1 mM PMSF. All flow through was collected and diluted 3-fold with 25 mM MES

pH 6.0, and 1 mM DTT and then loaded directly onto a pre-equilibrated S-sepharose column. The S-sepharose column was washed with two column volumes of 25 mM MES, pH 6.0, and 1 mM DTT, and then the protein was eluted in 6 mL fractions with a 250 mL linear salt gradient from 0-500 mM NaCl. The protein eluted from this column at ~ 120 mM NaCl. Fractions containing PLCδ-PH, as determined by the OD at 280 nm and a SDS-PAGE gel, were pooled and ammonium precipitated to 75% saturation, 0.476 g/mL NH_4SO_4, overnight at 4 ºC. The precipitate was centrifuged at 17,000 x g for 15 minutes and the pellet was resuspended in a minimal volume of 25 mM MES pH 6.0, 150 mM NaCl, and 1 mM DTT by gentle mixing. The protein was aliquotted into microcentrifuge tubes and centrifuged at maximum speed for two minutes to pellet particulates. The protein was syringe filtered through a 0.22 µm filter and loaded onto a Superdex 200 gel filtration column. PLCδ-PH ran as a 20 kDa protein. The fractions containing protein, as determined by SDS PAGE gel, were pooled together and dialyzed overnight versus 2 L HNa100. The protein solution was concentrated using Microsep concentrators (Pall Filtron) and aliquotted into 50 µL samples that were frozen in liquid N_2 and stored at -80 ºC. A typical gel showing various stages of the purification of PLCδ-PH is shown (Figure 16).

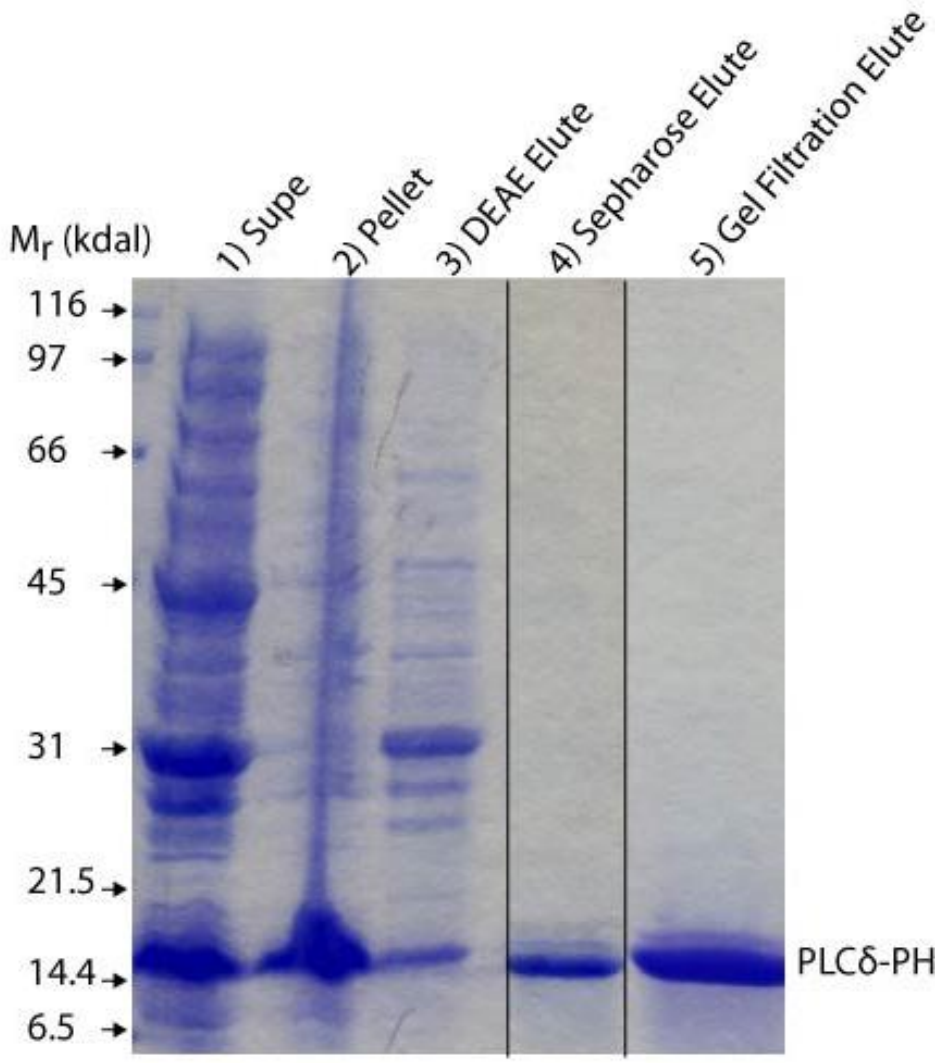

Figure 16 Purification of PLCδ-PH

Figure 16: A Coomassie-stained SDS-PAGE gel of the purification of PLCδ-PH. Lane 1) Supernatant of lysed cells. 2) Pellet of lysed cells. 3) Elution from DEAE column. 4) Elution from S-Sepharose elution. 5) Elution from gel filtration column. Arrows specify location of molecular mass markers. Lanes are non-continuous and are taken from 2 gels of the same protein preparation. Lanes from elutions with little or no protein have been excluded. The calculated molecular mass of PLCδ-PH is 20 kDa.

2.6.7 GFP-Tagged Myo1c-Tail

Small amounts of GFP-tail, GFP-tail-K892A and GFP-tail-R903A were purified for binding experiments by transient expression in HEK-293T cells (Hokanson, Laakso et al. 2006). Transfected cells (~$1x10^9$ cells per transfection) were collected by sedimentation, flash frozen in liquid N_2, and stored at -80 °C. GFP-proteins were purified in a 1-day procedure. Pellets of ~$1x10^9$ cells were suspended in 15 mL lysis buffer (10 mM HEPES pH 7.0, 1 mM EGTA, 300 mM NaCl, 5mM DTT, 0.5% Igepal, 1mM PMSF, 0.01 mg/mL aprotinin, and 0.01 mg/mL leupeptin), lysed by 8 strokes in a Dounce homogenizer, and centrifuged for 1 hour at 100,000 x g. The supernatant was incubated on ice with 10 µg/mL RNase A and 5 µg/mL DNase I for 20 minutes. After dilution, the final NaCl concentration of the supernatant was 100 mM; the supernatant was then passed through a 0.22 µm syringe filter and loaded immediately onto a MonoQ column (Amersham Biosciences). Protein was eluted from the MonoQ column using a linear salt gradient, and GFP-proteins were detected by monitoring GFP fluorescence. Fractions containing GFP were diluted to 100 mM final NaCl concentration, and $CaCl_2$ was added to attain 1 mM free Ca^{2+}. The protein was loaded immediately back on the MonoQ column and eluted with a linear salt gradient in column buffers containing 1 mM free Ca^{2+}. The addition of Ca^{2+} results in the dissociation of a CaM from myo1c (Zhu, Beckingham et al. 1998; Sokac and Bement 2000). We found that this CaM dissociation causes the GFP-proteins to elute from the MonoQ column at a lower salt concentration, resulting in their separation from Ca^{2+}-insensitive proteins. 5 µM CaM and 5 mM EGTA were immediately added to the

eluted GFP-proteins, and the proteins were dialyzed overnight versus HNa100. GFP-tail, GFP-tail-K892A, and GFP-tail-R903A were > 90% pure as determined by SYPRO-red staining of SDS-PAGE gels (Figure 17). GFP-proteins were stored on ice and used in binding assays within 2 days of purification. Yields of pure GFP-proteins were low (2 – 3 µg per transfection), but the preparations provided enough material to perform binding assays. A Western blot analysis with anti-GFP is shown (Figure 17 *inset*).

293T cells transfected with GFP-myolc-tail were also lysed and purified in the presence of phosphatase or phosphatase inhibitors. Phosphatase inhibitor was added to 293T cells during pellet resuspension and lysis. Cells lysates were then separated into two fractions; 400 U/µL of lambda protein phosphatase was added to one, then both fractions were purified separately as described above.

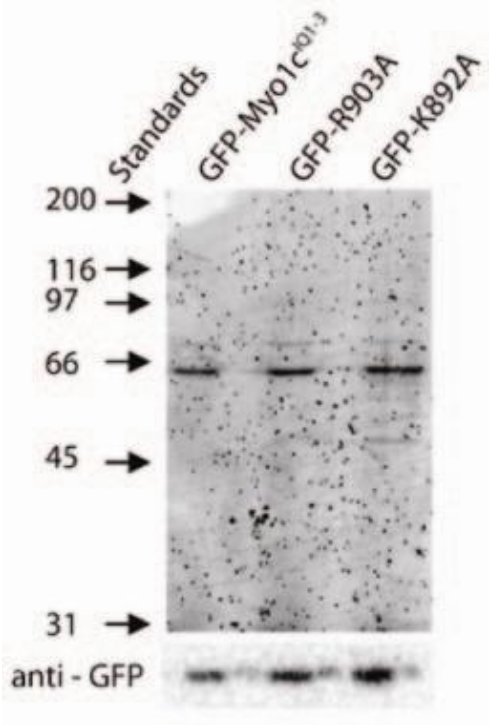

Figure 17 Purification of GFP-tail constructs

Figure 17: A SYPRO-red stained SDS-PAGE gel showing purified GFP-tail constructs. Lane 1) GFP-tail. Lane 2) GFP-tail-R903A. Lane 3) GFP-tail-K892A. Bottom) Western blot of purified GFP-myo1c-tail constructs stained with anti-GFP antibody. Figure originally published in (Hokanson, Laakso et al. 2006).

2.6.8 Mouse Myo1c-Tail Monoclonal Antibody (M2)

Frozen hybridoma cells containing a monoclonal antibody for the epitope PVVKYDRKGYKPRPRQLLL in mouse myo1c (M2), a gift from Peter Gillespie (Oregon Health and Science University, Portland, Oregon), were rapidly thawed and transferred to 5 mL warm RPMI 1640 medium containing 10% FBS and 1:100 penicillin and streptavidin. Cells were started in a 6-cm tissue culture plate and split 1:5 into larger volume plates each time cell densities reached 1 million cells/mL until cell volume reached 0.5 L. Supernatant was collected by centrifuging cells at 2500 x g for 5 minutes at 4 °C. The supernatant was filtered through a 0.22 µm filter and loaded onto a pre-equilibrated 1 mL HiTrap Protein G HP column (GE healthcare) at 4 °C. The HiTrap column was washed with 20 mL PBS and the protein was eluted with 5 mL 100 mM glycine pH 2.5 into 0.5 mL fractions containing 25 µL 1 M Tris pH 9.5 to neutralize the pH. Fractions were run on an SDS-PAGE gel; those containing antibody, with bands appearing at 30 and 50 kDa (Figure 18), were pooled and dialyzed verses 2 L PBS overnight, followed by 6 hours versus 500 mL 50% PBS, 50% glycerol. Supernatants collected from a 500 mL preparation yielded ~ 1.5 mg antibody.

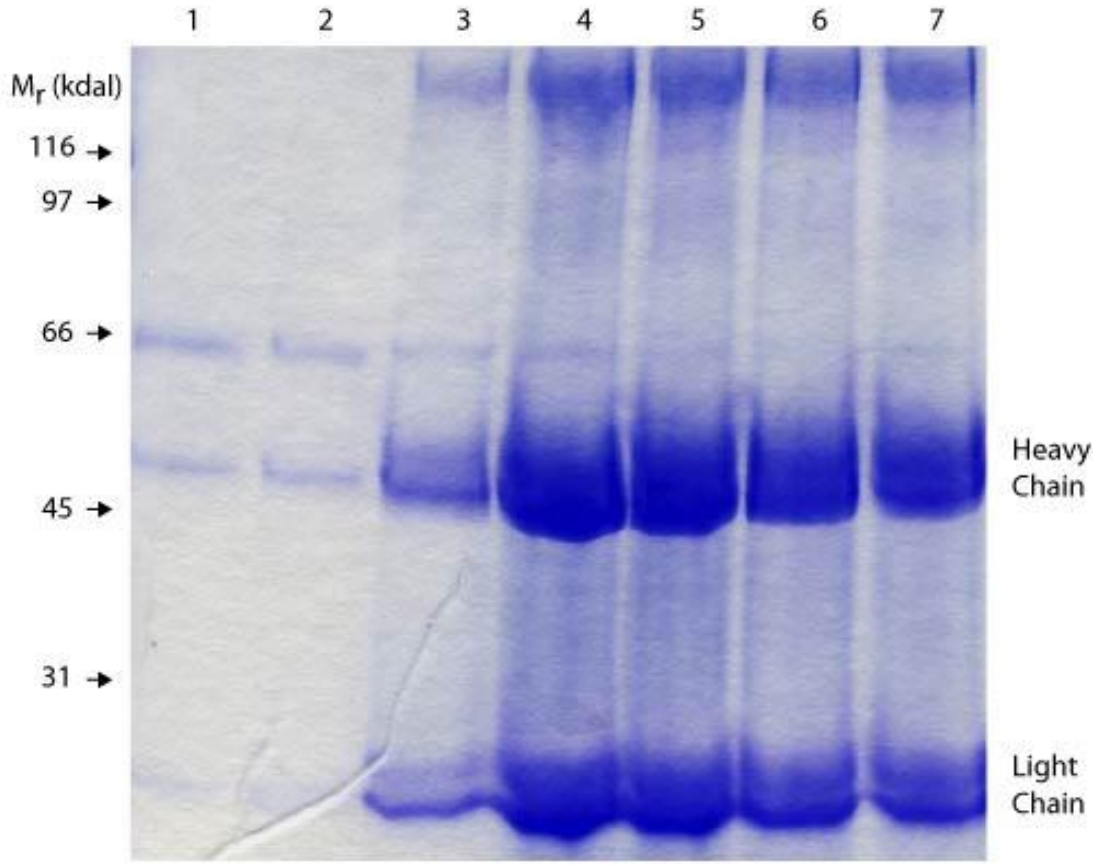

Figure 18 Purification of M2 antibody

Figure 18: A Coomassie-stained SDS-PAGE gel of the purification of M2. Lanes 1-7) Elutions of HiTrap column. Arrows specify location of molecular mass markers. The calculated molecular mass of the light and heavy chain subunits of an antibody are ~30 and 50 kDa.

2.7 Assays

2.7.1 Lipid Preparation

Lipid components were mixed in the desired ratios in chloroform and dried under a stream of nitrogen. Phospholipid vesicles containing PIP_2 were also prepared by first placing the methanol/water/chloroform solution in a 35 °C water bath for five minutes and then applying maximum vacuum in a rotovap for 30 minutes to ensure uniform inclusion of PIP_2 and PC (Gambhir, Hangyas-Mihalyne et al. 2004). This method was used to ensure that all of the chloroform was removed from the lipid samples; however, we found that LUVs formed using either of these two methods were identical, and therefore, we primarily prepared LUVs using a stream of N_2 gas.

2.7.2 Sucrose-Loaded LUVs

Large unilamellar vesicles (LUVs) with 100 nm diameter were prepared by extrusion (Hokanson and Ostap 2006). Lipids to be used in sedimentation experiments were resuspended in 176 mM sucrose, 12 mM HEPES pH 7.0, to a total concentration of 1 or 2 mM. This solution was used to increase the density of the LUVs so they would form a pellet in our sedimentation assays while maintaining the same osmolarity as our HNa100 buffer. Five cycles of rapid freeze-thaw using ethanol/dry-ice and a 37 °C water bath, followed by a one minute incubation in a bath sonicator, were applied before passing each lipid solution through a 100-nm filter (11 times) using a mini-extruder (Avanti Polar Lipids). LUVs were dialyzed overnight versus HNa100. LUVs were stored at 4°C under N_2 gas and discarded after 3 days. PS and PIP_2 percentages

reported throughout the text are the mole percentages of total PS and PIP_2 in a background of PC. Lipid concentrations are given as total lipid unless otherwise noted.

We checked that the diameter of our LUVs were uniformly 100 nm, by using dynamic light scattering (DLS) to measure the dispersion of sizes. LUVs were consistently found to be 100 nm in diameter with very little dispersion. We did find that under high divalent cation levels, such as Ca^{2+}, the dispersion of LUV sizes tended to increase as well as the average size of LUVs (Figure 19) due to a known effect of Ca^{2+} to the lipid vesicle structure (Bentz and Duzgunes 1985).

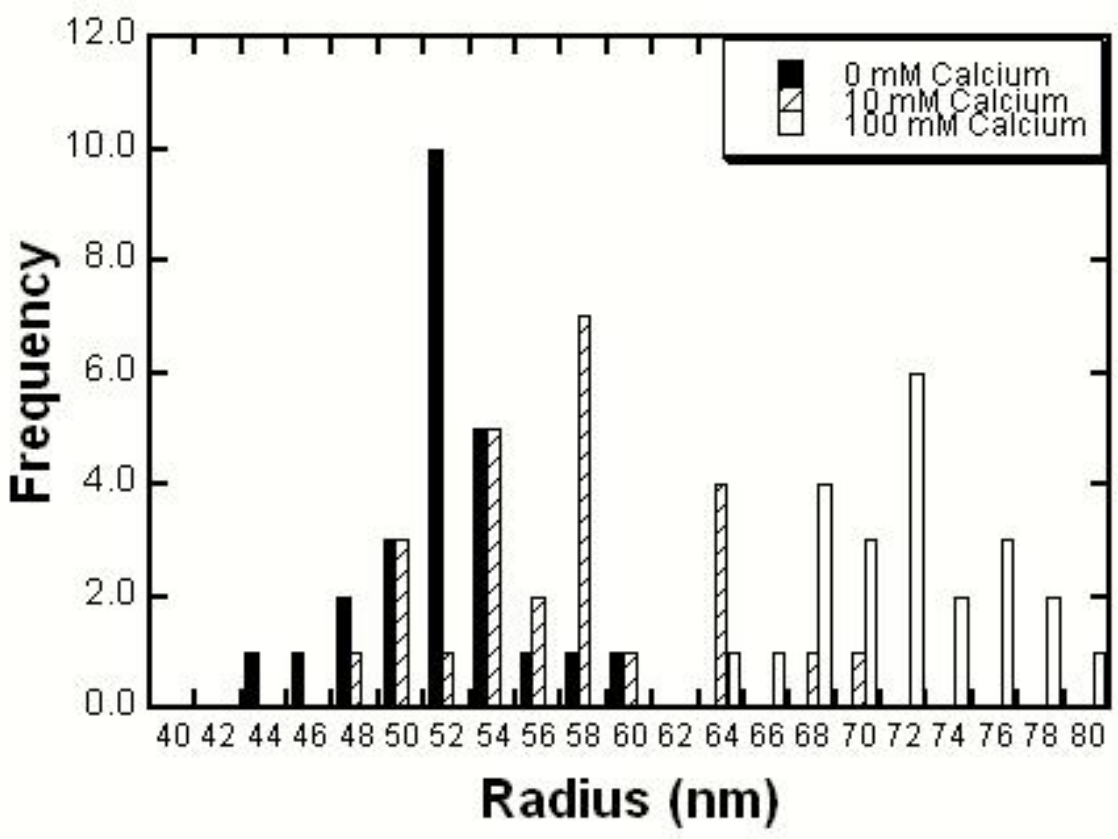

Figure 19 Ca^{2+} effect on DLS of LUVs

Figure 19: A histograph of the distribution of LUVs by DLS. Size distribution of 2% PIP_2 LUVs with 0 mM (black bars), 10 µM (hashed bars), or 100 µM Ca^{2+} (open bars) by DLS. Frequency of radii from 28 scans per each sample is shown. Note that the addition of Ca^{2+} causes the size distribution to shift to the right and become more dispersed.

2.7.3 Phosphorous Assay

To check that the concentrations of LUVs we were calculating were correct, we determined the total amount of phosphorous in a typical LUV sample following a modified procedure of Fiske & Subbarow from Avanti Polar Lipids (Fiske and Subbarow 1925). We used 0 - 0.0456 µmoles KH_2PO_4 to make phosphorous standards along with our samples of LUVs made up of various lipids. Solvent was removed with a stream of N_2 and 90 µL of 8.9 N H_2SO_4 was added to each tube. All samples were heated to 210 ºC in an aluminum heating block for 25 minutes. Tubes were removed and left to cool for 5 minutes before adding 30 µL of H_2O_2. Tubes were reheated at 210 ºC for 30 minutes, then allowed to cool to ambient temperature before adding 780 µL of H_2O. We then added 100 µL of 2.5% ammonium molybdate tetrahydrate solution and again vortexed each tube five times. We next added 100 µL of 10% ascorbic acid and vortexed each tube five times. A marble was placed over each tube to minimize evaporation and tubes were heated to 100 ºC for seven minutes. Absorbance of standards was measured at 820 nm using a UV/Visible spectrophotometer and used to generate a linear calibration curve to determine the concentration of phosphorous in each LUV sample. Predicted concentrations of LUVs were found to be accurate within 5%.

2.7.4 Sedimentation Assay

To test the binding of myo1c-tail to LUVs, we sedimented LUVs in a TLA100 rotor (Beckman), with a r_{ave} of 3.45 cm at 63,000 rpm to produce forces of 150,000 x g according to:

Equation 1

$$g_{cen} = \frac{(\omega)^2 r}{g}$$

where ω is the angular velocity in revolutions per second, r is the average radius of the rotor, and g is a gravitational constant of 980 cm/s^2.

2.7.4.1 Defining Pellet

We determined that sucrose loaded LUVs sedimented to the bottom 10% of a centrifuge tube when centrifuged at 150,000 x g after 20 minutes, but that they do not form a stable pellet. 200 µL samples of LUVs made with 5% dansyl labeled PS were centrifuged at 150,000 x g for 30 minutes. Five samples at sequential depths were carefully extracted from each centrifuge tube. We checked the samples for fluorescence at 340:500-620 nm and found that no lipid was found in the top 90% of the tube, but ~100% of the expected lipid was found in the bottom 10% (Figure 20). Following removal of the supernatant, HNa100 was added to the tubes to suspend any pellet; no florescence was found in this sample. This experiment was repeated with LUVs that did not contain dansyl labeled lipids, but were monitored by total phosphorous as described above; the results were identical. We thus define the "pellet" as the bottom

20% of the sample in a centrifuge tube after a 30 minute spin at 150,000 x g for all of our sedimentation assays.

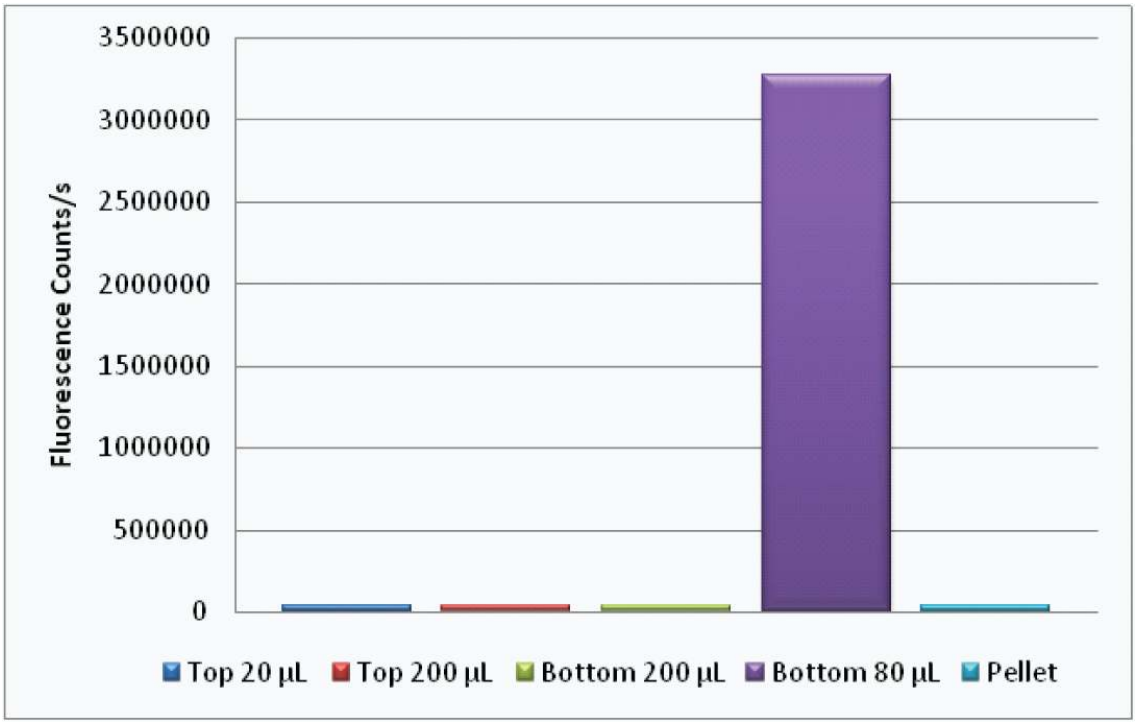

Figure 20 Sedimentation assay pellet

Figure 20: Quantification of the fluorescence of the lipid gradient of sucrose-loaded LUVs after centrifugation. A 500 µL sample of LUVs containing 5% dansyl-labeled PS was centrifuged at 150,000 x g for 30 min. Successive aliquots of the supernatant were removed and analyzed for fluorescence at 340:500-620 nm. After removal of supernatant, 40 µL HNa100 was added to centrifuge tube and analyzed as pellet.

2.7.4.2 Nonspecific Interactions

Nonspecific interactions between our protein and the walls of the polycarbonate centrifuge tubes caused a significant loss of protein, which was a concern since our experiments used protein concentrations of 40 nM to stay well below the K_d of binding. Nonspecific binding is thought to be due to the highly basic charge interaction with the acidic polycarbonate. Without protection, the myo1c-tail would practically disappear, as assessed by SDS-PAGE gel.

Two different strategies were combined to solve this problem. All tubes were coated with a bath sonicated solution of 40 μM PC hydrated in HNa100. This formed a thin film on the polycarbonate, which prevented myo1c from binding. The addition of non-specific blocking proteins to the samples was also used to help resolve this issue. Three different proteins were tested; CaM, fibrinogen, and GST (Figure 21). CaM showed no increase in recovery of myo1c from polycarbonate tubes; fibrinogen and GST both showed close to 100 % recovery. We selected GST because of its low molecular weight and availability, and added 0.25 mg/mL to all centrifugation samples.

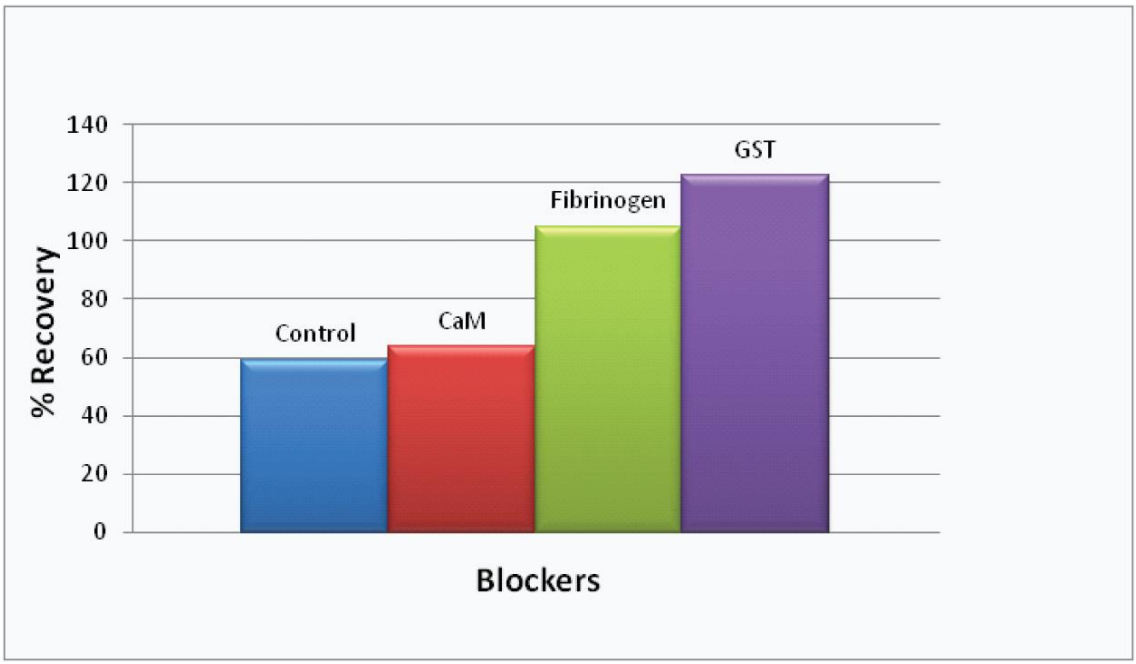

Figure 21 Nonspecific blockers

Figure 21: Quantification of the recovery of myo1c-tail after sedimentation in the presence of proteins to block nonspecific interactions to the polycarbonate tubes. CaM, Fibrinogen, or GST (5 mg/mL) were added to 40 nM myo1c-tail and centrifuged at 150,000 x g for 30 minutes. Samples were analyzed for the percentage of myo1c-tail recovered from supernatant after centrifugation.

2.7.4.3 Sedimentation

Protein binding to LUVs was determined by sedimentation assays conducted with 200 µl samples in an ultracentrifuge with a TLA-100 rotor (Beckman). Polycarbonate centrifuge tubes were incubated for an hour in 50 µM solution of PC in HNa100. GST (0.25 mg/ml) was added to every sample. Sucrose-loaded LUVs were sedimented at 150,000 x g for 30 min at 25 °C. The top 160 µL of each sample was removed and analyzed as supernatant. We called the remaining 40 µL the "pellet," although it contains approximately 20 % of the supernatant. The pellets were re-suspended with 10 µL SDS-PAGE sample buffer and boiled for three minutes. Bound proteins were resolved by SDS-PAGE and stained with SYPRO-red (Invitrogen) for quantization as described below. A sample gel with standards is shown (Figure 22). Supernatants containing GFP-proteins were assayed for GFP fluorescence in a fluorimeter. Gels were scanned using a gel scanner, and data were analyzed with MetaMorph (Universal Imaging).

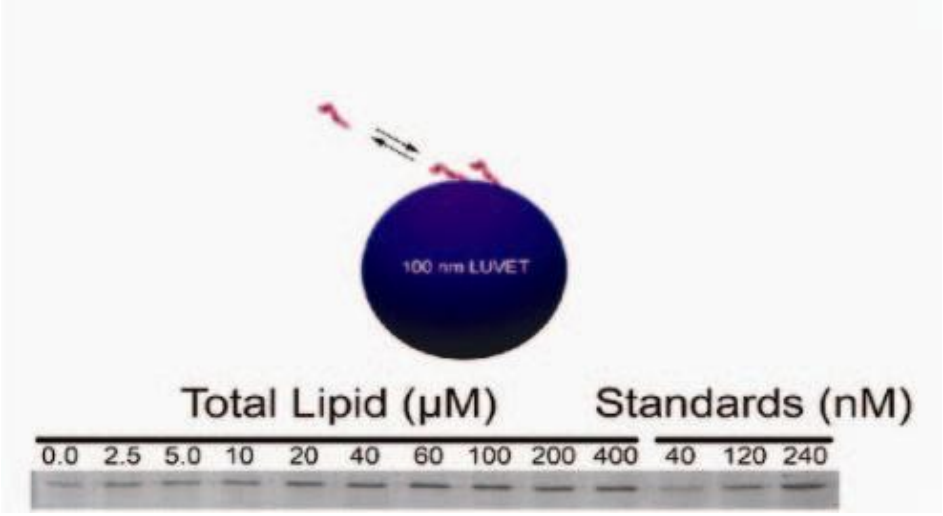

Figure 22 Sedimentation assay

Figure 22: A representative SYPRO red stained SDS-PAGE gel from a sedimentation assay. Top) Approximate scale representation of a 100 nm LUV and a full length myo1c binding. Bottom) SYPRO-red stained SDS-polyacrylamide gel of myo1c-tail from the pellets of a sedimentation assay with 0 - 400 μM LUVs (total lipid) containing 2% PIP_2. The last 3 lanes are myo1c-tail standards used for normalization. Bottom figure originally published in (Hokanson and Ostap 2006)

2.7.5 Gel Filtration

Gel filtration allows for the separation of molecules based on hydrodynamic radius. Columns are made up of beads with small pores that increase the run volume of smaller molecules, while proteins too large to fit in the pores flow by in a smaller run volume. Therefore, a column containing beads with pore sizes that are relative in size to the hydrodynamic radii of the small molecules of interest can be used to test for the direct binding of these small molecules to larger proteins. The population of small molecules bound to the larger proteins will elute much earlier than the population of free small molecules. To separate free Ins(1,4,5)P_3 from myo1c-tail bound Ins(1,4,5)P_3, we initially tried Sephadex G-25 resin, but found that the myo1c-tail bound to the resin through presumably nonspecific interactions. Therefore, we used ToyoPearl HW40F resin, which did not interact with myo1c-tail, but did retard the elution of free Ins(1,4,5)P_3.

Gel filtration assays were preformed as described (Lemmon, Ferguson et al. 1995). ToyoPearl HW40F resin (10 mL) was resuspended and packed into a 9 mm diameter column. The gel filtration column was equilibrated with 10 column volumes HNa100; protein samples of 50 µL PLCδ-PH (10 µM) or 10 µM myolc-tail mixed with 2-fold excess ^{3}H-Ins(1,4,5,)P_3 in HNa100 buffer were carefully loaded onto the top of the column bed without disturbing the resin. After the protein and Ins(1,4,5)P_3 mixture was fully immersed into the column bed, HNa100 was added to the column in 3 x 100 µL aliquots and then used to fill the column. Fractions were collected every ~200 µL starting as soon as the protein and Ins(1,4,5)P_3 mixture was loaded onto the column.

The elution position of protein was determined by absorbance at 280 nm. Scintillation counting was used to detect the ^{3}H-Ins(1,4,5)P_3 elution position by measuring the counts per minute of 50 µL of each fraction in 5 mL of scintillation fluid.

2.7.6 Digestions

Trypsin was used to do controlled digests of myo1c-tail at various concentrations and time points. Trypsin and soybean inhibitor (SI) were made up to 5 mg/mL stock solutions in HNa100. Trypsin was added in 1:100 to 1:2000 ratios by weight to myo1c-tail plus or minus Ins(1,4,5)P_3 and incubated for 0 to 40 minutes before each reaction was quenched with SI. Samples were then run on an SDS-PAGE gel and imaged by Coomassie staining or by Western blot.

2.7.7 Florescence Studies

Florescence resonance energy transfer (FRET) is a fluorescence technique that measures the fluorescence resonance energy transfer of one fluorophore, a donor, to another fluorophore, an acceptor, when the two fluorophores are in close proximity to one another (Lankiewicz, Malicka et al. 1997). LUVs containing both BODIPY FL-PIP_2 and BODIPY TMR-PIP_2 were used to detect the clustering of PIP_2 upon protein binding. These fluorescent tags were chemically attached to the acyl chains of PIP_2 and should not have affected the binding of proteins to the inositol head-group. We excited our donor, fluorescein (FL), at 495 nm, which resulted in an emission spectrum that overlapped with the excitation spectrum of our acceptor, tetramethylrhodamine (TMR).

We measured the emission of any consequently excited TMR at 575 nm. Emission and excitation spectra of the fluorophores are shown (Figure 23). When the two fluorophores are close enough to each other, the emission of the donor fluorophore is transferred to the acceptor fluorophore. A decrease in the fluorescence of the donor and an increase in the fluorescence of the acceptor were then seen as an increased number of fluorophores were clustered together. Thus, the fluorescence ratio of FL/TMR decreased when the fluorescent PIP2 molecules were clustered together by the binding of a protein (Figure 24).

LUVs with 0.4% BODIPY FL-PIP_2 and 0.4% BODIPY TMR-PIP_2 in a background of PC were titrated with 0 – 1 µM myo1c-tail or MARCKS peptide (a gift from Dr. Mark Lemmon). FRET from FL to TMR was detected by exciting FL at 500 nm and measuring TMR emission fluorescence at 575 nm.

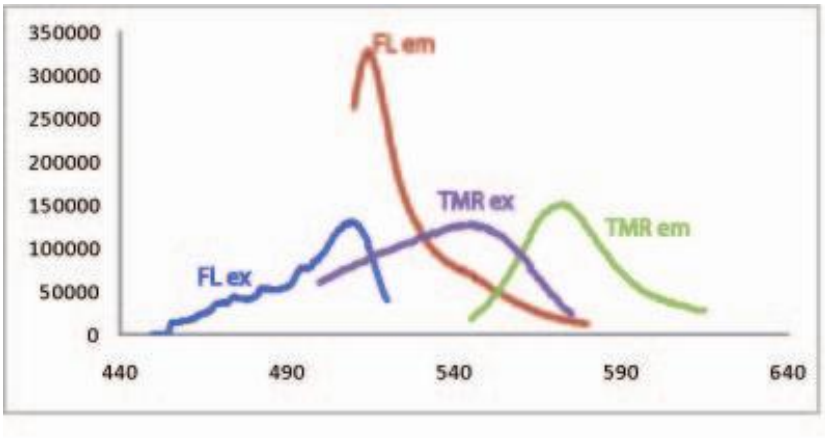

Figure 23 Excitation and emission spectra of FL and TMR

Figure 23: The fluorescence excitation and emission scans of FL and TMR labeled PIP_2. FL excites at 505 nm and emits at 513 nm. TMR excites at 532 nm and emits at 574 nm.

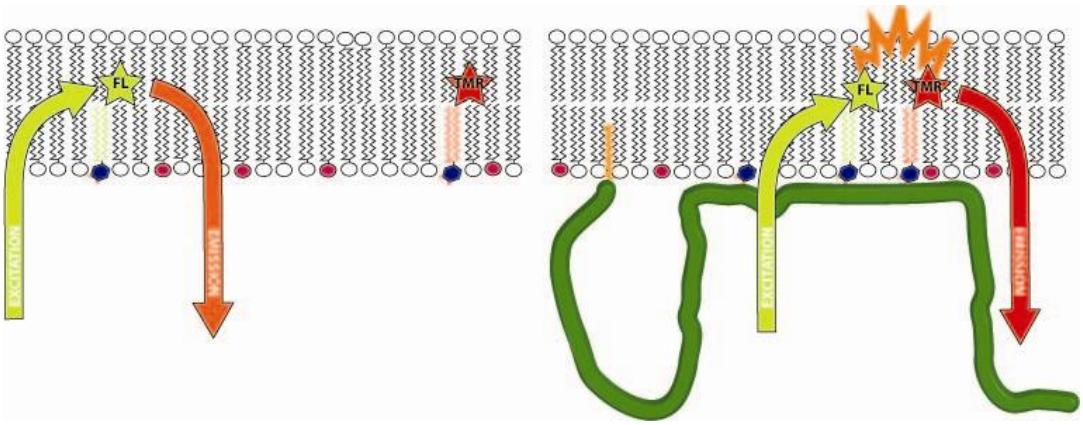

Figure 24 FRET from clustering PIP_2

Figure 24: A schematic of FRET. Upon excitation, yellow arrow, the donor molecule, FL, becomes excited and emits light, orange arrow. This emission either leaves the system (left) or is transferred to an acceptor molecule, TMR (right). The latter is the case when the two fluorophores are near each other as depicted on the right by the presence of MARCKS.

2.8 Live Cell Imaging

Cells were placed on 40-mm glass cover slips and mounted in a temperature-controlled flow chamber (Bioptechs, Butler, PA) for microscopic observation and perfused with DMEM, 10 mM HEPES, and 10% FBS (Tang and Ostap 2001). Cells were visualized through a 63x oil immersion objective with an inverted fluorescence microscope (Leica). The temperature of the flow chamber and microscope objective was maintained at 37 °C throughout the experiment. Images were acquired with a digital camera (Hamamatsu) and Metamorph software (Universal Imaging). The fluorescence excitation light was shuttered (Sutter Instruments), and exposure times were between 0.1 and 1.0 s.

2.8.1 TIRF/FRAP

TIRF is a technique designed to reduce background fluorescence of a specimen by exciting fluorophores within 100 nm of the objective (Axelrod, Thompson et al. 1983). Evanescent waves that excite fluorophores are generated when an objective with a high numerical aperture is used to bring incident light in at an angle larger than the critical angle with respect to the surface, and is totally reflected at the glass-water interface. The resulting evanescent electromagnetic field decays exponentially from the interface, and thus penetrates to a depth of approximately 100 nm into the sample medium. This technique allowed us to look at events that occurred at and directly above the plasma membrane without the background fluorescence of the entire cytosol.

2.8.1.1 TIRF

Objective-type total internal reflection fluorescence (TIRF) microscopy was performed on a modified Leica DMIRB microscope fitted with a Nikon 1.45 NA objective (Axelrod 2001). Samples were illuminated through the rear port of the microscope with a 488 nm laser beam (Melles Griot) focused on the back focal plane of the objective. Images were acquired with a digital camera (Hamamatsu) and Metamorph software (Universal Imaging). A computer controlled filter wheel (Sutter Instruments) containing neutral density filters was placed in the beam path to allow for attenuation of the beam.

2.8.1.2 FRAP

We combined TIRF with fluorescence recovery after photobleaching (FRAP) to measure dissociation rates of membrane bound myo1c. We were able to bleach either an entire cell or a ~ 10 µm spot on a cell expressing GFP-tagged constructs and measured the recovery of fluorescence over time. The recovery of fluorescence was due to new, unbleached fluorophores replacing bleached fluorophores at either the membrane, or diffusing in the cytosol just above the membrane. Since the association of myo1c to the membrane was measured to be diffusion limited (Tang, Lin et al. 2002), we were able to interpret the recovery of fluorescence as dissociation rates of bleached protein. Photobleaching by TIRF illumination was accomplished by removing the neutral density filter and decreasing the beam diameter.

TIRF/FRAP was performed as follows. Five prebleached TIRF images were acquired 5 - 10 s apart with a 100 ms acquisition time, followed by a 1 s bleaching TIRF pulse, followed by the immediate acquisition of images 1 - 2.5 s apart with 100 ms acquisition time. The bleach illumination was 10 - 100-fold more intense (depending on the cell intensity) than the imaging illumination.

2.9 Data Analysis

2.9.1 Binding Data Analysis

To quantify the amount of protein in each lane from our sedimentation binding assays, the integrated intensity of each protein band on the scanned gels was subtracted from the integrated intensity of the region directly above the protein band to correct for variations in background. Protein standards of known concentration were run on each gel to ensure that the intensity of the protein bands were within the linear range of the scanner and to translate integrated intensity to moles of bound protein (Figure 22). We reported the binding affinity of myo1c protein constructs to LUVs as a molar partition coefficient in terms of total lipid concentration (K_{eff}^{lipid}) or in terms of the accessible acidic phospholipid concentration (K_{eff}^{acidic}). The molar partition coefficient, K, is defined by:

Equation 2

$$\frac{[P]_m}{[L]} = K[P]$$

where $[P]_m$ is the molar concentration of the protein bound to the membrane, [P] is the free protein concentration, and $[L]$ is the total lipid concentration (Peitzsch and McLaughlin 1993). In our experiments $[L]$ is in 1000-fold excess to $[P]_m$ so loss of $[L]$ after binding does not need to be considered. By defining $[P]_{tot}$:

Equation 3

$$[P]_{tot} = [P]_m + [P]$$

binding curves can be fit to:

Equation 4

$$\frac{[P]_m}{[P]_{tot}} = \frac{K[L]}{1 + K[L]}$$

where K equals the concentration of lipid at which half of the protein binds and is given in M^{-1}. Binding data were fit to hyperbolae using KaleidaGraph.

All data were normalized from integrated intensities to molar concentrations by fitting internal standards of known myo1c-tail concentration from each gel to a linear line. Data was further normalized to percentage of myo1c-tail bound by:

Equation 5

$$\%Bound = \frac{[M_x] - [M_0]}{[M_t] - [M_0]}$$

where M_x is the concentration of myo1c-tail in the pellet in the presence of x lipid, M_0 is the concentration of myo1c-tail in the pellet in the absence of lipid, and M_t is the concentration of myo1c-tail calculated if 100% of it was in the pellet.

Binding data plotted as a function of [NaCl] were fit to an abbreviated equation derived from Debye-Hückel theory that describes the change in dissociation constant with ionic strength by:

Equation 6

$$logK = logK_0 - \frac{2Az_R z_L\sqrt{I}}{1 + rB\sqrt{I}}$$

where $logK$ is the log of the dissociation constant, A and B are thermodynamic constants equal to 0.509 and 2.391 nm^{-1} respectively, z_R and z_L are the charges on the receptor and ligand respectively, I is the ionic strength , and r is the effective interaction distance between receptor and ligand (Meltzer, Lurtz et al. 2006). Ionic strength is defined by:

Equation 7

$$I = \frac{1}{2}\sum_i m_i z_i^2$$

where m is the molar concentration of the ion, and z is the charge.

2.9.2 Competition Data Analysis

Soluble inositol phosphate competition data were fit to:

Equation 8

$$f_b = \frac{[PIP_2]}{K_{eff}^{acidic}\left(1 + \frac{[InsP_x)}{K_{InsP_x}}\right) + [PIP_2]}$$

where $[PIP_2]$ is the concentration of accessible PIP_2, $[InsP_x]$ is the concentration of the soluble inositol phosphate, K_{InsPx} is the affinity of the inositol phosphate for myo1c, and

K_{eff}^{acidic} is the effective dissociation constant of the myo1c-PIP_2 interaction in terms of accessible concentration of PIP_2 (Kubala, Plasek et al. 2004).

2.9.3 TIRF/FRAP Analysis

For presentational purposes, the photobleached region of each cell was normalized by dividing the image by the same region acquired 20 – 30 s before the bleach pulse, and then multiplied by 1000 to allow visualization of a 12-bit image. This normalization allows the fluorescence recovery to be visualized without the complication of cell intensity variation.

For analysis, the average background intensity was subtracted from the image, and the integrated intensity of the bleached spot was normalized by dividing by the intensity before the bleach. Thus, the intensity of the spot before the bleach is set to one, and absence of fluorescence is set to zero. After the bleaching pulse, the illumination required for visualization of the recovery time-course resulted in further photobleaching (< 15%) in some cells. This non-FRAP bleaching was corrected for by subtracting the rate of photobleaching as determined in an area away from the FRAP region. The effective rate of fluorescence recovery was determined by fitting the recovery transient to the sum of two exponential rates using KaleidaGraph (Synergy Software).

2.10 Molecular Modeling and Structure Prediction

2.10.1 Phyre Protein Fold Recognition Server

We used the Phyre server (www.sbg.bio.ic.ac.uk/phyre/) to initially reveal the secondary structural similarities of the tail domain to a PH domain. The Phyre server predicts the three-dimensional structure of a protein sequence by "threading" it through known structures and scoring it for compatibility (Kelley, MacCallum et al. 2000). To identify potential structural homologs, we performed a BLAST search on the myo1c-tail sequence, identifying phosphatidylinositol-dependent protein kinase-1 (PDK1) as a limited sequence match. Since PH domain of Pdk1 had been crystallized with Ins(1,3,4,5)P_4 (PDB 1W1D) and our myo1c-tail sequence showed 61% identity over the PIP_2 binding region of PDK1, we used this structure for a detailed structural comparison.

2.10.2 *Ab Initio* Structural Prediction

To provide further speculative structural insight into the binding of PIP_2 by the myo1c- tail, we collaborated with Dr. Dave Sept (Washington University, St. Louis, MO) who ran the mouse myo1c sequence through Pfam to identify known domains (Bateman, Coin et al. 2004). Based on the Pfam analysis, he selected a region following the IQ motif as the tail region (P802-R1028) and used this sequence in *ab initio* structure prediction with Rosetta (Bonneau, Strauss et al. 2002), generating a total of 50 structures. Clustering the structural predictions based on root mean square deviation resulted in a top structural candidate, and the side-chains of this structure were

added in and minimized using PLOP (Jacobson, Pincus et al. 2004). This completed structure was then simulated using molecular dynamics in Gromacs 3.3 (Lindahl 2001). The simulation used the OPLS/AA force field, TIP3P water, and periodic boundary conditions with Particle Mesh Ewald for long range electrostatics. After heating the system in 50K steps and equilibrating for 1 ns, the structure was simulated for a total of 20 ns at 300K. There were some minimal structural rearrangements during the simulation, but the basic structure of the protein remained constant throughout the simulation. Finally, to identify potential structural homologs, we performed a BLAST search on the myo1c-tail sequence, identifying phosphatidylinositol-dependent protein kinase-1 (PDK) as a limited sequence match. Since PDK1 had been crystallized with Ins(1,3,4,5)P_4 (PDB 1W1D) and our myo1c tail sequence showed 61% identity over the PIP_2 binding region of PDK1, we used this structure for a detailed structural comparison.

3 Results

In this section, data will be presented from an investigation into the interactions of myo1c with the lipid membrane. In this study, sedimentation assays were used to characterize the binding constants of myo1c for LUVs composed of various ratios of PS and PIP_2, as well as inositol phosphates. Constructs defined in chapter two were expressed in NRK cells to determine localization and *in vivo* activity. These results reveal that myo1c binds tightly to PIP_2 through a specific interaction in its tail domain.

3.1 Mechanism for Membrane Binding

To understand biochemically how myosin-Is interacted with the plasma membrane, we obtained steady state binding constants by performing a quantitative investigation under different parameters. Sedimentation assays using LUVs were used as the primary experiment for quantitatively determining the interactions between myo1c and phospholipids. This was an ideal system to use because it allowed us to do *in vitro* experiments with a fluid bilayer system that mimicked the phospholipid bilayer of the inner leaflet in the plasma membrane (Buser and McLaughlin 1998). Through extrusion techniques, we were able to precisely control the radii of our LUVs to 50 nm, as verified by DLS. This gave us a uniform binding substrate to work with, as well as accurate control over the molar ratios of various lipid contained within the vesicles. All sedimentation assays were performed using LUVs with PC as the background phospholipid.

3.1.1 Myo1c-Tail Binds LUVs Containing High Levels of PS

To determine if myo1c bound to lipid membranes containing PS, we tested the binding of a myo1c construct containing the 3 IQ motifs and tail domain (myo1c-tail) (Figure 11) to LUVs composed of 20% PS, 40% PS, 60% PS, and 80% PS in a PC background using our sedimentation assay as illustrated (Figure 25A). Myo1c-tail, 40 nM, was sedimented in the presence of 0 – 400 μM LUVs. The pellets were run on an SDS-PAGE gel and analyzed for the amount of myo1c-tail present. We plotted the percentage of myo1c-tail bound as a function of lipid concentration to determine the effective dissociation constants using Equation 4 and Equation 5, which were expressed in terms of total lipid (K_{eff}^{lipid}) or accessible acidic phospholipid (K_{eff}^{acidic}), for the interaction between myo1c-tail and LUVs containing varying amounts of PS in a background of PC. We used a low concentration of myo1c-tail (40 nM) to ensure that we stayed below the effective dissociation constant of myo1c : lipid.

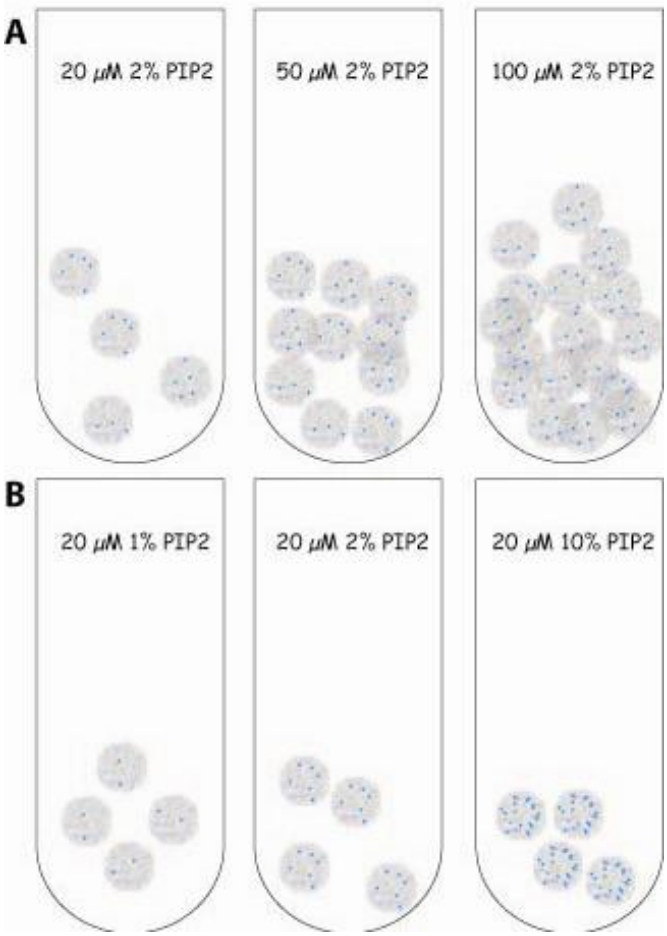

Figure 25 Total lipid *vs.*mol % binding assay

Figure 25A-B: A representation of the centrifuge tubes in the sedimentation assays. Shown is a comparison between an increase in concentration and an increase in mol %. A) An increase in the concentration increases the number of LUVs, but keeps the density of PIP_2 (blue dots) constant. B) An increase in mole % increases the density of PIP_2 within the LUVs, but keeps the number of LUVs constant.

We were unable to detect binding of myo1c-tail to LUVs containing only PC, or to LUVs containing physiological molar concentrations of PS ~20% (Figure 26). Myo1c-tail only bound to PS containing LUVs when the molar concentration of PS was increased to 60% or higher. At these high, non-physiological concentrations of PS, myo1c-tail bound with K_{eff}^{lipid} = 11 ± 2.0 μM (K_{eff}^{acidic} = 3.2 ± 1.0 μM) to 60% PS LUVs, and with K_{eff}^{lipid} = 4.1 ± 0.70 μM (K_{eff}^{acidic} of 1.7 ± 0.060 μM) to 80% PS LUVs (Table 1). These data confirmed previous studies showing that myosin-I bound to anionic lipids (Adams and Pollard 1989; Hayden, Wolenski et al. 1990), and that its binding was dependent on the molar concentration of PS (Tang, Lin et al. 2002); however, it also showed that the association could not solely be based on non-specific electrostatic interactions, as physiological levels of PS do not support binding. Therefore, we hypothesized that for myo1c to bind to the membrane, additional factors must be required.

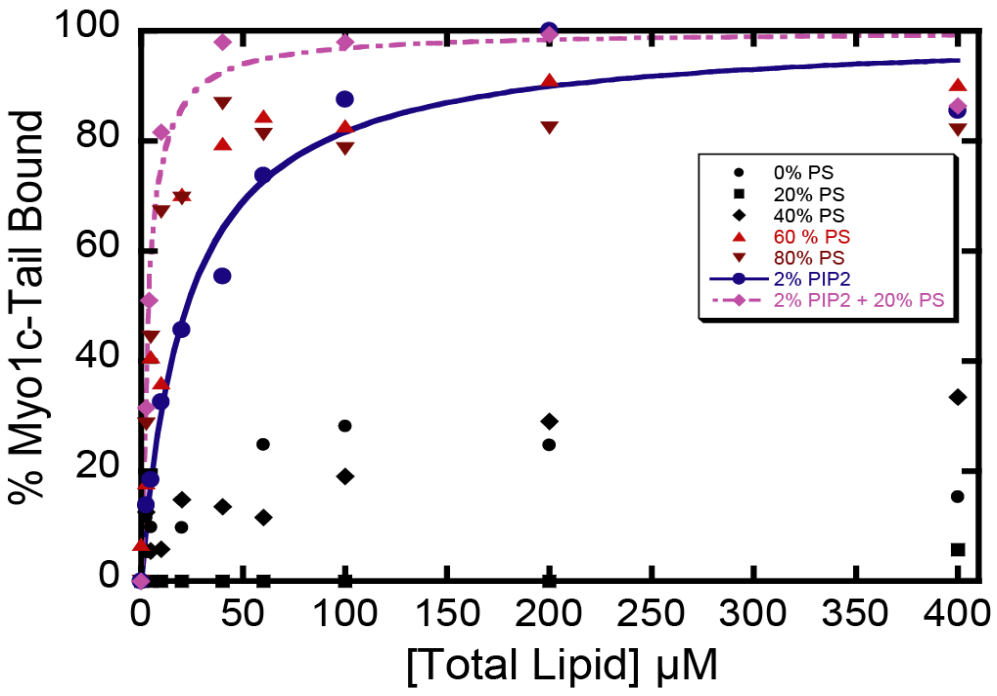

Figure 26 Sedimentation assays

Figure 26: The association of the myo1c-tail with LUVs. Lipid concentration dependence of 40 nM myo1c-tail binding to LUVs composed of PC and (●) 0% PS, (■) 20% PS, (◆) 40% PS, (▲) 60% PS, (▼) 80% PS, (●) 2% PIP_2, and (◆)20% PS + 2% PIP_2. Each point is the average of 2-6 measurements. The solid and dashed curves are the best fits of the 2% PIP_2 and 20% PS + 2% PIP_2 data to equation 2.4, respectively. The K_{eff} of each data set is listed Table 1.

Table 1 Effective dissociation constants for myo1c-tail binding to LUVs. [a]

LUV composition	K_{eff}^{lipid} (μM)[c]	K_{eff}^{acidic} (μM)[d]
0% PS	> 400	N.A.
20% PS	> 400	> 40
40% PS	> 400	> 80
60% PS	11 ± 2.0	3.2 ± 1.0
80% PS	4.1 ± 0.70	1.7 ± 0.060
2% PIP_2	23 ± 5.0	0.23 ± 0.050
2% PIP_2 + 20% PS	± 1.5	0.44 ± 0.17

[a]10 mM HEPES, pH 7.0, 100 mM NaCl, 1 mM EGTA, 1 mM DTT, 1 μM CaM

[b]The mole percentages PS and PIP_2 are reported with the remainder composed of PC.

[c]Effective dissociation constants expressed in terms of total phospholipid. Errors are standard errors of the fit.

[d]Effective dissociation constants expressed in terms of accessible acidic phospholipid. Errors are standard errors of the fit.

3.1.2 Myo1c-Tail Binds LUVs Containing Low Levels of PIP_2

We next studied binding interactions between myo1c and LUVs containing a highly regulated and essential signaling phospholipid, PIP_2, using our sedimentation assay. Although the physiological concentrations of PIP_2 in the inner membrane are only 1 - 2 % (as compared to 20 - 30% for PS) (Verkleij, Zwaal et al. 1973), it has three to four times the effective negative charge as PS and has been shown to bind specifically to many membrane associated proteins (DiNitto, Cronin et al. 2003). Myo1c-tail, 40 nM, was sedimented in the presence of 0 – 400 μM 2% PIP_2 LUVs. Myo1c-tail bound to 2% PIP_2 LUVs in a PC background with K_{eff}^{lipid} = 23 ± 50 μM (K_{eff}^{acidic} = 0.23 ± 0.050 μM) (Figure 26, Table 1). These data confirmed that the interaction between myo1c and the plasma membrane could not be entirely electrostatic, as myo1c bound tightly to LUVs composed of 2% PIP_2 and not to LUVs comprised of 40% PS, which contained five to seven times the effective charge. Myo1c-tail clearly showed a binding specificity to LUVs containing PIP_2 over those containing PS.

We determined the affinity of myo1c-tail for 2% PIP_2 + 20% PS LUVs to be K_{eff}^{lipid} = 4.0 ± 1.5 μM (K_{eff}^{acidic} = 0.44 ± 0.17 μM) (Figure 26, Table 1). While the affinity for accessible lipid was two-fold lower, the affinity for total lipid (which is more relevant to membrane binding) was roughly six times greater than to LUVs of just 2% PIP_2 alone. Therefore, although myo1c-tail did not bind to 20% PS alone, PS appeared to demonstrate an additive effect when in the presence of 2% PIP_2.

3.1.3 Myo1c Membrane Binding is Salt Sensitive

To test if the binding of myo1c-tail to LUVs composed of PS or PIP_2 has an electrostatic component, we measured the binding as a function of the amount of NaCl in solution. Binding data were fit to Equation 6, an abbreviated equation derived from Debye-Hückel theory (Meltzer, Lurtz et al. 2006) that relates the change of dissociation constants to the changes of ionic strength.

Myo1c-tail, 40 nM, and 60 μM LUVs were sedimented in the presence of 0 – 1 M NaCl. We found that the interaction of myo1c-tail to 2% PIP_2 LUVs had a slightly higher dependence on the ionic strength of the solution than with 60% PS LUVs (Figure 27A). A fit of the data to Equation 6 yielded net charges of -4.7 and -1.6 with interaction distances of 0.43 and 0.12 nm for 60% PS and 2% PIP_2 respectively (Figure 27B). Considering that PIP_2 has a net charge of -4 at pH 7.0, if we assumed 1:1 binding between myo1c and PIP_2, the effective charge for the region of myo1c-tail that interacts with PIP_2 would be 0.39, while the region that interacts with PS, charge of -1, would be 4.7. This implied that if the same region of myo1c-tail interacts with both PIP_2 and PS, up to 12 molecules of PS could be required for tight binding.

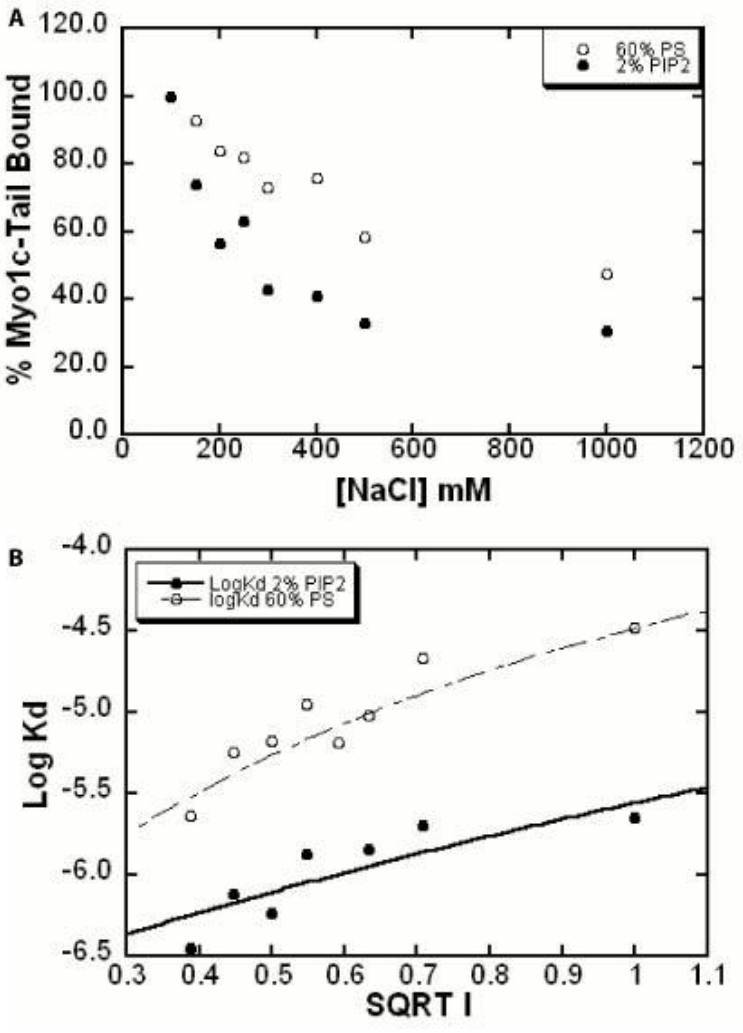

Figure 27A-B: The effect of ionic strength on myo1c-tail binding to LUVs. A) Dissociation of 40 nM myo1c-tail from 60 μM 60% PS (❍) or 2% PIP_2 (●) LUVs as a dependence of NaCl concentration. B) The same data plotted as the log of the K_d as a function of the square-root of the ionic strength. The solid and dashed curves are the best fits of the 2% PIP_2 and 60% PS data to Equation 6, respectively.

Figure 27 Salt dependence and Debye Hückel

3.1.4 Myo1c Does Not Cluster PIP_2

Some PIP_2 binding proteins, such as MARCKS, have been shown to cluster multiple PIP_2 molecules within close proximity to increase the density of anionic charges (Gambhir, Hangyas-Mihalyne et al. 2004). We used FRET to determine if myo1c was able to cluster PIP_2 labeled at the ends of one of its acyl chains with a donor fluorophore, FL, and PIP_2 labeled at the ends of one of its acyl chains with an acceptor fluorophore, TMR, on LUVs.

We measured the steady state fluorescence signal from FRET for both 0 – 5 μM MARCKS peptide and 0 – 10 μM myo1c-tail bound to 200 or 250 μM LUVs containing 0.8% of fluorescently labeled PIP_2 and plotted the ratios of TMR/FL emission spectra as a function or protein concentration. We observed no change in the FRET ratio with the addition of up to 1 μM myo1c-tail (Figure 28A), but saw a significant decrease in the FRET ratio with the addition of MARCKS peptide that appeared to saturate at around 10 μM (Figure 28B). This was due to a significant decrease in emission of FL at 514.5 nm, but little increase in the emission of TMR at 572.5 nm (Figure 28C). As a control, we confirmed that myo1c-tail was able to bind to LUVs containing 0.8% fluorescently labeled PIP_2 by using our standard binding assay. Although we did not observe a true FRET signal between our fluorescently labeled PIP_2 with the addition of MARCKS, the decrease of TMR fluorscence suggests that MARCKS affected the lateral distribution of PIP_2 in LUVs, whereas myo1c-tail did not.

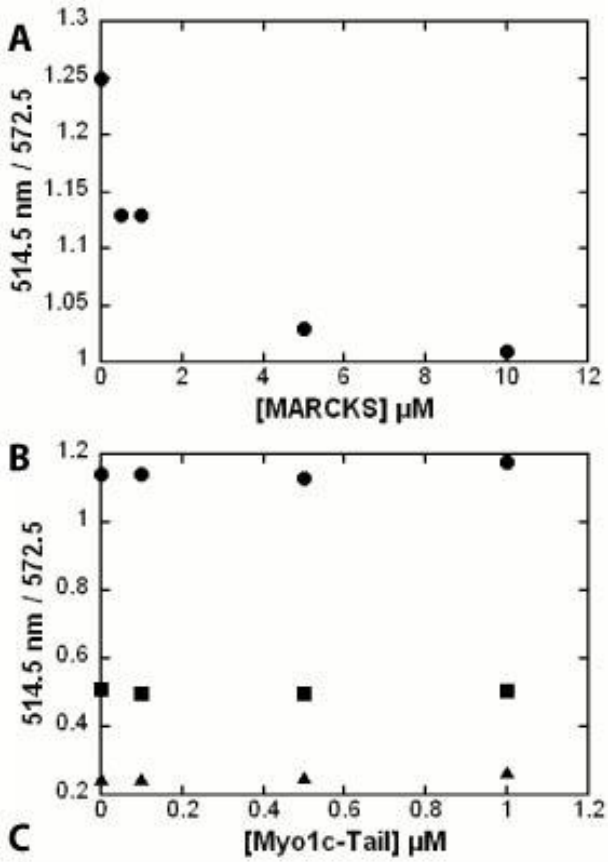

Figure 28A-C: FRET ratios from PIP_2 clustering. LUVs containing 0.5% (●), 0.8% (■), or 1.2% (▲) FL and TMR labeled PIP_2 were incubated with increasing concentrations of A) myo1c-tail, or B) MARCKS peptide. The ratio of TMR fluorescence measured at 514.5 nm over FL fluorescence measured at 572.5 nm is plotted as a function of protein. C) Raw fluorescence spectra of FL and TMR emissions with increasing concentrations of MARCKS.

Figure 28 Myo1c and MARCKS FRET

3.1.5 Cooperative Binding of PIP_2

Membrane association of certain PIP_2 binding proteins, *e.g.* MARCKS (McLaughlin, Wang et al. 2002) and N-WASP (Papayannopoulos, Co et al. 2005), requires cooperative binding. A minimum negative density threshold must exist before binding occurs, which results in a sigmoidal binding curve (Figure 29A). This is in contrast to proteins that bind to PIP_2 directly and do not require multiple PIP_2 molecules to bind. Examples of this are PPB PH domain containing proteins, which have a hyperbolic binding curve (Figure 29B).

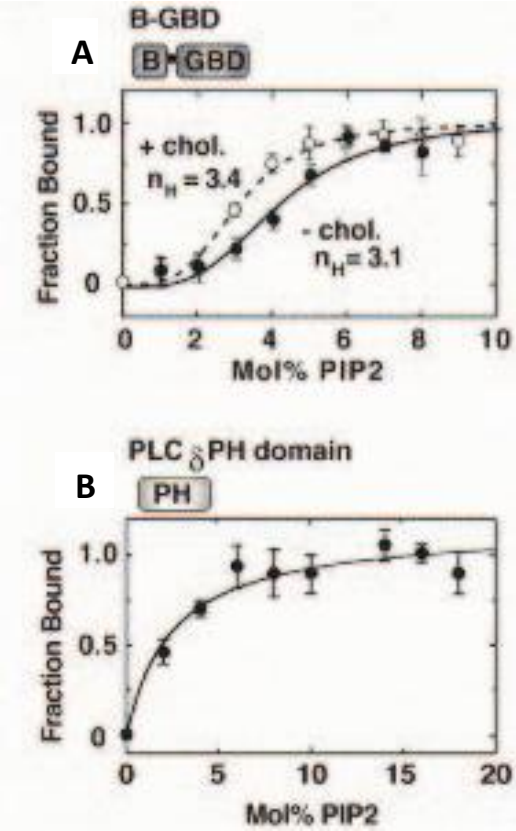

Figure 29A-B: Figures are taken from (Papayannopoulos, Co et al. 2005). Binding isotherms for A) N-WASP, and B) PLCδ-PH were measured with a fluorescence perturbation assay from. A) Cooperative binding requiring a minimal density of PIP_2 before binding occurs. Note the lag phase from 0 – 2 Mol% PIP_2. B) Direct binding to the head group of PIP_2 does not require a minimum density of PIP_2.

Figure 29 Cooperative binding curves

To determine if myo1c bound PIP_2 in a cooperative manner, we measured 40 nM myo1c-tail binding to increasing molar concentrations of PIP_2 while maintaining the same total lipid concentration at either 30 or 60 μM (Figure 25B). The resulting binding curve of myo1c-tail bound as a function of increasing molar concentrations of PIP_2 had a hyperbolic dependence (Figure 30), signifying that the binding was not cooperative; if binding was cooperative, then we would have expected to see a sigmoidal binding curve with a lag-phase at low molar concentrations of PIP_2. Moreover, when we plotted the percentage of myo1c-tail bound from our previous 2% PIP_2 binding experiments at varying lipid concentrations as a function of the concentration of accessible PIP_2 (Figure 30 *inset*), we found the concentration dependence of binding to be nearly identical. This mode of binding supported our previous conclusions from our stoichiometric data, suggesting that the binding ratio of myo1c to PIP_2 is 1:1.

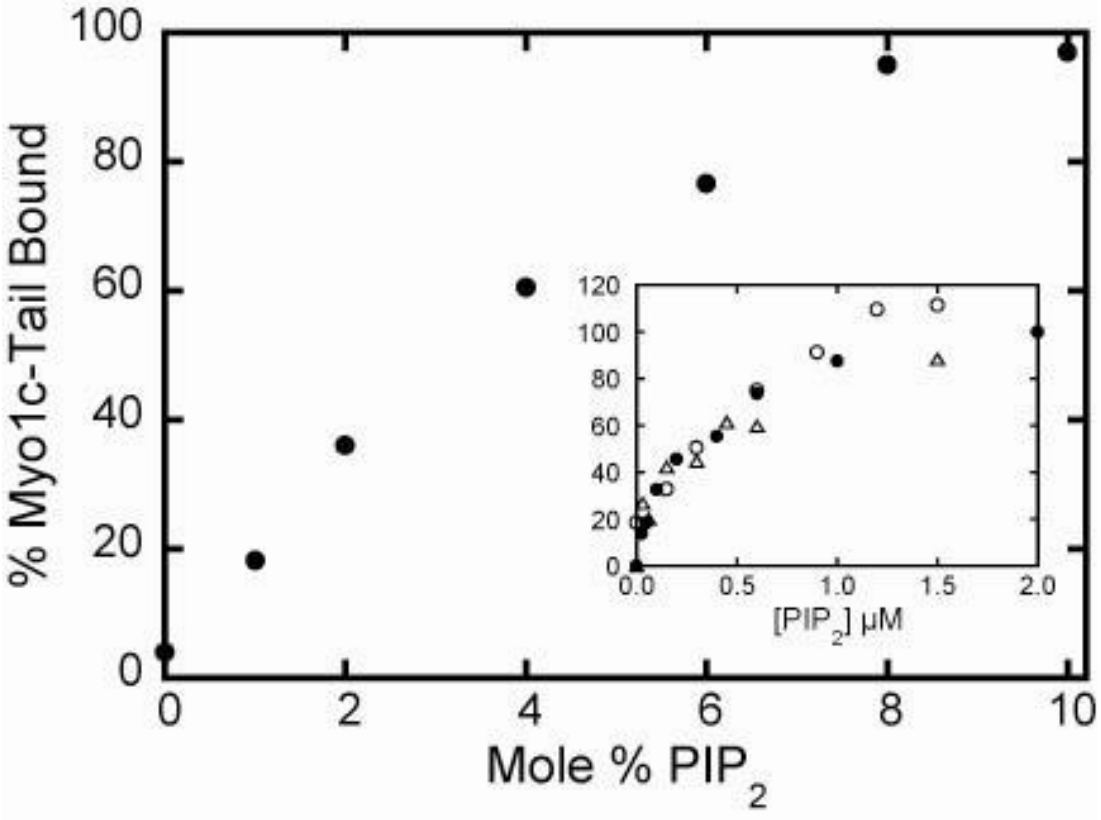

Figure 30 Myo1c binding as a function of mol% PIP_2

Figure 30: Figure was originally published in (Hokanson and Ostap 2006). Binding of 40 nM myo1c-tail to 30 µM LUVs (total lipid) composed of 0 – 10% PIP_2. The percent of membrane-bound myo1c-tail is plotted as a function of the percentage of PIP_2 in the LUVs, rather than total lipid concentration. Each point is the average of three measurements. (*Inset*) The same data plotted as a function of the accessible PIP_2 concentration (○). Data in the inset also include the percent of 40 nM myo1c-tail bound to (△) 60 µM LUVs containing 0 - 5% PIP_2 and (●) 0 – 400 µM LUVs containing 2% PIP_2 from Figure 22.

3.1.6 Calcium and CaM Myo1c-Tail Binding 2% PIP_2 LUVs

It had been proposed that the lipid binding site of myo1c was located in the regulatory domain and not in the tail domain (Swanljung-Collins and Collins 1992; Tang, Lin et al. 2002; Hirono, Denis et al. 2004). This model suggested that lipid binding required Ca^{2+}-dependent conformational changes in one or more CaM bound to the three IQ motifs in the regulatory domain. This conformational change or dissociation of CaM from an IQ motif was proposed to have the potential to expose basic polypeptide stretches that might be responsible for binding to anionic lipids (Figure 31). In order to test this model, we measured the effects of both Ca^{2+} and CaM on the steady-state binding of myo1c-tail to LUVs composed of 2% PIP_2 or 20% PS.

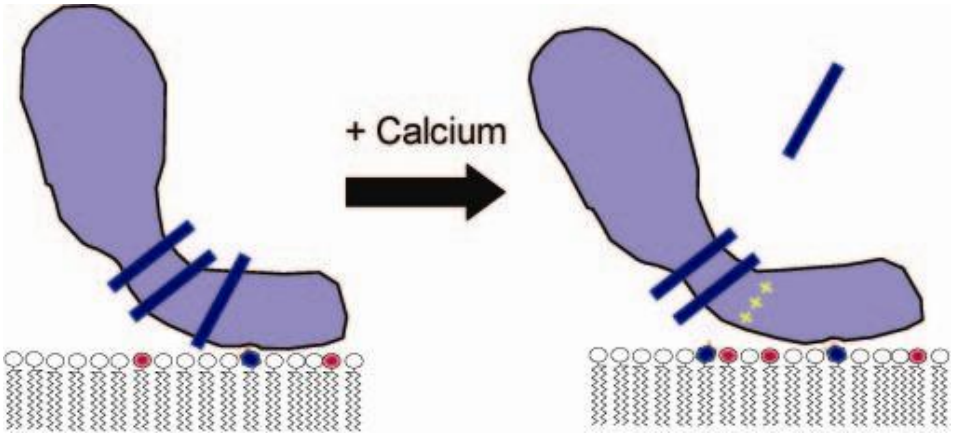

Figure 31 Ca^{2+} regulation of CaM reveals lipid binding site

Figure 31: A cartoon showing a proposed effect of Ca^{2+} revealing a lipid binding site. High levels of Ca^{2+} change the conformation and cause at least one bound CaM (blue bars) to dissociate. This reveals a basically charged IQ motif which could interact with acidic lipids shown in red.

Myo1c-tail, 40 nM, was sedimented in the presence of 0 – 200 µM LUVs with or without 10 µM free Ca^{2+}, or 40 nM myo1c-tail was sedimented with 60 µM LUVs in the presence of 0 – 100 µM CaM. We determined that the interaction of myo1c-tail and LUVs was neither inhibited by the addition of up to 100 µM CaM (Figure 32A), nor was there a significant increase in affinity in the presence of 10 µM free Ca^{2+} (Figure 32B). We concluded that the binding of myo1c-tail to 2% PIP2 LUVs was not affected by an increase in Ca^{2+} levels and was not dependent on the conformational changes of CaM bound to the IQ motifs.

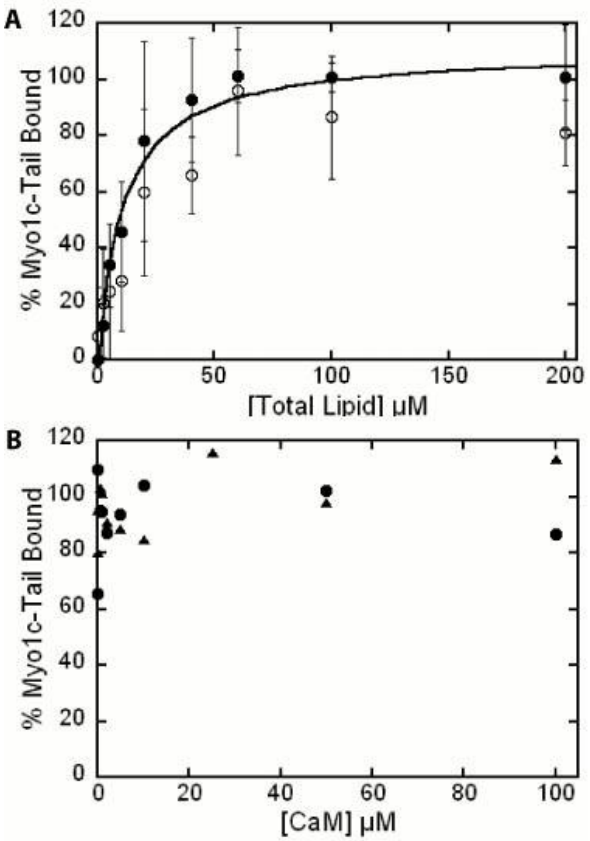

Figure 32A-B: Figures were originally published in (Hokanson and Ostap 2006). (*A*) 40 nM myo1c-tail binding to 60 µM LUVs containing (●) 2% PIP_2 or (▲) 60% PS LUVs in the presence of 0-100 µM calmodulin. Each point is the average of two measurements. (*B*) 40 nM myo1c-tail binding to 0 - 400 µM LUVs containing 2% PIP_2 in the (●) absence and (○) presence of 10 µM free calcium. The solid line is the best fit to a rectangular hyperbola. Error bars represent ± 1 standard deviation (n = 4-6).

Figure 32 CaM and Ca^{2+} dependence of myo1c-tail binding to PIP_2

3.1.7 Regulatory Domain Binds to PS with a Calcium Dependence

To further test if there were any contributions from the regulatory domain of myo1c for lipid binding, we ascertained the affinity of a myo1c construct containing the motor domain followed by the 3 IQ motifs (myo1c-motor) (Figure 11) for LUVs. This construct was designed to lack the tail domain so that the only possible lipid binding site would be the motor or regulatory domains. We tested the binding of 40 nM myo1c-motor to 0 – 200 μM LUVs composed of 20% PS, 40% PS, 60% PS, 80% PS, 2% PIP_2, and both 20% PS + 2% PIP_2 all in a PC background, in the absence and presence of 10 μM free Ca^{2+} using our sedimentation assays (Figure 33). In the absence of Ca^{2+}, myo1c-motor bound weakly to 40% PS LUVs (99 ± 24 μM), whereas 60% PS and 80% PS LUVs bound with affinities of 37 ± 5.6 μM and 23 ± 3.3 μM respectively (Table 2). In the presence of 10 μM free Ca^{2+}, the affinity of myo1c-motor for ≥ 40% PS LUVs increased ~10-fold to as high as 0.42 ± 0.27 μM for 80% PS LUVs; this was consistent with the proposal that positive charges in the IQ motif were revealed upon Ca^{2+}-induced dissociation of CaM.

Physiological levels of PS in biological membranes are ~ 20% - 30% PS, so it is unlikely that myo1c binding to high PS concentrations is physiologically relevant. However, it is possible that additional factors in the cell could cause PS to cluster and form micro-domains (Murray, Arbuzova et al. 1999). Given that our data showed a six-fold increase in affinity of myo1c-tail for 20% PS + 2% PIP_2 LUVs over that of 2% PIP_2 LUVs (Table 3.1), it was more likely that low concentrations of PS contributed to the binding energy when myo1c was attached to the membrane via

phosphatidylinositols. Therefore, we concluded that it was the tail domain of myo1c that was responsible for localization and binding to the membrane. Although the regulatory domain may have stabilized this interaction in a Ca^{2+} regulated manner once myo1c was already bound to the membrane through PIP_2, it was not sufficient for membrane binding alone.

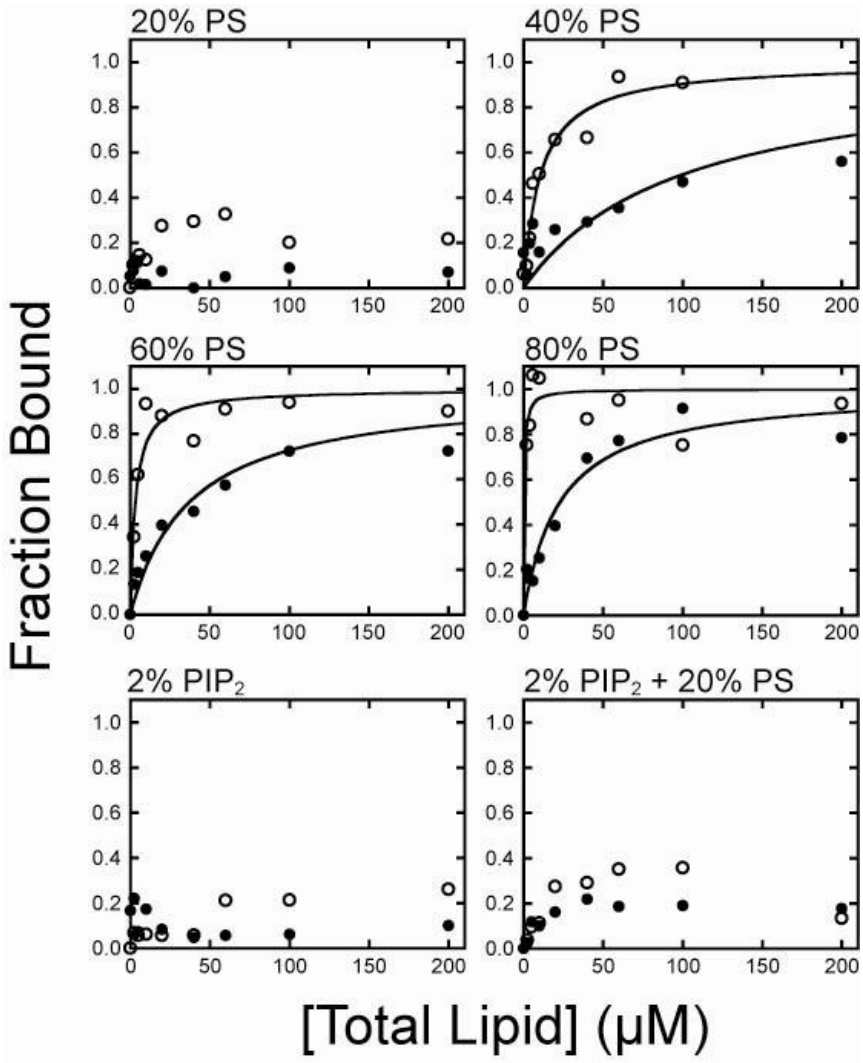

Figure 33 Myo1c-motor binding is Ca^{2+} dependent

Figure 33: Figure was originally published in (Hokanson, Laakso et al. 2006). Lipid concentration dependence of 40 nM myo1c-motor binding to LUVs composed of PC and 20% PS, 40% PS, 60% PS, 80% PS, 2% PIP_2, and 20% PS + 2% PIP_2 in the (●) absence and (○) presence of 10 μM free calcium. Each point is the average of 2 - 6 measurements. The solid and dashed curves are the best fits of the data to hyperbolae. The K_{eff}^{lipid} of each data set is listed in Table 2.

Table 2 Effective dissociation constants for myo1c-motor binding to LUVs. [a]

LUV Composition[b]	K_{eff}^{lipid} (μM)[c]	K_{eff}^{lipid} (μM)[c]
	- Ca^{2+}	+ Ca^{2+}
20% PS	> 400	> 400
40% PS	99 ± 24	11 ± 1.5
60% PS	37 ± 5.6	3.2 ± 0.83
80% PS	23 ± 3.3	0.42 ± 0.27
2% PIP_2	> 400	> 400
2% PIP_2 + 20% PS	> 400	> 400

[a] 10 mM HEPES, pH 7.0, 100 mM NaCl, 1 mM EGTA, 1 mM DTT, 1 μM CaM

[b] The mole percentages PS and PIP_2 are reported with the remaining lipid composed of PC.

[c] Effective dissociation constants expressed in terms of total phospholipid. Errors are standard errors of the fit.

3.2 Inositol Phosphate Binding and Inhibition Studies

In cells, many phosphatidyl inositols are hydrolyzed to form DAG and a soluble inositol phosphate by phospholipases (Figure 7). It was important for us to determine if myo1c was able to bind to the soluble head groups of phosphatidyl inositols. Polybasic proteins, e.g. MARCKS and N-WASP, are unable to bind soluble phosphatidyl inositol derivatives because they are not accessible in a multivalent manner like PIP_2 in the membrane (Papayannopoulos, Co et al. 2005). Phosphatidyl inositol binding proteins that have a specific interaction with the inositol head group bind to the phosphorylated inositol ring directly through an electrostatic association with the charged phosphates. The most studied is PLCδ-PH, which binds to $Ins(1,4,5)P_3$ as well as PIP_2 (Lemmon, Ferguson et al. 1995). Determining whether myo1c bound directly to the inositol ring would give insight into the mechanism of binding.

A secondary reason for determining if myo1c directly bound to inositol phosphates was the ability to test for inositol phosphorylation stereospecificity. Many relevant phosphatidylinositols were not available from biochemistry reagent suppliers, and those that were did not easily go into solution and/or did not contain long acyl chains that would ensure their incorporation into LUVs. A variety of soluble inositol phosphates were readily available from biochemistry reagent suppliers.

By using competitive inhibition binding studies, we were able to measure the K_d of myo1c-tail for a variety of inositol phosphates. We assumed that the myo1c-tail binds PIP_2 with a 1:1 stoichiometry and that myo1c-tail has an affinity of $K_{eff}^{acidic} = 0.23$

μM for PIP_2. Data was fit to Equation 8 to calculate binding affinities of inositol phosphates that bound to the PIP_2 binding site of myo1c-tail and displaced it from the LUVs. This fit also enabled us to determine the affinity for PIP_2 of proteins that displaced myo1c-tail from the LUVs by binding to PIP_2.

3.2.1 Myo1c and PLCδ-PH Domain Compete for PIP_2 Binding

To determine if myo1c-tail bound to the same site on PIP_2 as the canonical PIP_2 binding protein, PLCδ-PH, we tested if PLCδ-PH could competitively bind PIP_2 containing LUVs in the presence of myo1c-tail. Myo1c-tail, 100 nM, was sedimented in the presence of 60 μM 2% PIP_2 LUVs and 0-10 μM PLCδ-PH (Figure 34). We found that PLCδ-PH was able to effectively displace the myo1c-tail from the LUVs in a dose dependent manner. We calculated an effective dissociation constant for PLCδ-PH binding to PIP_2 of K_{eff} = 0.30 ± 0.030 μM, which was in close agreement with previously determined values (Lemmon, Ferguson et al. 1995).

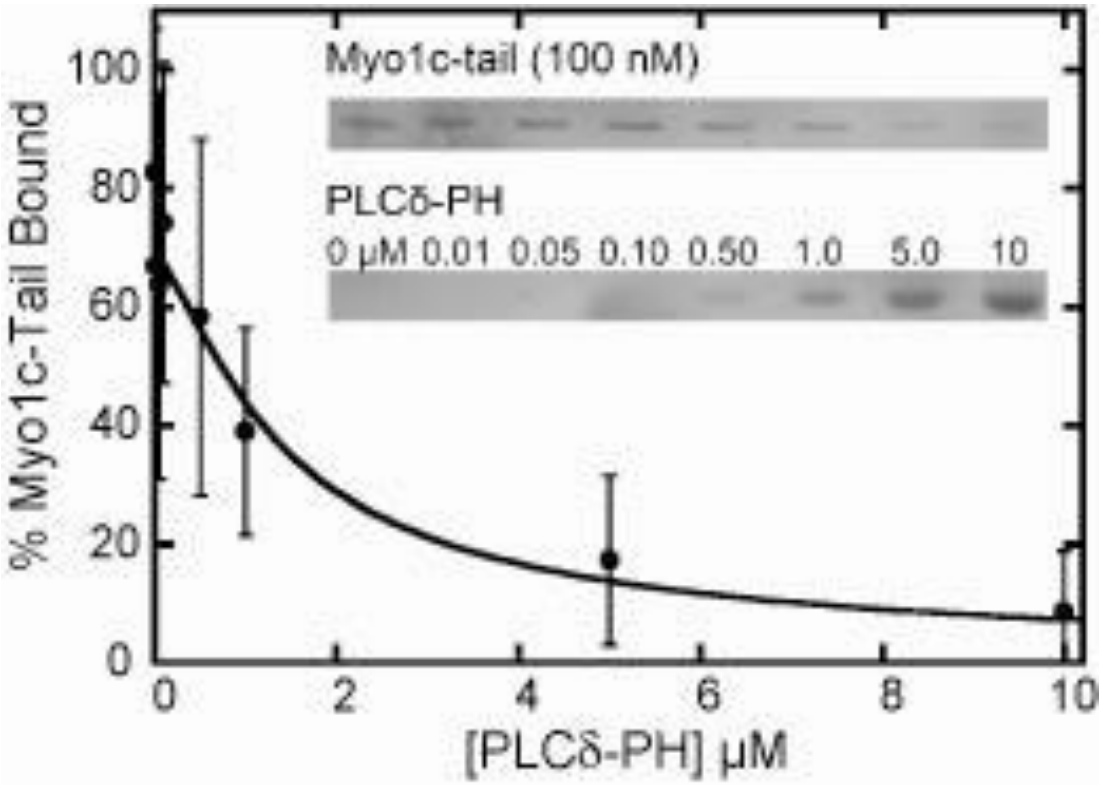

Figure 34 Myo1c and PLCδ-PH compete for PIP_2

Figure 34: Figure was originally published in (Hokanson and Ostap 2006). Binding of 100 nM myo1c-tail to 60 μM LUVs containing 2% PIP_2 in the presence of 0 – 10 μM PLCδ-PH. The inset is a SYPRO-red stained SDS-PAGE gel showing LUV-bound (top) myo1c-tail and (bottom) PLCδ-PH as a function of total PLCδ-PH concentration.

3.2.2 Myo1c Binds Directly to Ins(1,4,5)P_3

To ascertain whether myo1c-tail bound to the head group of PIP_2 directly, we measured its ability to bind [^{3}H]-labeled Ins(1,4,5)P_3 by gel filtration chromatography (Figure 35A-C). We used PLCδ-PH as a positive control because it had previously been shown to bind tightly to Ins(1,4,5)P_3 (Lemmon, Ferguson et al. 1995). Both PLCδ-PH and myo1c-tail eluted as single peaks from gel filtration columns. When PLCδ-PH and myo1c-tail were run with two-fold molar excess [^{3}H]-Ins(1,4,5)P_3, [^{3}H]-Ins(1,4,5)P_3 eluted as two peaks, one co-eluting with the PLCδ-PH or myo1c-tail, demonstrating a stable interaction, and the other corresponding to free [^{3}H]-Ins(1,4,5)P_3. As a negative control, [^{3}H]-Ins(1,4,5)P_3 eluted as a single, non-protein-bound peak when run on the gel filtration column with GST, a protein that does not bind Ins(1,4,5)P_3. The elution position of protein was determined by absorbance at 280 nm. Scintillation counting was used to detect the ^{3}H-Ins(1,4,5)P_3 elution position. These results suggest that myo1c bound to Ins(1,4,5)P_3 directly.

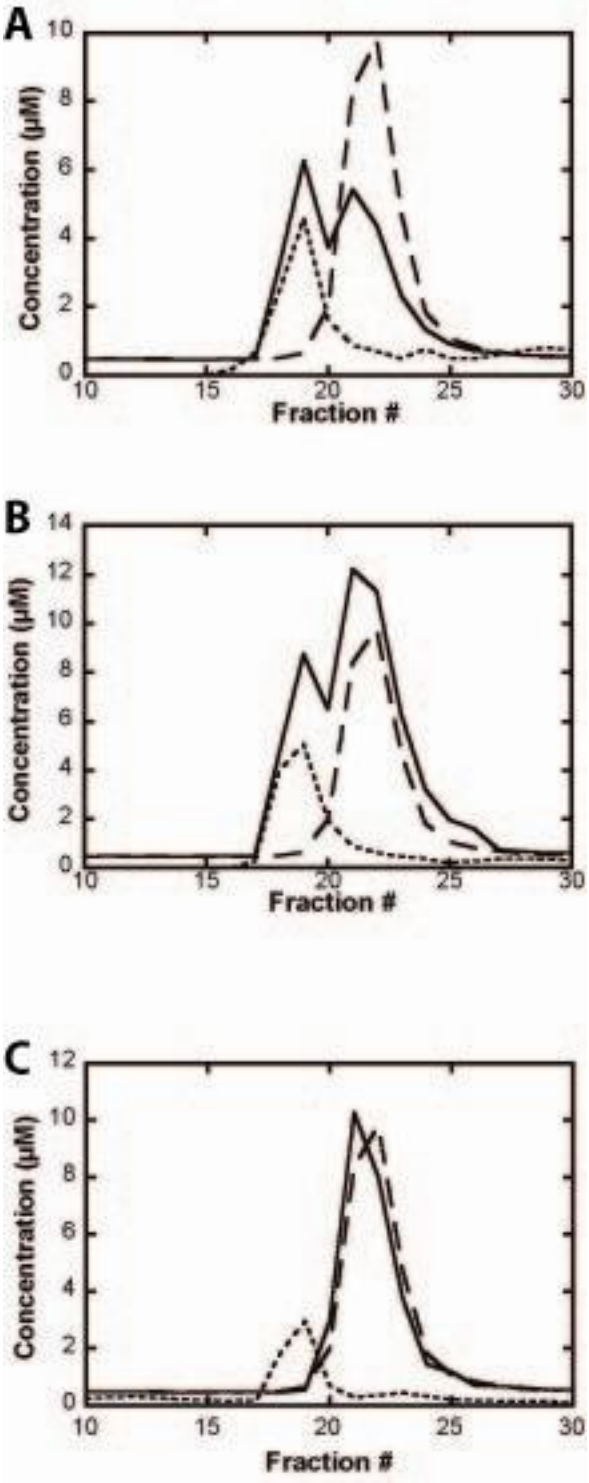

Figure 35A-C: Figures were originally published in (Hokanson and Ostap 2006). Myo1c-tail binds $InsP_3$. Gel filtration elution profiles of samples containing (*A*) 10 μM PLCδ-PH, (*B*) 10 μM myo1c-tail, or (*C*) 10μM GST in the presence of excess ^{3}H-Ins(1,4,5)P_3. The concentrations of $InsP_3$ (solid lines) and PLCδ-PH or myo1c-tail (dotted lines) are shown. $InsP_3$ run in the absence of protein in a separate experiment is also shown (dashed line) as a reference elution profile.

Figure 35 Gel filtration assay

3.2.3 Myo1c Binds Inositol Phosphates Promiscuously

To determine if myo1c binds to additional inositol phosphates, we tested the affinity of myo1c-tail for nine inositol phosphates by competitive binding. We measured the ability of Ins(3)P_1, Ins(1,3,4)P_3, Ins(1,4,5)P_3, Ins(1,2,6)P_3, Ins(1,3,4,5)P_4, Ins(1,2,5,6)P_4, Ins(1,3,4,6)P_4, Ins(1,2,3,5,6)P_5, and InsP_6 to compete with 2% PIP_2 LUVs for binding to myo1c-tail (Figure 36).

Inositol phosphates (0 – 50 μM) were mixed with 50 nM myo1c-tail and 60 μM 2% PIP_2 LUVs. At these concentrations, ~ 80% myo1c-tail was bound to the LUVs in the absence of inhibitor. Eight of the nine inositol phosphates, when fit to Equation 4, gave results within a factor of three ranging from 96 ± 32 nM for Ins(1,4,5)P_3 to 33 ± 7 nM for Ins(1,3,4,5)P_4. The one exception that we obsevered was Ins(1,2,6)P_3, which had a 10-fold lower affinity of 630 ± 130 nM (Table 3). These affinities were over 2-fold tighter binding than our measured affinity of myo1c-tail for PIP_2 (K^{eff}_{acidic} = 0.23 ± 0.050 μM), which suggested that Ins(1,4,5)P_3 may be able to effectively displace myo1c from the plasma membrane in the cell; however, additional binding energies contributed by PS binding may prevent this from occurring. The mono-inositol phosphate, Ins(3)P_1, failed to inhibit the interaction of myo1c with PIP_2 at concentrations up to 100 μM. These results suggested that the binding of myo1c-tail to phosphatidyl inositols is not solely dependent on the number of charges, but also on the positions of the charges. Moreover, myo1c may have some inositol phosphate binding specificity for phosphates at the 4 and 5 positions of the inositol ring, as the affinity of myo1c for Ins(1,2,6)P_3 is

10-fold weaker than all other inositol phosphates that contain a phosphate at one or both of these ring positions.

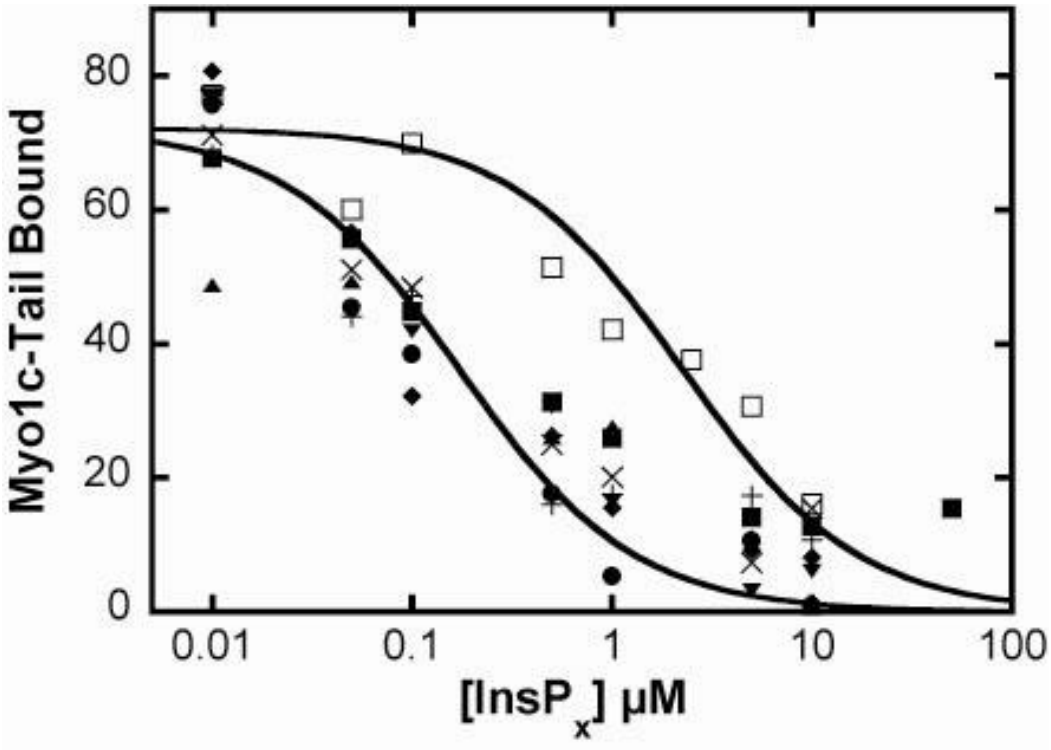

Figure 36 InsP$_x$ competitive binding assay (PIP$_2$)

Figure 36: Figure was originally published in (Hokanson, Laakso et al. 2006). Binding of 40 - 100 nM myo1c-tail to 60 µM LUVs containing 2% PIP_2 in the presence of 0 – 50 µM (■) Ins(1,4,5)P_3, (▲) Ins(1,3,4)P_3, (□) Ins(1,2,6)P_3, (●) Ins(1,3,4,5)P_4, (▼) Ins(1,2,5,6)P_4, (×) Ins(1,3,4,6)P_4, (+) Ins(1,2,3,5,6)P_5 and (♦) $InsP_6$ (*n* for each point = 4 - 14). Solid lines are fits to the (●) Ins(1,3,4,5)P_4 and (□) Ins(1,2,6)P_3 using Equation 4. Points at 0 µM $InsP_x$ are not shown due to logarithmic scale. The effective dissociation constants obtained from the fits are listed in Table 3.

Table 3 Effective dissociation constants for inositol phosphates binding to myo1c-tail.[a]

Inositol Phosphate[b]	K_d[c]
Ins(3)P_1	> 1 µM
Ins(1,4,5)P_3	96 ± 32 nM
Ins(1,3,4)P_3	61 ± 25 nM
Ins(1,2,6)P_3	630 ± 130 nM
Ins(1,3,4,5)P_4	33 ± 7.0 nM
Ins(1,2,5,6)P_4	53 ± 23 nM
Ins(1,3,4,6)P_4	67 ± 17 nM
Ins(1,2,3,5,6)P_5	44 ± 14 nM
InsP_6	48 ± 16 nM

[a]10 mM HEPES, pH 7.0, 100 mM NaCl, 1 mM EGTA, 1 mM DTT, 1 µM CaM

[b]The mole percentages PS and PIP_2 are reported with the remaining lipid composed of PC.

[c]Effective dissociation constants were determined by competition assays as described in Materials and Methods. Errors are standard errors of the fit.

3.2.4 Ins(1,4,5)P_3 Competes Weakly with Myo1c-Tail for PS Binding

We hypothesized that if the binding of myo1c to PS was due to a separate binding site than that for PIP_2, Ins(1,4,5)P_3 should not be able to inhibit binding of myo1c-tail to LUVs comprised of PS. We repeated our Ins(1,4,5)P_3 competition binding studies using 50 nM myo1c-tail bound to 60 µM LUVs composed of 2% PIP_2 + 20% PS, 2% PIP_2 + 60% PS, 20% PS, 60% PS, and 80% PS (Figure 37). Only weak inhibition was seen with up to 50 µM Ins(1,4,5)P_3 as most of the myo1c-tail remained bound to LUVs comprised of 2% PIP_2 + 20% PS or 2% PIP_2 + 60% PS. Myo1c-tail also remained mostly bound to LUVs of 60% and 80% PS with Ins(1,4,5)P_3 concentrations up to 50 µM.

We interpreted this data to signify that myo1c contained two separate binding sites. One site bound tightly and specifically to phosphatidyl inositols in a 1:1 ratio and could be inhibited by inositol phosphates; a second site bound to PS or anionic lipids in a Ca^{2+} dependent manner and was not inhibited by inositol phosphates. When both sites were bound to their respective substrates, *i.e.* LUVs with 2% PIP_2 + 20% PS, binding was six-fold tighter (Table 1) and myo1c was not displaced from the LUVs by Ins(1,4,5)P_3.

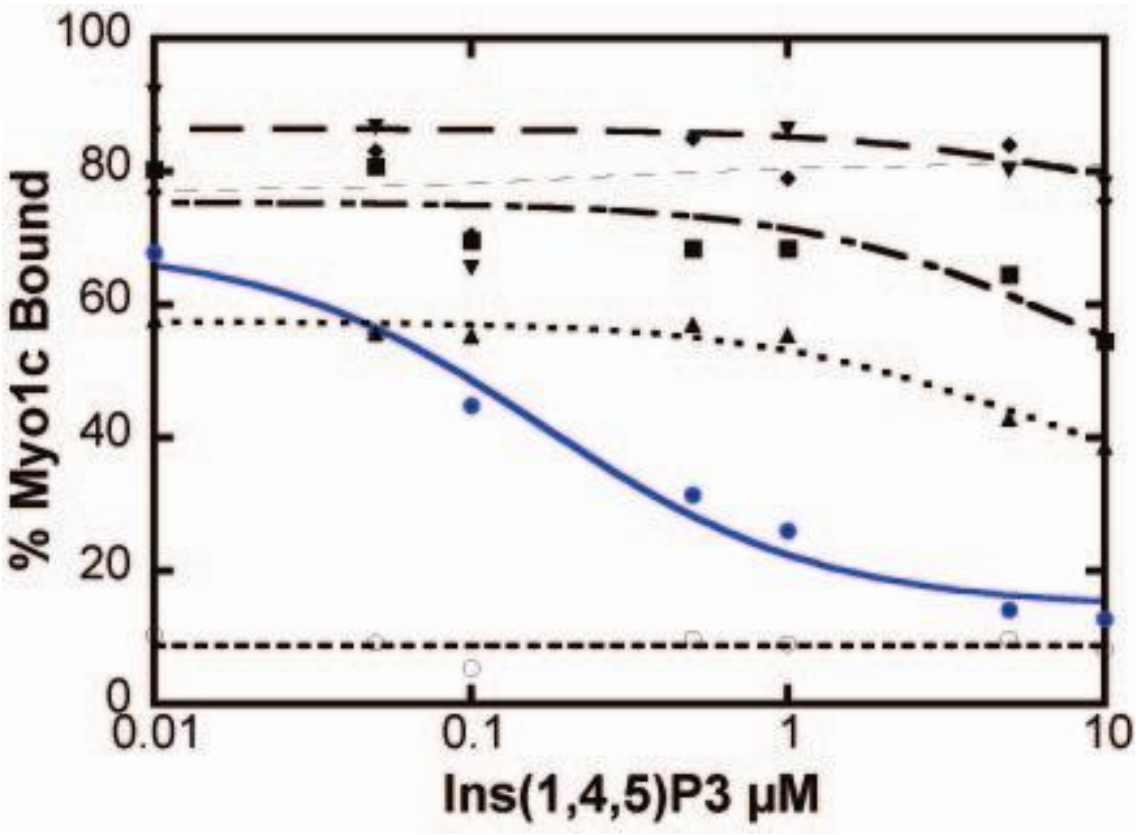

Figure 37 Ins(1,4,5)P_3 competitive binding assay

Figure 37: Binding of 50 nM myo1c-tail to 60 µM LUVs composed of (●, solid line) 2% PIP_2, (■ uneven dashed line) 2% PIP_2 + 20% PS, (◆, thin dashed line) 2% PIP_2 + 60% PS, (❍, lowest dashed line) 20% PS, (▲, dotted line) 60% PS, and (▼, long dashed line) 80% PS (*n* for each point = 4 - 14). Lines are fits to the using the Equation 4. Points at 0 µM $InsP_x$ are not shown due to logarithmic scale.

3.2.5 Ins(1,4,5)P_3 Protects Myo1c-Tail from Trypsin Digest

We found that Ins(1,4,5)P_3 protects myo1c-tail from trypsin digestion while attempting to obtain a small, stable construct of the lipid binding domain of myo1c. 100 µL aliquots of 0.3 mg/mL myo1c-tail were incubated with trypsin concentrations ranging from 0.15 - 3.0 µg/mL trypsin over 0 - 40 minutes before the reaction was quenched by the addition of equal amounts by weight of soybean inhibitor (SI). Myo1c-tail fragments were detected by Western blot and SYPRO red analysis (Figure 38A-B). A 1:1000 ratio by weight of trypsin to myo1c-tail for 40 minutes, or a 1:100 ratio by weight of trypsin to myo1c-tail for 10 minutes effectively digested the myo1c-tail to near completion. Digestion fragments from a 1:1000 ratio by weight of trypsin to myo1c-tail can be clearly seen in the SYPRO red stained gel after 5 minutes (Figure 38B). A 1:100 ratio by weight of trypsin to myo1c-tail sample with 10 µM Ins(1,4,5)P_3 was not digested after 10 minutes, whereas a sample with no Ins(1,4,5)P_3 was almost fully digested. Similar results have shown that myo1a is protected by lipid vesicles when digested with α-chymotrypsin (Hayden, Wolenski et al. 1990). We conclude from this finding that Ins(1,4,5)P_3 helped to protect myo1c-tail from trypsin digestion, possibly by stabilizing a folded conformation or blocking one or more cleavage sites.

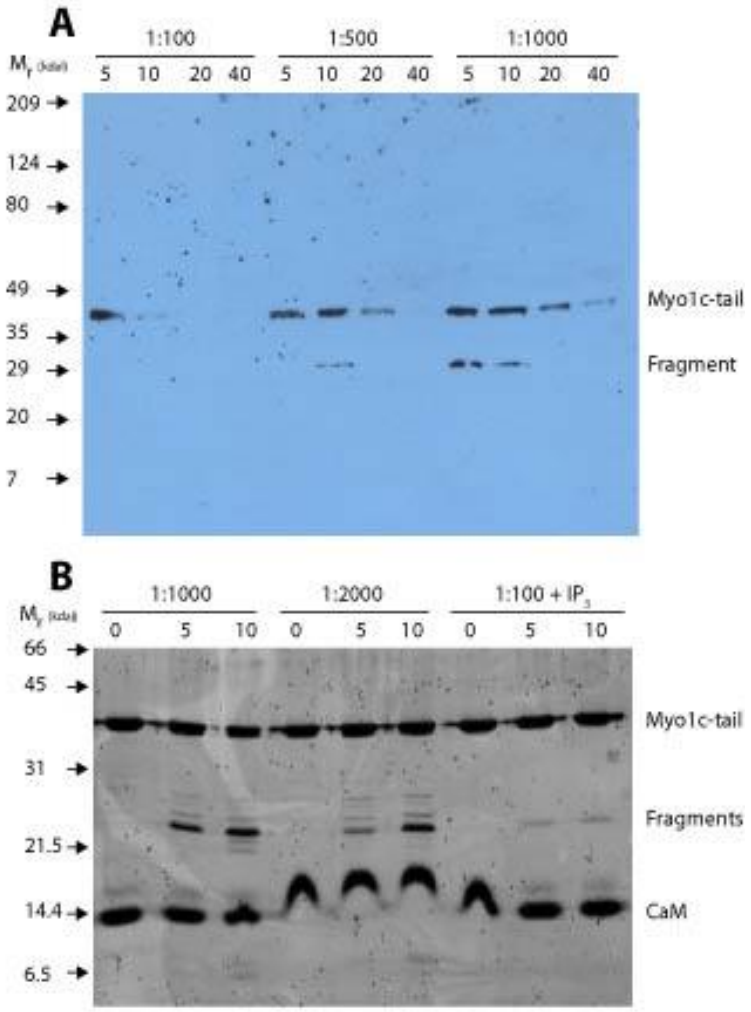

Figure 38 Myo1c-tail digest

Figure 38A-B: Western blot and SYPRO red stained SDS-PAGE gel of a myo1c-tail trypsin digest. A) Digestion times were 5, 10, 20, 40 minutes at three dilutions. Lanes 1 – 4 1:100 trypsin by weight, lanes 5 – 8 1:500 trypsin by weight, lanes 9 – 12 1:1000 trypsin by weight. B) Digestion times were 0, 5, 10 minutes at three dilutions. Lanes 1 – 3 1:1000 trypsin by weight, lanes 4 – 6 1:2000 trypsin by weight, lanes 7 - 9 1:100 trypsin by weight in the presence of 10 μM Ins(1,4,5)P_3.

3.3 *In Vivo* Localization Studies

We sought to show that the localization of myo1c in mammalian cells was consistent with the data from our *in vitro* binding assays. To test this, we expressed a myo1c-tail construct with a GFP-tag at the N-terminus in mammalian cells. We found that when a GFP-myo1c-tail chimera was expressed, it localized to the plasma membrane as shown previously (Figure 39) (Ruppert, Godel et al. 1995; Bose, Guilherme et al. 2002). We further used this construct to show that myo1c concentrated on cellular PIP_2 containing structures. All of our constructs expressed in various cell types showed no dominant inhibitory effects to any of the cell processes we checked for including ruffling, lamellipodia retraction, filopodia, presence of vesicles, cell size, or mitosis (Figure 40).

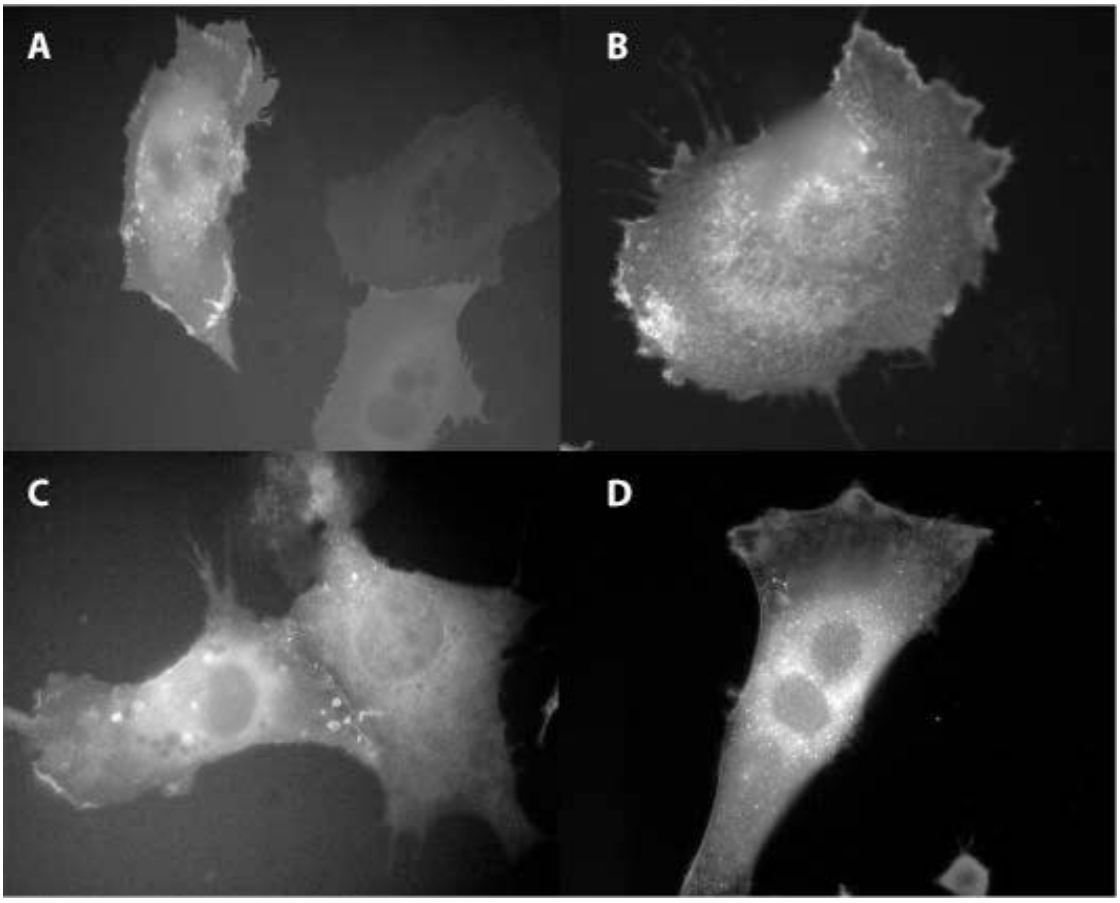

Figure 39 Myo1c-tail localization

Figure 39: The localization of myo1c-tail by epifluorescence. Four different cell types, A) NRK, B) CHO, C) COS-7, and D) HeLa, were transfected with GFP-tail and observed under epifluorescence. Note the punctuate staining and membrane localization in each cell type.

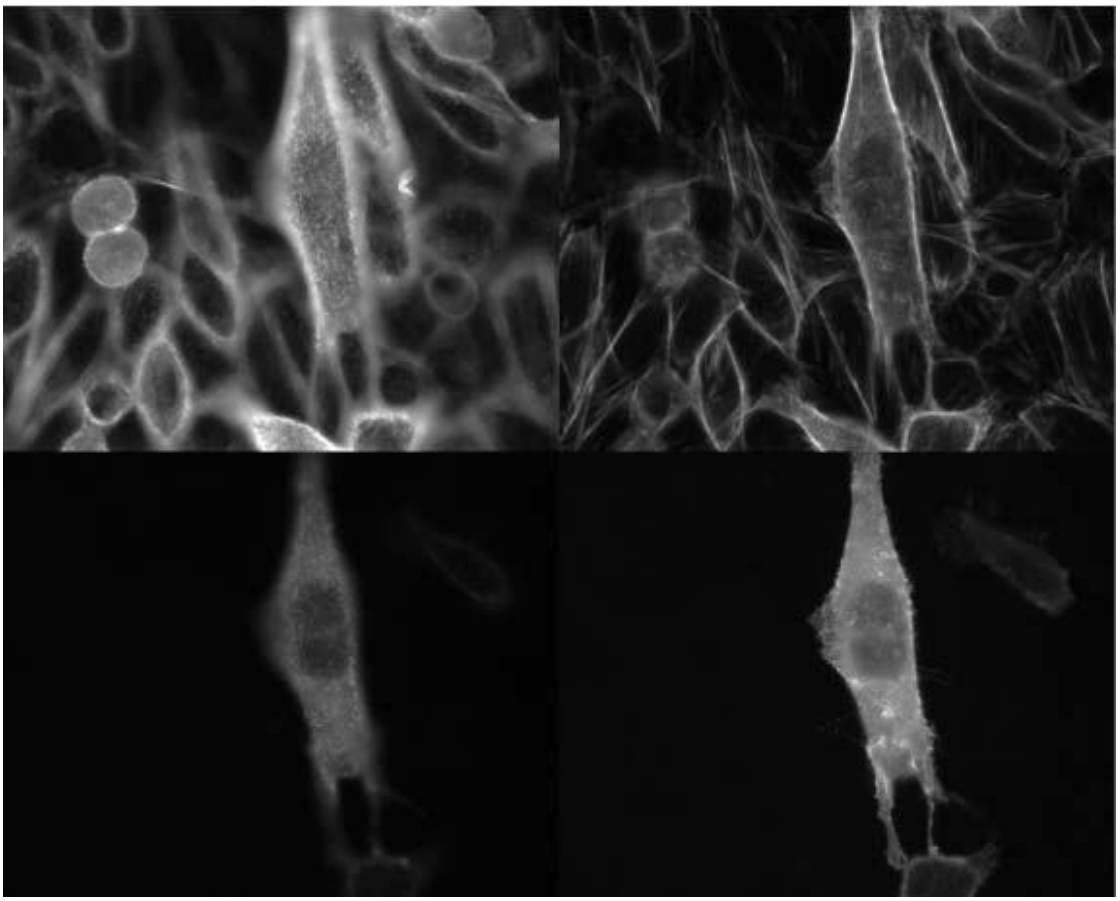

Figure 40 No dominant negative effect

Figure 40: Epifluorescence of CHO cells transfected with GFP-tail. Top images show fluorescence of actin labeled with rho-phalloidin. Bottom images show fluorescence of GFP-tail. The focal plane of images on left are focused at the top of the cells to observe filopodia, the focal plane of images on the right are focused at the edges of the cell.

3.3.1 Ionomycin Redistributes Myo1c-Tail to the Cytoplasm

PLC hydrolyzes PIP_2 into two second messengers, DAG, which is retained in the membrane, and $Ins(1,4,5)P_3$, which is soluble and contains the phosphorylated inositol ring. We hypothesized that the tail domain of myo1c should localize to the plasma membrane and translocate to the cytoplasm upon calcium activation of PLC if it binds tightly to cellular PIP_2 (Ryu, Suh et al. 1987). To observe changes in localization of myo1c after Ca^{2+}-induced activation of PLC, we added $CaCl_2$ and ionomycin, an ionophore which allows Ca^{2+} to cross the plasma membrane.

The addition of 10 μM ionomycin and 1.2 mM $CaCl_2$ to the growth medium of NRK cells expressing GFP-myo1c-tail resulted in the redistribution of GFP-myo1c-tail to the cytoplasm (Figure 41). The GFP-myo1c-tail reassociated with the plasma membrane upon washing out the $CaCl_2$ and ionomycin. In consideration of this result, we kept in mind that increased levels of Ca^{2+} in the cell from the addition of ionomycin can affect other factors in addition to activating PLC, all of which could potentially have inhibited myo1c localization. The two most obvious possibilities we considered were the activation of scramblases, which flip PS molecules to the outside of the cell and deplete their effective concentration on the inner-leaflet, and electrostatic shielding at the plasma membrane. Although this assay was relatively non-specific, it supported our findings that the myo1c-tail bound to PIP_2 and that calcium did not increase the affinity of myo1c for the plasma membrane.

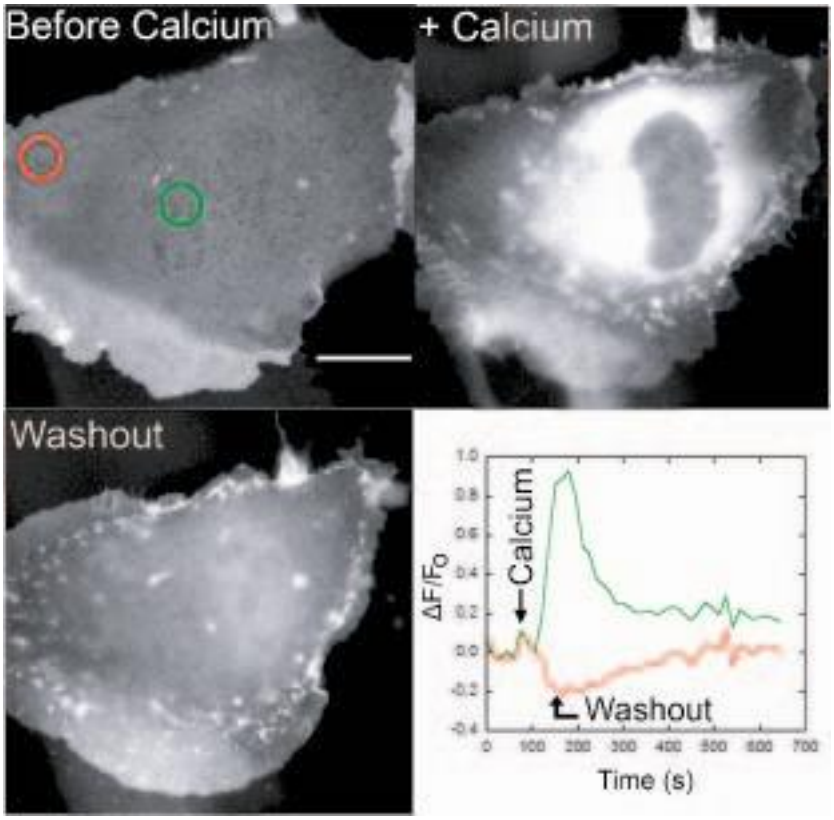

Figure 41 Ionomycin redistributes myo1c-tail

Figure 41: Figure was originally published in (Hokanson and Ostap 2006). Cellular distribution of GFP-tail during influx of calcium. Fluorescence micrographs of a transfected NRK cell showing GFP fluorescence before, during, and after incubation with 10 μM ionomycin in medium containing 1.2 mM $CaCl_2$. Scale bar is 15 μm.

3.3.2 Myo1c Found on Cellular PIP_2-Containing Structures

In addition to localizing to the plasma membrane, myo1c was found on cellular structures known to be enriched in phosphatidyl inositols. In NRK cells undergoing macropinocytosis, we found that GFP-myo1c-tail transiently concentrated on the membrane during the early phases of membrane internalization (Figure 42). Once the

macropinosome separated from the plasma membrane, the GFP-myo1c-tail dissociated from the membrane. This transient localization closely mirrored the localization of PIP_2-specific PH domains during macropinocytosis and phagocytosis (Cullen, Cozier et al. 2001; Simonsen, Wurmser et al. 2001), again supporting the proposal that myo1c primarily bound to cellular PIP_2.

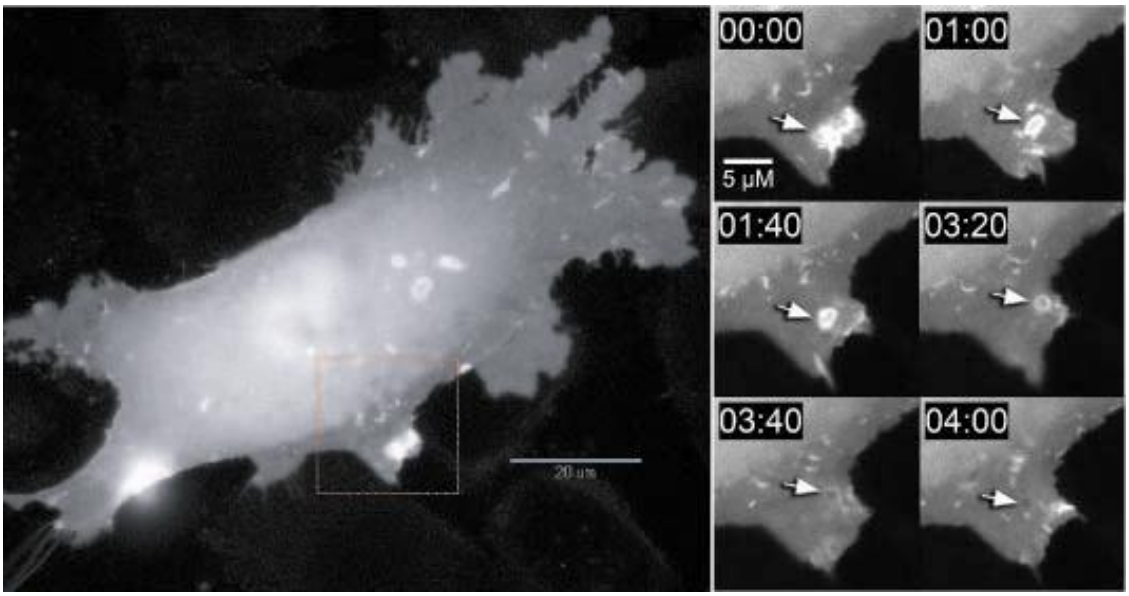

Figure 42 Macropinocytosis event

Figure 42: Figure was originally published in (Hokanson and Ostap 2006). Cellular distribution of GFP-tail during macropinocytosis. Fluorescence micrographs of a transfected NRK cell showing GFP fluorescence around a newly internalized macropinosome (arrow). Note the loss of fluorescence around macropinosome after it is internalized. The time stamp is min:sec, and the scale bar is 5 µm.

3.4 Identifying the PIP_2 Binding Site

Finding sequence homology to a PIP_2 binding domain proved to be quite difficult, as there was no structural information known and very little sequence homology found to the tail domain of myo1c in the databases. In addition, there was evidence that the myo1c tail domain may be extended and flexible due to its lack of density in electron micrographs of helical reconstructions of myo1a saturated actin filaments (Figure 48) (Jontes and Milligan 1997). Therefore, we followed the advice of Dr. Mark Lemmon (University of Pennsylvania) and turned to algorithms that predict secondary structure and match those to protein domains of known structures. From these, we were able to identify the region in the tail domain that binds to the membrane and locate residues directly responsible for PIP_2 binding.

3.4.1 Identification of a Putative PH Domain

Our searches in the NCBI database for PIP_2 binding proteins with sequence homology to myo1c yielded negative results. Undeterred, we searched for structural homologs of the myo1c tail domain using the Phyre server (www.sbg.bio.ic.ac.uk/phyre/) to identify a phosphatidylinositol binding site. Secondary structural analysis revealed that the myo1c tail domain had homology to PH domains, including specific sequence homology to the β1-loop-β2 phosphatidylinositol binding region (Figure 10) of PPB PH domains (Isakoff, Cardozo et al. 1998). This region contained the PH domain signature motif of conserved basic residues (K-X_n-

(K/R)-X-R) (Isakoff, Cardozo et al. 1998; Cronin, DiNitto et al. 2004), which we identified in myo1c (Figure 43A).

Two of the conserved basic residues in the β1-loop-β2 region of PH domains have been shown to be crucial for high affinity poly-phosphatidylinositol binding (Cronin, DiNitto et al. 2004). To determine if these residues also play a role in myo1c-PIP_2 interactions, we mutated the corresponding amino acids in a GFP-tail construct to alanines (GFP-tail-K892A and GFP-tail-R903A) (Figure 11). We expressed GFP-tail, GFP-tail-K892A, and GFP-tail-R903A in HEK-293T cells, and purified these proteins using a two-step purification scheme as described in chapter 2. The impact of these mutations on myo1c binding to PIP_2 will be discussed below.

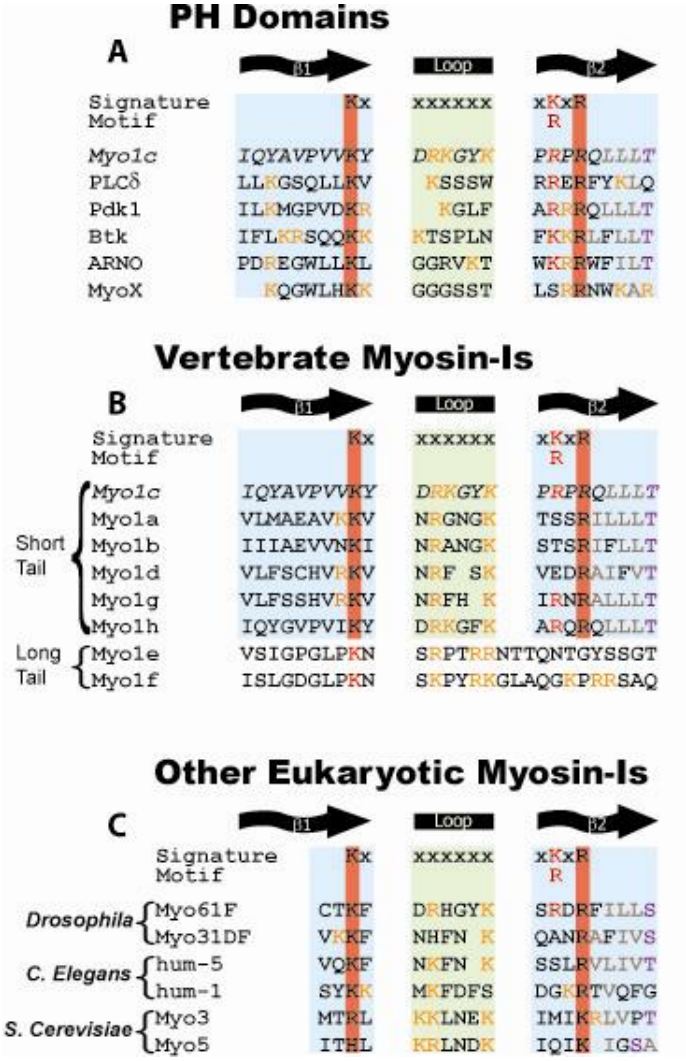

Figure 43 PH domain signature motif

Figure 43A-C: Figures were originally published in part in (Hokanson, Laakso et al. 2006). Alignment of mouse myo1c (residues 884 - 908) with the (A) β1-loop-β2 motif of PH domains, B) vertebrate myosin-I isoforms, and C) eukaryotic myosin-Is. Red bands and residues indicate conserved known basic residues important for membrane binding in PH domains, orange residues indicate all other basic residues, brown residues indicate conserved hydrophobic patch following the second key residue of β2, purple residues indicates conserved threonine at end of β2.

3.4.2 Signature PH Domain Motif Found in Many Eukaryotic Myosin-Is

There are eight myosin-Is expressed in humans, myo1a through myo1g. We were able to identify the PH domain signature motif (K-X_n-(K/R)-X-R) in all six short-tail myosin-Is (Figure 43B). Therefore, we hypothesized that these short-tail isoforms bind to phosphatidylinositols in a manner similar to myo1c. The two myosin-Is that did not contain the PH domain signature motif were myo1e and myo1f, the two long-tail isoforms of myosin-I. Long-tail myosin-Is have the addition of an SH3 and GP-rich domain in a C-terminal extension of their tail domains that starts after the first β-strand of the identified PH domain signature motif. This extension contains several positive charges that may be positioned for phosphatidylinositol binding. Long-tail myosin-I isoforms have been shown to bind acidic phospholipids (Adams and Pollard 1989; Stoffler, Ruppert et al. 1995), so it is possible that differences in this region may result in differences in membrane binding properties.

We also identified the PH domain signature motif in myosin-Is from other Eukaryotic species, including 61F and 31DF from *Drosophila*, hum-5 and hum-1 from *C. elegans*, and Myo3 and Myo5 from *S.* cerevisiae (Figure 43C). These myosin-Is may also bind to phosphatidylinositols in a manner similar to myo1c.

3.4.3 Point Mutations Inhibit PIP_2 Binding

We used sedimentation assays to calculate the effective dissociation constants, which are expressed in terms of total lipid (K_{eff}^{lipid}) or accessible acidic phospholipid

(K_{eff}^{acidic}), for the interaction between GFP-tail, GFP-tail-K892A, and GFP-tail-R903A and sucrose-loaded 2% PIP2 LUVs (Figure 44). GFP-tail, GFP-tail-K892A, and GFP-tail-R903A were sedimented in the presence of 0 – 400 μM LUVs. The supernatants were analyzed for the presence of GFP using a fluorimeter with a double monochromator to decrease the amount of light-scattering caused by the LUVs. Because the constructs were GFP fusion proteins, we were able to determine the fraction bound as a function of lipid concentration by monitoring the loss of fluorescence in the supernatant. The GFP-tail bound with K_{eff}^{lipid} = 24 ± 2.4 μM (K_{eff}^{acidic} = 0.24 ± 0.024 μM), which is almost identical to the K_{eff}^{lipid} for a myo1c-tail construct expressed in *sf*9 cells that does not contain GFP (Table 1). Remarkably, we did not detect any binding of GFP-tail-K892A and GFP-tail-R903A mutants to LUVs containing 2% PIP_2 at total lipid concentrations of up to 400 μM.

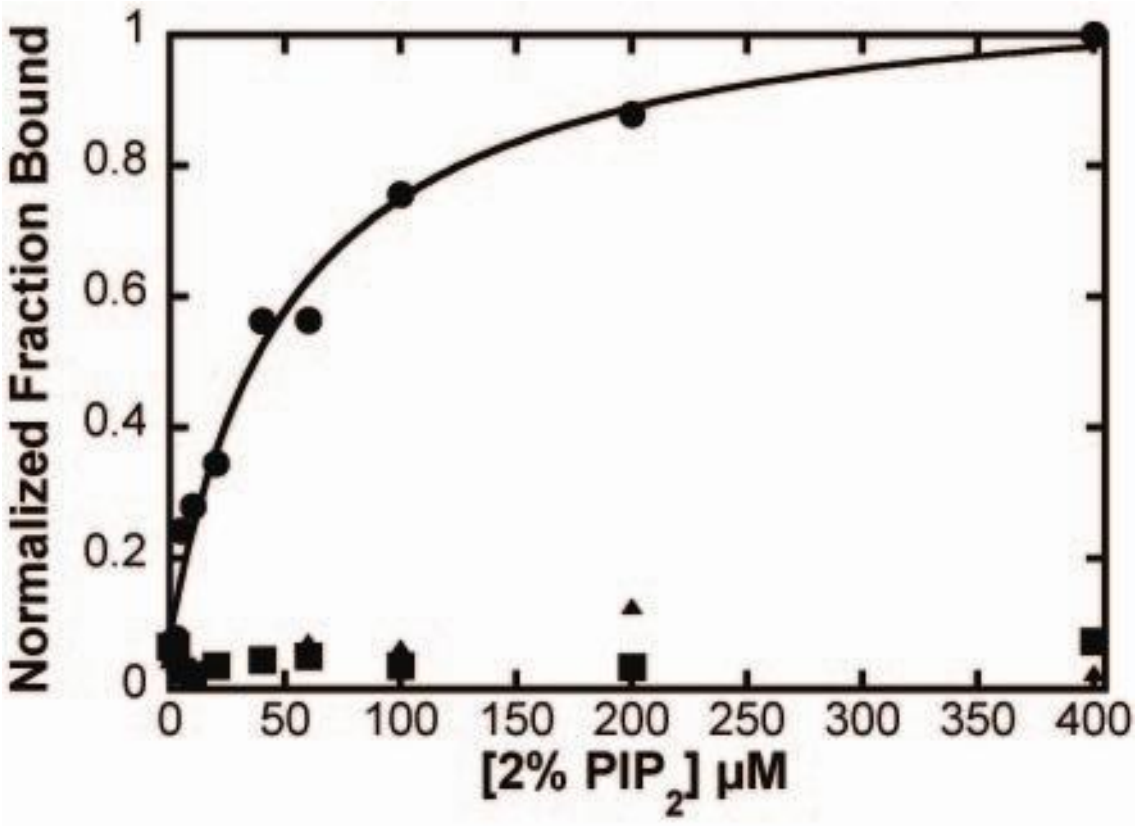

Figure 44 Association of GFP-tail constructs with PIP_2

Figure 44: Figure was originally published in (Hokanson, Laakso et al. 2006). Lipid concentration dependence of (●) 6.9 nM GFP-tail, (■) 9.7 nM GFP-tail-K892A, and (◆) 15 nM GFP-tail-R903A binding to LUVs composed of 2% PIP_2. Each point is the average of two measurements. The solid line is the best fit of the GFP-myo1c-tail data to a hyperbola, yielding, $K_{eff}^{lipid} = 53 \pm 11$ µM.

3.4.4 Full-Length Myo1c Localization is Identical to Myo1c-Tail

In all cell types tested (NRK, COS-7, CHO, HeLa, and 293T), GFP-tail was localized to the cell membrane and was concentrated in regions of membrane ruffling and retraction (Figure 39), as reported previously for endogenously expressed myo1c in NRK cells (Ruppert, Godel et al. 1995) and GFP-myo1c in NIH3T3 cells (Bose, Guilherme et al. 2002). In NRK cells, full length GFP-myo1c constructs that contained the K892A (GFP-myo1c-K892A) and R903A (GFP-myo1c-R903A) mutations were localized to the cytoplasm, with no significant population in the dynamic cell margins (Figure 45). Therefore, no significant population of GFP-myo1c-K892A and GFP-myo1c-R903A bound to the plasma membrane. We also tested a GFP-tail construct with a K296A mutation. This construct showed identical localization to GFP-tail, suggesting that not all basic residues in this region are essential for membrane association, and that membrane binding is not based on charge alone.

To test for dominant negative effects on motility and cell morphology, particularly at the cell edge, we over expressed GFP-myo1c-tail, GFP-myo1c-tail-K903A, and GFP-myo1c-K903A in NRK, COS-7, and CHO cells. We were unable to detect any differences in transfected versus nontransfected cells regarding cell size, ruffling, lamellipodia, filopodia, endocytosis, mitosis, and cell motility.

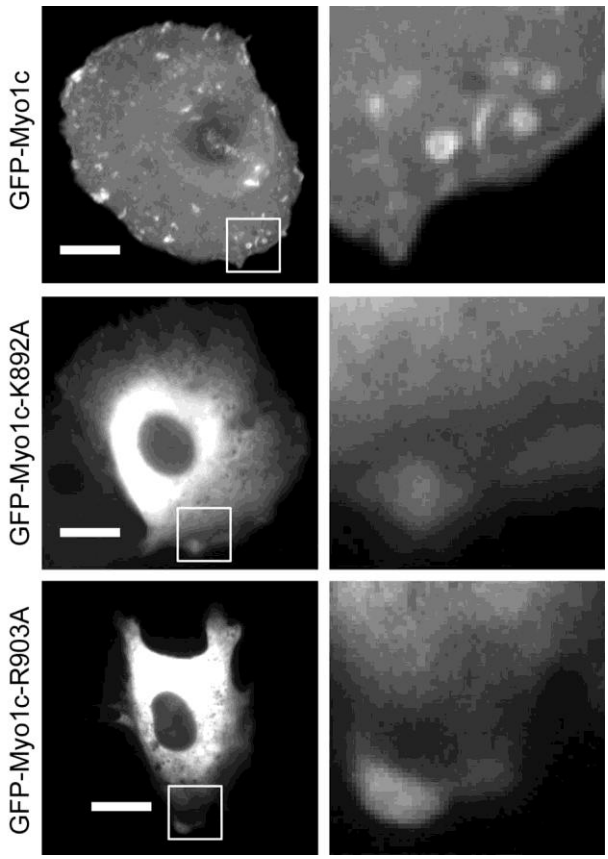

Figure 45 GFP-my1oc constructs localization

Figure 45: Figure was originally published in (Hokanson, Laakso et al. 2006). Epifluorescence micrographs of live NRK cells expressing (top) GFP-myo1c, (center) GFP-myo1c-K892A, and (bottom) GFP-myo1c-R903A. The boxes outline the expanded regions shown in the right column. Note the localization of wild-type GFP-myo1c within the membrane ruffles and macropinocytic regions, but not in the mutated proteins. The scale bars are 15 µm.

3.5 TIRF/FRAP Dissociation Studies

TIRF is a technique designed to reduce the background fluorescence of a specimen due to the nature of the evanescent electromagnetic field, which decays exponentially from the interface and thus penetrates to a depth of approximately 100 nm into the sample medium. We combined TIRF with FRAP to measure dissociation rates of membrane-bound myo1c. This technique allowed us to monitor events that occurred at and directly above the plasma membrane without the background fluorescence of the entire cytosol.

3.5.1 Point Mutations in the Putative PH Domain Affect Myo1c Localization

We monitored membrane association of GFP-tail, GFP-tail-K892A, and GFP-tail-R903A by TIRF/FRAP microscopy in live NRK cells to determine if the K892A and R903A mutations affect the dynamics of in vivo membrane binding (Figure 46). The fluorescence of all constructs was visible by TIRF microscopy, as was the fluorescence from cells expressing GFP only. The fluorescence after photobleaching of GFP-tail recovered in two phases. A fast phase (kfast) recovered within the first acquisition point (> 1 s-1), and a slow phase (kslow) recovered with an average rate of 0.060 ± 0.037 s-1 (Table 4). kslow ranged between 0.013 – 0.15 s-1 in the eighteen cells examined by TIRF/FRAP, but in all cases kslow was clearly resolved from kfast. Because myo1c binds acidic lipids at a diffusion-limited rate (Tang, Lin et al. 2002), we interpreted the slow recovery time to be the rate at which the photobleached GFP-

myo1c-tail dissociated from the membrane and the fast recovery to have been the diffusion of GFP-tail in the cytoplasm.

The fluorescence after photobleaching of GFP-tail-K892A and GFP-tail-R903A almost completely recovered within the first acquisition point at a rate > 1 s^{-1}, a response similar to control cells expressing GFP alone. Also, no slow phase was detected, which suggested that the myo1c proteins containing point mutations did not bind to the membrane. These results were consistent with the in vitro binding data (Figure 44).

To make certain the motor domain would not compensate for the point mutations in the tail domain of myo1c, we repeated these experiments with full length, GFP-tagged constructs. Again, the fluorescence of GFP-myo1c after photobleaching in TIRF/FRAP experiments recovered in two phases. The kinetics of the recovery phases were nearly identical to GFP-tail, indicating that the actin binding domain did not contribute significantly to the lifetime of plasma membrane attachment of the over-expressed protein (Table 4). The fluorescence after photobleaching of GFP-myo1c-K892A and GFP-myo1c-K903A almost completely recovered within the first acquisition point at a rate of > 1 s-1, confirming that the mutations in the full length protein did not bind tightly to the membrane. Therefore, we concluded that myo1c bound to membranes *in vitro* and *in vivo* via a region in the tail domain that was in part structurally homologous to the phosphatidylinositol binding site in certain PH domains.

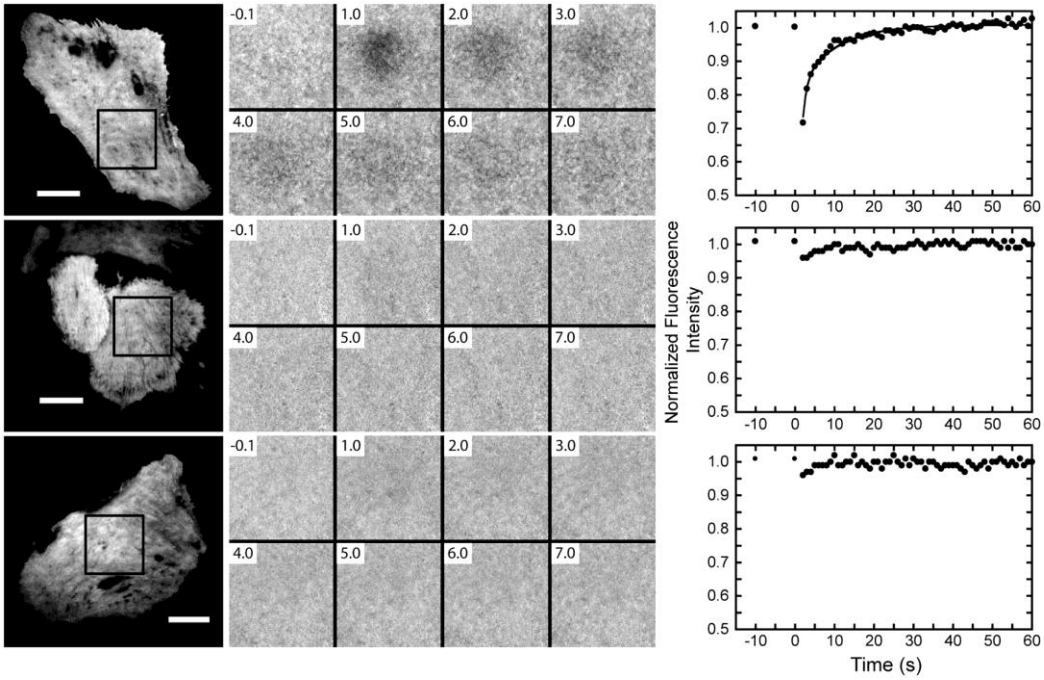

Figure 46 TIRF/FRAP of myo1c-tail constructs

Figure 46: Figure was originally published in (Hokanson, Laakso et al. 2006). TIRF/FRAP experiments of single NRK cells expressing (top row) GFP-tail, (center row) GFP-tail-K892A, and (bottom row) GFP-tail-R903A. (Left column) TIRF micrographs of NRK cells before photobleaching. The boxes outline the photobleached regions. The scale bar is 15 µm. (Center columns) Normalized time-lapse images of the photobleached regions (see chapter 2); elapsed times are given relative to the start of the bleach pulse. (Right column) Fluorescence recovery of GFP after photobleach. The bleach pulse occurs at time-zero. The solid line in the top graph is a fit of the data from this cell to the sum of two exponential rates (k_{slow} = 0.10 ± 0.010 s^{-1}).

3.5.2 Myo1c Tail Domain is Sufficient for Membrane Localization

To test whether the IQ motifs in the regulatory domain are necessary for membrane binding in live NRK cells, we performed TIRF/FRAP microscopy of GFP-myo1c-tail^{IQ2-3}, GFP-myo1c-tail^{IQ3}, and GFP-myo1c-tail^{IQ0} (Figure 11). The fluorescence after photobleaching of these constructs recovered in two phases, as seen with GFP-tail (Table 4). The fast phases recovered within the time resolution of the experiment (> 1 s-1), and the slow phases recovered with average rates between 0.041 – 0.049 s^{-1}, which were not significantly different from the k_{slow} determined for GFP-tail. Therefore, the regulatory domain was not necessary for membrane association *in vivo*. However, this finding did not rule out a role for the regulatory domain in targeting the motor to specific subcellular regions.

Table 4 Rates of fluorescence recovery from TIRF/FRAP experiments.

Myo1c construct[a]	k_{slow} (s^{-1})[b]	Range[c]
GFP-tail (18)	0.060 ± 0.037	0.013 – 0.15
GFP-myo1c (10)	0.050 ± 0.028	0.017 – 0.096
GFP-tail-K892A (4)	> 1 s^{-1}	> 1 s^{-1}
GFP-tail-R903A (7)	> 1 s^{-1}	> 1 s^{-1}
GFP-myo1c-K892A (7)	> 1 s^{-1}	> 1 s^{-1}
GFP-myo1c-R903A (9)	> 1 s^{-1}	> 1 s^{-1}
GFP only (4)	> 1 s^{-1}	> 1 s^{-1}
GFP-myo1c-tail$^{IQ2\text{-}3}$ (11)	0.049 ± 0.028	0.018 – 0.087
GFP-myo1c-tail^{IQ3} (16)	0.050 ± 0.021	0.019 – 0.089
GFP-myo1c-tail^{IQ0} (15)	0.041 ± 0.012	0.012 – 0.094

[a]The number of FRAP transients is reported in the parentheses.

[b]Values of k_{slow} were determined from fitting the data to the sum of two exponential transients. Values of k_{fast} determined from the fits are as fast as the time resolution of the acquisitions and are not reported. Errors are standard deviations.

[c]The minimum and maximum values for the experimental set of k_{slow} values.

4 Discussion

This chapter will interpret the results from chapter 3 and foresee their implications on the association of myo1c with the plasma membrane. Included will be the relevance of PIP_2 binding and the resulting specific interaction of myo1c with the membrane. The binding domain will be modeled and the mechanism of binding will be related to other membrane binding, as well as the force and dynamics of motors while bound to the membrane.

4.1 Mechanism of Membrane Binding

4.1.1 Original Hypothesis

It has been known since 1989 that myosin-Is are localized to the plasma membrane and bind to vesicles of anionic lipids (Adams and Pollard 1989). Myo1c has been shown to bind to LUVs composed of increasing molar concentrations of PS with increasing affinity (Tang, Lin et al. 2002). The regulatory and tail domain of myo1c has clusters of positively charged arginines and lysines, with an estimated pI of 10.8. Before this study, it was believed that the association of myo1c with the plasma membrane was primarily based on non-specific electrostatic interactions (Hayden, Wolenski et al. 1990; Doberstein and Pollard 1992). We initially modeled one patch of basic residues, PEWKQQLQQKAVASEIFKGKK, as an α-helix using Swiss PDB Viewer (Figure 47A-B); it appeared as an amphiphatic helix with all of the basic charges aligned on one side of the helix. Therefore, we originally predicted this cluster of positive charges to be the lipid binding site of myo1c.

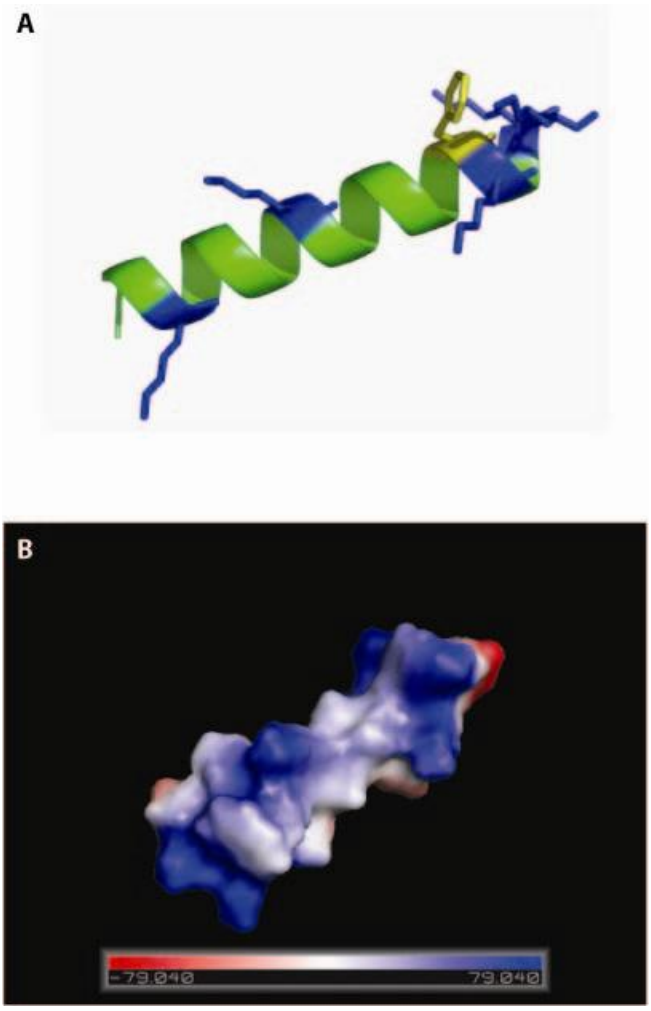

Figure 47 Predicted lipid binding site

Figure 47A-B: A predicted α-helix calculated with Swiss PDB viewer and stylized using Pymol. The structure was predicted using energy minimizations of the sequence from the text. A) Predicted α-helix, basic residues are displayed in blue, aromatic residues are displayed in gold. B) Electrostatic potential map of the helix in "A". Note the amphiphatic nature of the helix with basic residues facing the top side.

4.1.1.1 Electrostatic Binding

Like myo1c, MARCKS has been shown to bind PS through electrostatic interactions (McLaughlin, Wang et al. 2002). The ED of MARCKS has been well studied and contains 13 basic residues, five phenylalanines, and a myristoylated N-terminus (Figure 8). MARCKS has no set structure when it is bound or unbound to the membrane (Arbuzova, Schmitz et al. 2002). It combines myristoylation, hydrophobic insertions, and electrostatic interactions to bind to the plasma membrane in a non-specific manner. Based on binding data from MARCKS (McLaughlin, Wang et al. 2002) and helical reconstructions of a myosin-I showing the lack of electron density in the tail domain (Figure 48) (Jontes and Milligan 1997), we initially hypothesized that myo1c bound to the membrane in a non-specific manner similar to the ED of MARCKS. We further hypothesized that the structure of the myo1c tail domain might be disordered and that interacting with the membrane could induce the folding of an amphiphatic helix, creating a highly concentrated positive electrostatic potential that would bind to the negatively charged membrane. Membrane localization of the ED of MARCKS requires an interaction with multiple PS molecules. It was predicted and subsequently demonstrated that the ED preferentially bound to lipid headgroups in which the negative charges were already clustered. The prime candidate for a lipid with such a head group was PIP_2, which has a charge of -4 at pH 7 (McLaughlin, Wang et al. 2002). Since PIP_2 only contributes ~ 1% of the plasma membrane, the binding interaction between myo1c and PIP_2 would have to require a tight 1:1 stoichiometry of myo1c : PIP_2, or a cooperative binding to multiple PIP_2 molecules.

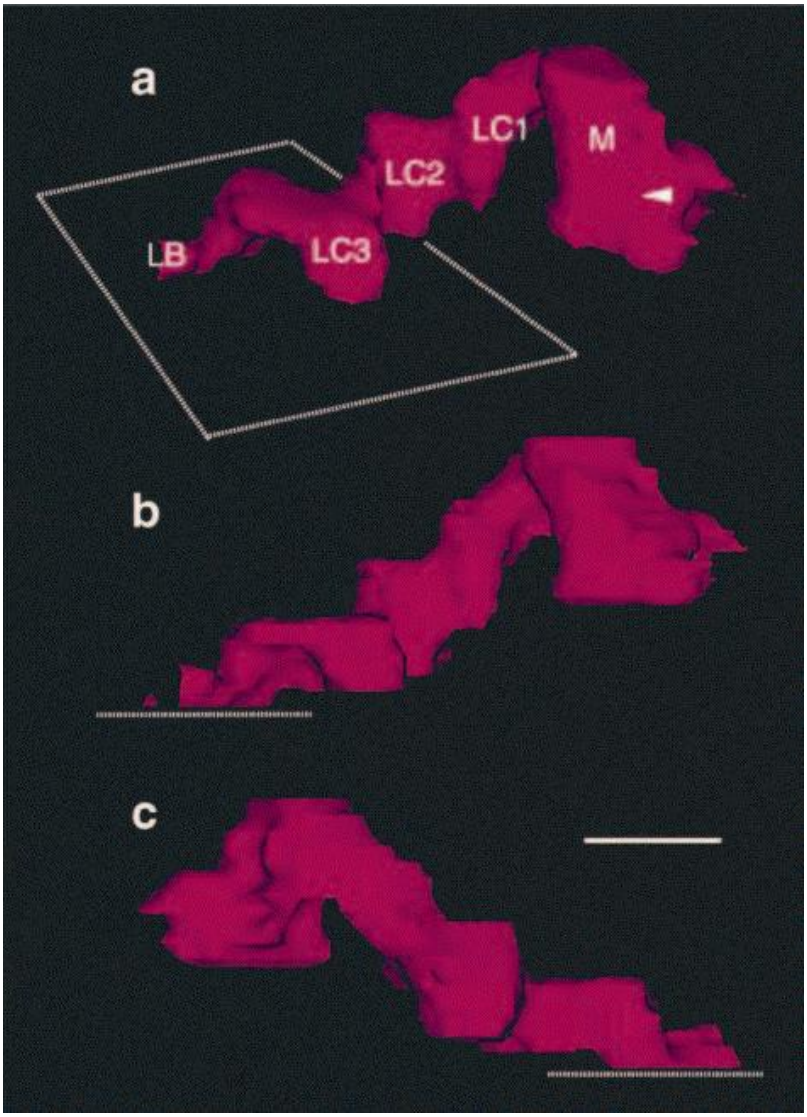

Figure 48 3D model of myo1a

Figure 48A-C: A three dimensional model of myo1a from (Jontes and Milligan 1997). A) M, motor domain; LC1, 2, and 3, the three CaM light chains; LB, lipid binding domain. The deduced actin binding site is indicated by the arrow. The plane of the membrane is illustrated by the dotted lines. B) and C) are side views of the model. The scale bar represents 45 Å.

4.1.1.2 Myo1c Binds PIP_2 Headgroup

To determine if MARCKS's non-specific binding mechanism was an appropriate model for the interaction between myo1c and PIP_2, we measured the binding of myo1c-tail to PIP_2 and found that like MARCKS, myo1c bound PIP_2 preferably over PS (Table 1). However, unlike proteins with polybasic EDs, (McLaughlin, Wang et al. 2002) , the interaction did not appear to be cooperative, as determined by the lack of a lag phase when myo1c bound to increasing molar concentrations of PIP2 (Figure 29). In addition, myo1c was unable to cluster multiple PIP_2 molecules together upon binding to the membrane, as measured by FRET. Moreover, we determined that myo1c bound to Ins(1,4,5)P_3 directly, and that this interaction was slightly tighter than that for PIP_2. Proteins with polybasic EDs cannot bind to soluble inositol phosphates derivatives because they are not presented in a multivalent manner within the membrane like phosphatidyl inositols. This is referred to as a reduction of dimensionality and can increase the effective concentration of a substrate 1000-fold (Adam 1968). Thus, the interaction of myo1c for PIP_2 was not cooperative, but specific for the headgroup of the lipid. This led us to form a new hypothesis that the mechanism of myo1c binding to the membrane was more similar to the specific interaction of PLCδ-PH with PIP_2 (Lemmon and Ferguson 2001) rather than the electrostatic interaction of the polybasic ED of MARCKS with multiple PIP_2 molecules.

4.1.2 Myo1c Tail Domain Binds PIP_2

We now know that myo1c binds to the membrane through a specific interaction with the head group of PIP_2 and other phosphatidyl inositols. The myo1c tail domain is necessary and sufficient to localize myo1c to the membrane. This high affinity interaction drives the association of myo1c to the plasma membrane and other membrane regions rich in poly-phosphatidyl inositols. We show through sedimentation assays that myo1c binds PIP_2 with a partition coefficient of K_{eff}^{acidic} = 0.23 μM. The interaction of myo1c with PIP_2 has a 1:1 stoichiometry as evidenced by our data from PIP_2 molar percentage experiments, as well as our data showing that myo1c can bind to $Ins(1,4,5)P_3$. All evidence points to a similar binding mechanism to the canonical PIP_2 binding PLCδ-PH domain. This similarity is further supported by our data showing that mutating one of two conserved residues of the PH domain signature motif, both essential for PIP_2 binding in certain PH domains, in the myo1c-tail completely eradicates binding to PIP_2 and membrane localization.

Many PH domains contain a specific binding pocket for the phosphorylated inositol rings of phosphatidyl inositols. These pockets are made up of multiple hypervariable loops that form hydrogen bonds to the phosphates on the inositol rings of phosphatidyl inositols (Lemmon and Ferguson 2001). The first of these loops between β-strand 1 and β-strand 2 is where the PH domain signature motif lies. Slight variations in the non-conserved residues found on these loops give rise to the binding specificity to particular phosphatidyl inositols (Cronin, DiNitto et al. 2004). We found that myo1c bound promiscuously to many inositol phosphates through our competitive inhibition

assays. Although no structure is known for the tail domain of myo1c, we hypothesize that it contains a binding pocket made up of loops containing basic residues required for hydrogen bonding with the phosphates of phosphatidylinositols. Myo1c shares sequence homology with many other myosin-I isoforms from vertebrates and other eukaryotes; slight differences in the non-conserved residues of these loops may lead to stereo-specific interactions with particular phosphatidyl inositols, much like that seen in the hypervariable loops of PH domains (Lemmon and Ferguson 2001). This would lead to an isoform specific localization of myosin-Is in the cell due to the non-uniform expression and localization of phosphatidyl inositols. Although all of our membrane binding data with myo1c supports characteristics of its tail domain containing a phosphatidylinositol binding PH domain, we are unable to classify it as a PH domain because no structure is known.

4.1.3 Biological Relevance of PIP_2 Binding

Phosphatidylinositols are concentrated in actin-rich structures where they regulate the activity of several cytoskeletal proteins, including activators of the Arp2/3 complex, actin severing and capping proteins, and actin monomer binding proteins (Insall and Weiner 2001; Yin and Janmey 2003). PIP_2 production spatially and temporally regulates phagocytosis, macropinocytosis, endocytosis, ion channel function and cell protrusion. Myosin-I isoforms are also enriched in these regions and function in these processes (Yin and Janmey 2003). One role of phosphatidylinositols in actin-rich

structures may simply be to serve as spatially and temporally regulated membrane anchors for myosin-I isoforms, allowing the recruitment of myosin-I to function in endocytosis (Novak, Peterson et al. 1995; Jung, Wu et al. 1996; Swanson, Johnson et al. 1999; Ostap, Maupin et al. 2003), secretion (Bose, Guilherme et al. 2002), and membrane retraction. However, myosin-I isoforms may also use their barbed-end-directed motor activity to keep the fast-growing ends of the actin filament oriented toward the membrane and phosphatidylinositol regulators of the cytoskeleton (Jung, Remmert et al. 2001).

Myosin-I isoforms may also link phosphatidylinositols to other regulatory proteins. For example, β-catenin and dynamin have been shown to bind myosin-I in *Drosophila*, where they play a role in the control of left-right asymmetry during development (Hozumi, Maeda et al. 2006; Speder, Adam et al. 2006). However, the function of myosin-I in these processes is not understood, and it is not known if the motor and phosphatidylinositol binding activity of myosin-I drives the localization of these proteins, or if myosin-I is targeted to specific regions by binding to these proteins. PHR1, a recently identified integral membrane protein present in the sensory cells of the inner ear, binds myo1c and may link it to stereocilia membranes (Etournay, El-Amraoui et al. 2005). Myo1c is the likely motor that drives mechanical adaptation in hair cells (Batters, Arthur et al. 2004; Gillespie and Cyr 2004), and depletion of PIP_2 inhibits this adaptation (Hirono, Denis et al. 2004). Therefore, it is likely that PHR1 and PIP_2 act to link myo1c to the adaptation complex (Hirono, Denis et al. 2004; Etournay, El-Amraoui

et al. 2005). It is interesting to speculate that control of the levels of membrane phosphatidylinositol regulates the assembly of this motor complex.

4.1.4 The Regulatory Domain and Membrane Association

The original hypothesis of a membrane induced, α–helical binding site could still hold true for a separate, secondary membrane binding site. In fact, our data showed that there was an electrostatic component to the binding of myo1c to the membrane, given that myo1c bound to LUVs comprised of ≥ 60% PS and that the addition of NaCl was able to inhibit binding of myo1c to either LUVs of PS or PIP_2. However, it is more likely that our data supports a model which implicates the regulatory domain as the secondary binding site of myo1c (Swanljung-Collins and Collins 1992; Tang, Lin et al. 2002; Hirono, Denis et al. 2004). This model was derived from the existence of several basic residues in the three IQ motifs of the regulatory domain. A Ca^{2+}-induced conformational change or dissociation of one or more of the three CaM bound to the IQ motifs could reveal positive charges (Figure 31).

Our sedimentation assays confirmed that the regulatory domain of myo1c was capable of binding negatively charged phospholipid membranes *in vitro* in a Ca^{2+}-dependent manner, as proposed for myo1a (Collins and Swanljung-Collins 1992) and myo1c (Tang, Lin et al. 2002; Hirono, Denis et al. 2004). A myo1c construct lacking the tail domain but still containing the regulatory domain was able to bind to LUVs comprised of ≥ 40% PS with high affinity in the presence of 10 μM Ca^{2+}. We also

found that the affinity of the myo1c-tail interaction increased ~5-fold with the inclusion of 20% PS in LUVs that contained 2% PIP_2. This indicated that the regulatory domain could potentially play a secondary role in membrane attachment, with the primary association occurring via phosphatidylinositol-tail interactions. Nevertheless, this secondary binding site alone could not explain the physiological binding of myo1c to the membrane since the typical inner leaflet of the membrane contains less than 30% PS. For myo1c to bind to the plasma membrane in a cell, it must rely on its primary lipid binding site in the tail domain.

TIRF/FRAP experiments revealed that the regulatory domain was not necessary for plasma membrane association in live cells. Although the high expression levels of the GFP constructs and the short acquisition integration time prevented us from confidently examining subtle changes in subcellular localizations, we were able to detect membrane binding of GFP-myo1c-tail^{IQ0} with dissociation rates similar to GFP-myo1c. One can speculate that although the motor and regulatory domains are not required for membrane association, they may have an effect on the subcellular localization to micro domains on the membrane. In fact, the motor domain has been shown to be required for correct subcellular localization of other myosin-Is (Ruppert, Godel et al. 1995; Tang and Ostap 2001; Bahler and Rhoads 2002); however, our IQ motif deletion constructs did not contain a motor domain, so we could not study this directly. Although we could rule out the requirement of the regulatory domain for

plasma membrane attachment, further experiments are required to determine its role in myosin-I targeting (Cyr, Dumont et al. 2002).

4.2 Discovery of the PIP_2 Binding Site.

4.2.1 Identifying a Putative PH Domain

We were able to identify the PIP_2 binding site of myo1c through discovering predicted secondary structure homology to a specific region in poly-phosphatidylinositol binding (PPB) PH domains. This region contained the PH domain signature motif of conserved basic residues (K-X_n-(K/R)-X-R) (Isakoff, Cardozo et al. 1998; Cronin, DiNitto et al. 2004). We validated this sequence similarity to PPB PH domains by testing single point mutations in our myo1c construct that are conserved and known to disrupt PIP_2 binding in these domains. As with PPB PH domains that contain (K-X_n-(K/R)-X-R), these point mutations completely eradicated myo1c binding to PIP_2 *in vitro* and disrupted membrane localization *in vivo*. These data supported our finding that the tail domain of myo1c is both sufficient and necessary for membrane localization in the cell.

In a collaboration with Dave Sept (Washington University, St. Louis, MO), we preformed *ab initio* structural prediction calculations of residues P802-R1028 within the myo1c tail domain. These calculations resulted in a modeled structure that could not be classified as a PH domain, but showed some structural similarity to PH domains (see chapter 2). These similarities included the β1-loop-β2 region (Figure 49B) and a β-

sheet core structure, although it was not continuous (Figure 49A). Specifically, when compared with the PH domain of PDK1, we saw that the structural alignment over the β1-loop-β2 region was very good (Figure 49), giving a protein backbone RMSD of 3.5 Å with a sequence identity of 61% (Figure 43). However, the computation predicted neither a seven stranded β-sheet core, nor a distinct C-terminal α-helical cap as defined in all PH domain structures (Lemmon and Ferguson 2001), which may have been a limitation of the computational method, or may reflect actual differences in the structure.

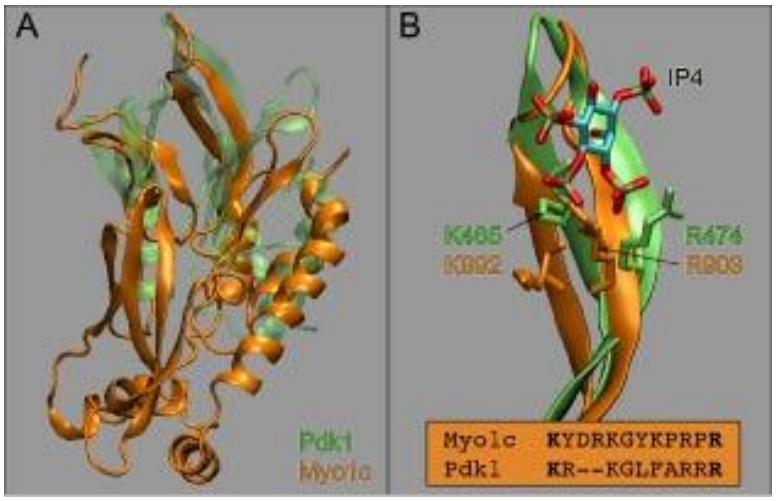

Figure 49 Predicted PIP_2 binding structure

Figure 49A-B: Figure was originally published in (Hokanson, Laakso et al. 2006). A) Predicted structure for the myo1c tail region (orange) compared with the Pdk1 structure (green). (B) Detailed comparison of the β1-loop-β2 region of PDK1 and the predicted structure of the Myo1c tail. Two of the residues in Pdk1 involved in coordinating the Ins(1,3,4,5)P_4 molecule align with our two mutations at K892 and R903 (see sequence inset).

Since our *ab initio* modeling cannot identify a PH domain in the myo1c tail, it is possible that this region is a novel PIP_2 binding motif with only partial sequence and structural elements similar to PH domains. It is also possible, and perhaps likely, that the *ab initio* model is wrong. Low electron density of the tail domain from electron microscopy and helical reconstructions suggests this region may be flexible (Jontes and Milligan 1997). A flexible region could enable a myo1c bound to PIP_2 to bind to an actin filament at various places along its helical pitch. Therefore, more binding sites would be available on a given actin filament, which would increase the chance of it binding to myo1c as it approaches the membrane from varying angles.

This alternative model is quite intriguing since it may lead to the discovery of a new phosphatidyl inositol binding domain found among the short-tail vertebrate myosin-Is, as well as myosin-Is from many other eukaryotes. As discussed earlier, slight differences in sequence could lead to subtle changes in spatial or temporal localization. Defining this binding site is an important step in our understanding of the interaction between myosin-Is and the membrane. Knowing which residues are important to membrane binding will help in the understanding of diseases and drug targeting involving myosin-I motors.

Further characterizing this domain will also help in understanding the seemingly redundant nature of expressing multiple myosin-I isoforms in the same cell. It has been shown that knocking down the expression of a single myosin-I isoform shows little to no phenotype in some cells because there are complimentary myosin-I isoforms that

will take its place (Jung, Wu et al. 1996). In fact, a myo1a knock out mouse showed ectopic recruitment of myo1c to the region where myo1a normally resides (Tyska, Mackey et al. 2005). In many of the cases studied, there appears to be an overlap of localization as well as function. Myo1c and myo1e are both found at the vesicles containing cortical granules within a short time span, yet play unique roles (Sokac, Schietroma et al. 2006; Schietroma, Yu et al. 2007). We found no obvious dominant negative effects from the over-expression of either GFP-tail or GFP-myo1c-R902A (Figure 40). To further define the membrane binding domain, detailed structural information is imperative. This will allow a better understanding of the structural diversity within the myosin-I isoforms needed to decipher their overlapping, but possibly non-redundant functions.

4.2.2 Inositol Phosphate Specificity

We showed through gel filtration and competitive binding assays that myo1c bound to inositol phosphates directly with similar affinities to PIP_2. These affinities were similar to those of PH domains specific for inositol phosphate $Ins(1,4,5)P_3$, including PLCδ, K_d = 0.21 μM (Lemmon, Ferguson et al. 1995), $Ins(1,3,4,5)P_4$, including Btk, K_d = 0.040 μM (Baraldi, Carugo et al. 1999), and Pdk1, K_d = 0.014 μM (Komander, Fairservice et al. 2004). We found that although myo1c seemed to be quite promiscuous and bound to most of the inositol phosphates with affinities within a factor of three, it bound to $Ins(1,2,6)P_3$ with a 10-fold weaker affinity and did not bind

$Ins(3)P_1$ detectably. Therefore, the binding affinity was not based on the charge of the inositol phosphate alone, but was dependent on the positions of the phosphates on the inositol ring. Our experiments suggested that phosphates at the 4 or 5 positions were required for tight binding, while phosphates at the other positions did not prevent binding.

Myo1c should be able to bind lipids that have headgroups listed in Table 3, with PIP_2 ($Ins(1,4,5)P_3$ headgroup) and PIP_3 ($Ins(1,3,4,5)P_4$ headgroup) being the most prevalent in the membrane and the most relevant to the proposed functions of myo1c (Yin and Janmey 2003). The plasma membrane concentration of PIP_2 is much higher than PIP_3 in both unstimulated and stimulated cells (Insall and Weiner 2001; Dormann, Weijer et al. 2002). Thus, in the absence of other phosphatidylinositol binding proteins, we would expect myo1c to interact with PIP_2 based on its higher concentration (McLaughlin and Murray 2005). However, our *in vitro* biochemical experiments may not take into account the presence of other cellular phosphatidylinositol binding proteins. Further cellular experiments are required to determine *in vivo* specificity and binding of myo1c.

4.2.3 Phosphatidylinositol Binding by Other Myosin-I Isoforms

Alignment of myo1c with the seven other vertebrate myosin-I isoforms showed sequence conservation in the β1-loop-β2 motif region of the putative PH domain. The highest sequence similarity was among the short tail myosin-I isoforms (myo1a, myo1b,

myo1c, myo1d, myo1g). Thus, we proposed that the short-tail isoforms will bind to phosphatidylinositols in a manner similar to myo1c. We also found extended sequence similarities of this region to myosin-Is from other species including 61F and 31DF from *Drosophila*, hum-5 and hum-1 from *C. elegans*, and Myo3 and Myo5 from *S. cerevisiae*. However, given that this region was not completely conserved, it is possible that the different short-tail isoforms differ in their phosphatidylinositol affinity and specificity. This would enable different myosin-I isoforms to localize to different sub-regions on the plasma membrane depending on local concentrations of phosphatidylinositols.

Long-tail myosin-I isoforms have been shown to bind acidic phospholipids (Adams and Pollard 1989; Miyata, Bowers et al. 1989; Stoffler, Ruppert et al. 1995). However, vertebrate long-tail myosin-I isoforms (myo1e and myo1f) contain only the N-terminal portion of the PH domain signature motif. Although their sequences diverge from the signature motif in the putative loop region, they do contain several positive charges that may be positioned for phosphatidylinositol binding. It is possible that without hypervariable loops like those found in PPB PH domains, myo1e and myo1f may bind to the membrane in a manner more similar to the ED of MARCKS than to a PH domain.

4.3 Myo1c Lipid Binding Sites

4.3.1 Physiological Role of Binding PIP_2

We hypothesize that since levels of PIP_2 in the inner leaflet of the plasma membrane are estimated to be 5 - 10 µM, which is 10 – 1000 fold higher than most other phosphatidyl inositols (PtdIns4P is 3 µM) (Stephens, Jackson et al. 1993; McLaughlin, Wang et al. 2002), myo1c will more often bind PIP_2 preferentially over other phosphatidyl inositols. This leads to important implications within the cell including subcellular localization, PIP_2 sequestering, limited lateral diffusion rates, possible regulation, and tight binding.

4.3.1.1 Localization to High Concentrations of PIP_2 at the Membrane

PIP_2 has been implicated to exist at high local concentrations on the plasma membrane and in membrane structures within the cell (McLaughlin, Wang et al. 2002). This can be due to synthesis of PIP_2 at these regions, sequestering and clustering of PIP_2 by proteins, or segregation of PIP_2 into micro-domains. A higher local concentration should result in the recruitment of myo1c. This not only affects the spatial localization of myo1c, but also the temporal localization; additionally, the local concentrations of PIP_2 in the cell can be very dynamic. We have shown an example of this in NRK cells where myo1c tracks with a macropinosome enriched with PIP_2. One of the most important implications of high local concentrations of PIP_2 for myo1c is the role of myo1c as a motor in the adaptation response in hair cells.

4.3.1.2 Role of PIP_2 Binding in Hair Cells

PIP_2 has a distinct distribution in hair cells, being present only above the ankle link region of stereocilia and excluded from the basal region and apical surface of hair cells (Hirono, Denis et al. 2004). Inhibition of PIK4 reduces the rates of both slow and fast adaptation and causes a loss in transduction current (Hirono, Denis et al. 2004). Myo1c is required for the slow and fast adaptation in hair cells (Holt, Gillespie et al. 2002; Gillespie 2004), and it has been shown that the second IQ motif is necessary for proper myo1c localization in stereocilia (Cyr, Dumont et al. 2002; Phillips, Tong et al. 2006). The second IQ motif of myo1c is thought to interact with the cytoplasmic domain of cadherin 23, a component of the tip link, but is not sufficient for proper localization (Siemens, Lillo et al. 2004; Phillips, Tong et al. 2006). From these and other studies it is clear that the mechano-signal transduction and the adaptation response in hair cells requires both PIP_2 and myo1c.

We hypothesize that disrupting PIP_2 levels in hair cells disrupts the ability of myo1c motors to be linked to the transduction channel and facilitate an adaptive response. One model that would explain this is that myo1c binds to PIP_2 through its tail domain and cadherin 23 through its second IQ motif, linking myo1c to both the transduction apparatus and to the surrounding membrane while it is bound to the bundled actin filaments through its motor domain. These interactions could cluster the estimated ensemble of 50 – 200 myo1c motors to the transduction apparatus and enable them to adapt to the transduction channel opening. Without either of these interactions present, transduction ceases and adaptation is lost.

An opposing model is that the IQ motifs bind to both cadherin 23 and PIP_2. Since the IQ motifs of myo1c are highly basic, it is reasonable to assume that they could provide a secondary binding sight to a high local concentration of PIP_2 and would be sufficient for localization. In fact, this has been confirmed using PIP strips (Hirono, Denis et al. 2004) and a myo1c construct containing only the IQ motifs. However, we believe that this interaction is not physiological and only exists due to the abnormally high density of PIP_2 present on the PIP strips, as our myo1c-motor construct did not bind to up to 10% PIP_2 LUVs. Any positively charged peptide is likely to bind to PIP strips; however, this does not mean that it will bind to PIP_2 at physiological concentrations in the cell. Therefore, I believe that the IQ motifs are responsible for binding to cadherin 23 or another transduction apparatus receptor, and that the tail domain is responsible for binding to PIP_2.

4.3.1.3 Sequestering PIP_2

We showed that myo1c is unable to cluster multiple PIP_2 molecules together; however, one can imagine how multiple myo1c molecules decorating an actin filament might be able to align a string of PIP_2 molecules along the actin filament. In a branched network of actin filaments close to the plasma membrane, this could create a high density of PIP_2 molecules that have a low lateral diffusion coefficient and are unable to bind to other proteins. A secondary effect of this is that if PIP_2 binds laterally to intermembrane proteins, this would give rise to the pickets in the picket fence model

that correlates with the mesh size of the actin cytoskeleton. More on this will be discussed later. Through a signaling event or regulation of myo1c, these PIP_2 molecules could be released, creating a local high concentration of PIP_2 for other proteins to bind. This has been shown previously with MARCKS protein which can bind to multiple PIP_2 molecules (Glaser, Wanaski et al. 1996).

Our digestion experiments with trypsin revealed that myo1c is protected from digestion in the presence of $Ins(1,4,5)P_3$. Binding to PIP_2 in the cell may protect myo1c from being degraded by protecting sites targeted by proteinases. Selecting non-membrane bound myo1c for degradation could be a way to regulate the over-expression of myo1c and limit its presence in the cytoplasm.

4.3.2 Physiological Role of the Regulatory Domain in Membrane Association

The primary proposed role of the regulatory domains of all myosins is that it acts as a lever arm that transduces the force of the motor domain. It has been shown that light chains, most likely CaM, bind to the long single α-helix to give it enough rigidity to hold firmly in place during a powerstroke. Without light chains bound, it is thought that the lever becomes flaccid (Zhu, Beckingham et al. 1998). From our binding data collected with the myo1c-motor construct and myo1c-tail with LUVs of 20% PS and 2% PIP_2, it is apparent that the regulatory domain plays a role in membrane binding. Once myo1c has been localized to the plasma membrane via the tail domain

binding to PIP_2, it is likely that at least one of the IQ motifs will contribute to binding by a conformational change or dissociation of a CaM.

4.3.2.1 Sequestering of the Lever Arm

One consequence of the regulatory domain binding to the membrane is that it will shorten the effective lever arm of the motor considerably depending on which of the IQ motifs binds to the membrane. Myo1c has a powerstroke of 4.2 nm (Batters, Arthur et al. 2004) and it has been shown that the number of IQ motifs linearly affects the length of the working powerstroke of myosin-V (Sakamoto, Wang et al. 2003). If the IQ motif furthest from the motor domain loses its CaM and binds to the plasma membrane, it will essentially change the length of the powerstroke from three IQ motifs to two. This shortening of the lever arm could be a way to regulate the length of the powerstroke in the cell. However, if the IQ motif closest to the motor is affected, it will also shorten the length of the powerstroke considerably. This would have a drastic affect on the function of the myo1c and may even inhibit it from acting as a conventional molecular motor. In this latter case, myo1c would instead act as a very short tether, maintaining a bond between the actin cytoskeleton and the plasma membrane.

Although an IQ motif providing an additional binding site to the plasma membrane may shorten the length of the powerstroke, it may provide an additional anchoring point. As will be discussed later in more detail, for a myosin-I to be an

effective motor while it is bound to the membrane, it must remain anchored in the membrane and not fluid during a powerstroke. Although it has been shown that PIP_2 has a much lower lateral diffusion rate than other lipids (Cho, Kim et al. 2005), an additional binding site to multiple PS molecules may stabilize myo1c positioning on the membrane.

4.3.2.2 Stabilizing Myo1c in the Absence of CaM

Another possibility for the function of the regulatory domain in myo1c binding to the plasma membrane is to prevent the aggregation of myo1c. Ca^{2+} was found to prevent myo1c from dissociating from 60% PS LUVs, even after washout with EGTA (Tang, Lin et al. 2002). This suggests that in the presence of excess Ca^{2+}, myo1c binding to the membrane is irreversible in the absence of excess CaM. Myosins are notorious for aggregating when they are in the absence of light chains. When a CaM dissociates from myo1c, binding to the membrane may be a way for myo1c to prevent aggregation, thus stabilizing its regulatory domain and preventing it from binding to potentially harmful binding partners that would cause aggregation. Therefore, the plasma membrane could act much like a chaperone protein, binding to unstable regions of the protein until a light chain is available for binding.

4.3.2.3 Lower Dissociation Rates

We propose that the main function of the regulatory domain of myo1c bound to the membrane is that it changes the kinetics of membrane association by decreasing the dissociation rate. The K_{eff}^{lipid} increases 10-fold when 20% PS is added to LUVs comprised of 2% PIP_2. Since association rates are fast and diffusion limited (Tang, Lin et al. 2002), the only way to explain this is that the dissociation rates decrease 10-fold. This would allow myo1c to proceed through more ATPase cycles (1 s^{-1}) while still bound to the membrane if it is acting as a motor, or keep myo1c associated with the membrane longer if the primary role of myo1c bound to the plasma membrane is to act as a tether.

4.4 Force and Function.

The apparent second-order association rate (k_a) of myo1c for 60% LUVs is ~0.16 μM^{-1} s^{-1}. For binding in terms of LUV concentrations, this rate can be considered as diffusion limited at 2 x 10^{10} M^{-1} s^{-1}. (Tang, Lin et al. 2002). We measured the partition coefficient of myo1c to 2% PIP_2 + 20% PS LUVs to be K_{eff}^{lipid} = 4.0 ± 1.5 µM. If we ignore that K_{eff}^{lipid} is not a true K_d, and that the association rate for 60% PS LUVs is the same as for 2% PIP_2 + 20% PS LUVs, we can calculate a dissociation rate in accordance with:

Equation 9

$$K_d = \frac{k_d}{k_a}$$

An apparent k_d calculated as 0.040 s^{-1} for myo1c dissociating from 2% PIP_2 + 20% PS LUVs *in vitro*. As mentioned, there are limitations to this calculation so this number should be taken lightly as an approximation. This calculated value is in close agreement with the *in vivo* dissociation rates we measured in our TIRF/FRAP experiments (0.05 s^{-1}). Since the ATPase rate of myo1c is 1 s^{-1} (Gillespie, Gillespie et al. 1999), myo1c should be able to go through ~20 ATPase cycles before dissociating from the membrane at high ATP concentrations. Whether the ATPase activity of a myo1c can produce force relative to the membrane to which it is bound will be discussed below.

It is well established that the plasma membrane is fluid and dynamic. One of the biggest questions that still remains regarding myosin-Is is if they can act as a motor while bound to the membrane. When forces are applied in plane with the membrane, can a myosin-I molecule that is bound remain anchored during a powerstroke? When forces are applied perpendicularly, can myo1c stay bound to the membrane, thus stretching and deforming the membrane itself, or will it be pulled off? These are two fundamental questions that still need to be answered to understand the functions of myo1c.

4.4.1 Forces Planar to the Membrane

Testing the notion of myo1c remaining anchored in the plasma membrane while experiencing forces in plane with the membrane is essential to identifying the possible

functions of myosin-Is (Figure 50). For myo1c to be functional as a motor while bound to the membrane, it must be stationary at forces up to 2 pN, the estimated force of a myo1c powerstroke (Gillespie and Cyr 2004). We can estimate the minimum velocity of an individual powerstroke of myo1c by dividing the powerstroke distance of 4.2 nm by the lifetime of actin attachment 50 ms (Gillespie and Cyr 2004) to get a velocity of 0.084 µm/s. To withstand forces of up to 2 pN, the drag coefficient of myo1c on the membrane would have to be greater than 2.4 x 10^{-11} N·s/µm in accordance with:

Equation 10

$$F = v\gamma$$

where F is the force against the plane of the membrane, v is the velocity of the powerstroke, and γ is the drag coefficient. Using the Einstein relation,

Equation 11

$$D = \frac{kT}{\gamma}$$

where D is the lateral diffusion coefficient, and kT is the Boltzman constant at 37 °C, 4.11 x 10^{-15} N·µm, this would require the lateral diffusion coefficient of a myo1c bound to the plasma membrane to be less than 1.7 x 10^{-4} $\mu m^2/s$.

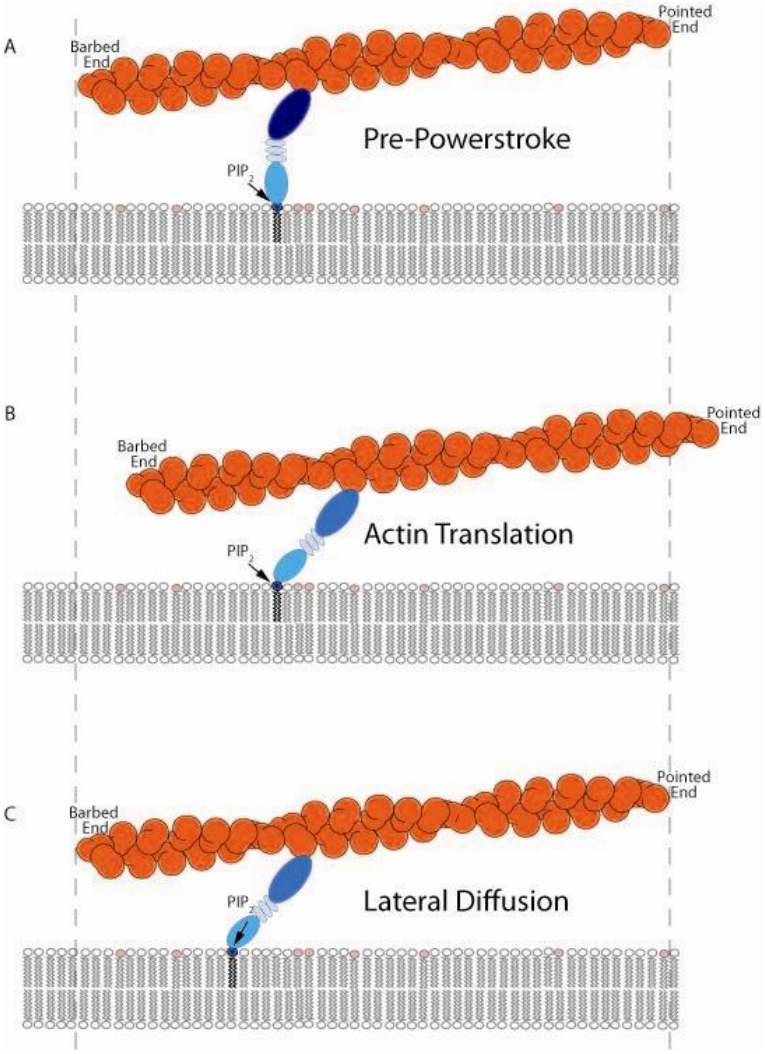

Figure 50 Forces planar to the membrane

Figure 50: Cartoon of myo1c producing forces planar to the membrane. A) Myo1c bound to both actin and PIP_2 pre-powerstroke. B) Myo1c bound to the membrane remains stationary as the actin filament is translated relative to the membrane after a powerstroke. C) Actin filament remains stationary as myo1c bound to PIP_2 laterally diffuses in the membrane after a powerstroke.

4.4.1.1 Lateral Diffusion

A diffusion coefficient of 1.7 x 10^{-4} $\mu m^2/s$ is much slower than the diffusion rates measured for many lipids (6 $\mu m^2/s$) (Scandella, Devaux et al. 1972) and integral membrane proteins (0.5-2 $\mu m^2/s$) (Snapp 2003). Diffusion rates of phosphatidyl inositol associated proteins, such as PLCδ-PH domain, have been measured using FRAP to be close to cytoplasmic diffusion rates (3.5 $\mu m^2/s$); however, no controls for the possibility of the dissociation of bleached proteins from the membrane and association of unbleached protein were shown (Brough, Bhatti et al. 2005). Additionally, it was found for eGFP-PH123 that the mean-squared deviation in position did not increase with time and remained close to the limit of position detection (0.03 μm^2) (Mashanov, Tacon et al. 2004).

Interestingly, the diffusion rate for PIP_2 was recently measured to be as low as 3.9 e^{-4} $\mu m^2/s$ in mouse arterial myocytes (Cho, Kim et al. 2005). The diffusion rate was found to be dependent on the cytoskeleton and is ten thousand times slower than other phosphatidyl inositols measured in the same study. PIP_2 with a lateral diffusion coefficient of 3.9 e^{-4} $\mu m^2/s$ would provide the approximate resistance for a myo1c motor to translate an actin filament in relation to the plane of the membrane during a powerstroke.

There are many possibilities that could account for the five orders of magnitude difference in lateral diffusion rates between PIP_2 and other lipids. It has been suggested that lipids can segregate into microdomains created by mismatches in hydrophobic

thickness, van der Waals interactions, and acyl chain entropy (Marguet, Lenne et al. 2006). Thus, PIP_2 could be segregated into these microdomains which may have a lower overall diffusion rate than the rest of the membrane. Although PIP_2 has a polyunsaturated chain and should not partition into microdomains without other factors acting on it (McLaughlin, Wang et al. 2002), studies have shown that some microdomains are enriched in PIP_2 (Golub, Wacha et al. 2004).

A possibility that also accounts for the dependence on the cytoskeleton is that the lateral diffusion of PIP_2 could be limited by the mesh size of the cytoskeleton, a model commonly referred to as the picket fence model (Sako and Kusumi 1995). In this model, it is suggested that the actin cytoskeleton acts as a fence that encloses a domain of lipids and lipid-bound proteins. Transmembrane proteins that are associated with the cytoskeleton act as pickets in the membrane and further limit the mobility of lipids from diffusing outside of these domains. The actin cytoskeleton lies close to the plasma membrane at just 10.2 nm (Morone, Fujiwara et al. 2006). The mesh sizes created by the actin network differ from cell types, ranging from 0.0027 μm^2 in FRSK cells and to 0.039 μm^2 in NRK cells. These measurements correlate well with the measured lateral diffusion of a fluorescently labeled phospholipid used in the same study, which diffused within a compartment of 0.0021 μm^2 in FRSK cells and 0.043 μm^2 in NRK cells (Morone, Fujiwara et al. 2006). However, this model alone cannot explain the five magnitude difference in lateral diffusion rates of PIP_2 to other phospholipids. Incorporating the findings that so many proteins bind to PIP_2 and not to

other phospholipids might be enough to explain the lower diffusion rates. The lateral diffusion rates of these proteins would be limited by the cytoskeleton, thus limiting PIP_2 bound to them, while phospholipids not bound to proteins would be free to diffuse.

An alternative explanation is that the low lateral diffusion rates observed for PIP_2 may be the effect of myo1c binding rather than the cause of myo1c having a low lateral diffusion rate while it is bound to PIP_2. The most likely explanation for the five magnitude lower diffusion rate of PIP_2 to other phospholipids is a direct link between PIP_2 and the cytoskeleton. It has been shown that PIP_2 levels regulate membrane dynamics and cell shape by locally increasing and decreasing the interactions between the plasma membrane and actin cytoskeleton (Raucher, Stauffer et al. 2000). The low diffusion rate of PIP_2 could be the effect of myo1c or another protein linking the phosphatidyl inositol directly to the cytoskeleton. If PIP_2 is linked to the cytoskeleton through a protein tether, it would significantly inhibit its lateral diffusion, which would explain the large difference between lateral diffusion rates between PIP_2 and other phospholipids. With the cytoskeleton being within 10.2 nm of the plasma membrane (Morone, Fujiwara et al. 2006), it is plausible that myo1c may function as a protein tether, especially given that a similar myosin-I, myo1a, has an estimated length of 22 nm (Jontes and Milligan 1997). However, PIP_2 would not be able to anchor myo1c to the membrane if myo1c is the reason for the lateral diffusion rate of 3.9×10^{-4} $\mu m^2/s$.

4.4.2 Force Perpendicular to the Membrane

An alternative function of myo1c bound to the membrane is to deform the membrane by applying forces perpendicular to the membrane rather than in the plane of the membrane (Figure 51). We estimate that these interactions will withstand forces greater than 40 pN because under similar conditions, the detachment forces of myelin basic protein from the membrane has been measured to be more than 40 pN (Mueller, Butt et al. 1999). Myo1c could function in the deformation of the membrane to induce vesicle fusion or scission, as well as lamellipodia and neuronal growth cone retraction and expansion. The force required to pull out a membrane tether *in vitro* was measured to reach ~50 pN and required the coordinated pulling of multiple motors (Leduc, Campas et al. 2004). At these forces, it is feasible that an ensemble of myo1c motors bound to PIP_2 on the membrane could pull out a membrane tether without being pulled off the membrane.

It is not necessary for myo1c to actively produce force to function in processes that deform the membrane. In both endocytic and exocytic events at the membrane, myo1c may act as a tether, connecting the growing barbed ends of actin filaments to sites of membrane deformation. This has been proposed as the function of myo1c in compensatory endocytosis of fertilized *Xenopus* eggs (Sokac, Schietroma et al. 2006). Actin polymerization alone can produce forces of up to 1 pN (Footer, Kerssemakers et al. 2007). Linking the growing ends of actin to the membrane at sites of endocytosis may induce stall forces on myo1c, keeping it bound to actin in an ADP bound state as the forming vesicle pulls the myo1c towards the pointed ends of an actin filament. This

would allow actin filaments to be properly oriented to produce the forces on the plasma membrane required for vesicle formation.

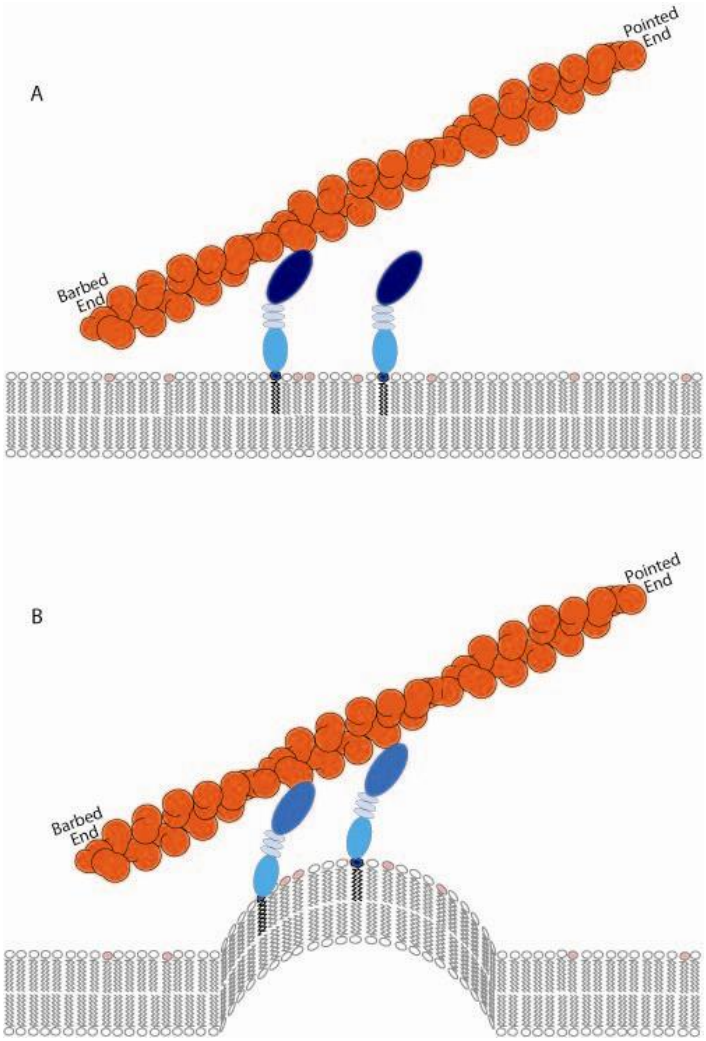

Figure 51 Forces perpendicular to the membrane

Figure 51: Cartoon of myo1c producing force perpendicular to the membrane. A) Myo1c bound to both actin and PIP_2 pre-powerstroke. B) Myo1c after powerstroke deforms the membrane as it pulls up perpendicularly to the membrane.

4.4.3 Model for Myo1c Recruitment to the Membrane

Myo1c diffusing in the membrane is under no load and acts as a low duty-ratio motor of 0.05 (Gillespie 2004). Myosin-Is have been shown not to bind to actin that is saturated with tropomyosin like filaments found in stress fibers. Thus, myo1c will diffuse until it reaches the dynamic actin network near the plasma membrane that is not coated with tropomyosin. Near the plasma membrane, myo1c will bind to free PIP_2 through its tail domain and then further strengthen its avidity through interactions of its regulatory domain with anionic lipids. PIP_2 and tropomyosin-free actin created by phosphatidylinositol production or release from sequestering proteins, and the activation of new actin polymerization respectively, will create newly available binding sites for myo1c. Myo1c will localize to these areas of high local concentrations of PIP_2 on the membrane. As myo1c bound to the membrane binds to actin and goes through its catalytic cycle, the motor will become strained, and its duty ratio will increase at stall forces (Figure 52). Myo1c in this state will act as a tether, linking the actin cytoskeleton to the plasma membrane.

An ensemble of myo1c motors in such a state has been hypothesized to maintain the tension on transduction channels in hair cells (Batters, Arthur et al. 2004). When the channel opens and tension is released, the ensemble of motors climbs up the actin filaments in the stereocilia until the channel is closed and the tension is reset. At the membrane, myo1c motors are held in an isometric contraction, linking the membrane to the underlying cytoskeleton; force from actin polymerization will act on the membrane as barbed ends are kept close to the membrane interface by myo1c (Figure 52). These

forces have been proposed to be involved in such processes as membrane fusion, compensatory endocytosis, and neuronal growth cone turning (Bose, Guilherme et al. 2002; Wang, Liu et al. 2003; Sokac, Schietroma et al. 2006). If the strain on myo1c is below its stall force, myo1c will complete its powerstroke, resulting in the translocation of the actin filament. This could be the result of a free actin filament, or many myo1c motors working together to produce a cooperative force. Therefore, an ensemble of myo1c motors working cooperatively could produce forces necessary to deform the membrane or even pull out a lipid tubule (Figure 52). In conclusion, myo1c has been determined be involved in many cellular processes at the membrane involving the actin cytoskeleton. Although many of the functional details are still elusive, knowing that myo1c binds tightly to PIP_2 is an important step to understanding the possible roles for myo1c.

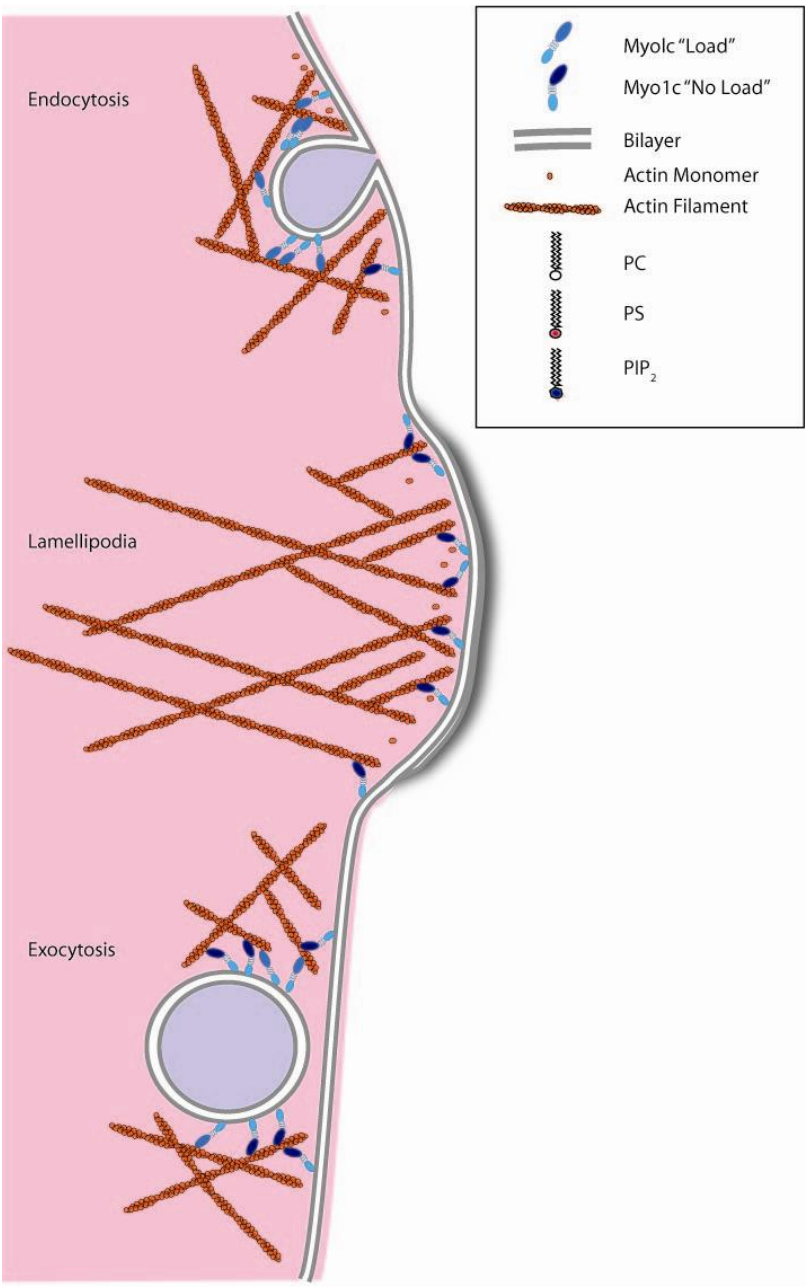

Figure 52 Model of Myo1c functions at the plasma membrane

Figure 52: Cartoon of 3 possible functions of myo1c at the membrane involved in endocytosis, lamellipodial extention, and exocytosis.

4.5 Future Directions

We have characterized the mechanism by which myo1c binds to the plasma membrane. Myo1c binds to the membrane through a direct interaction with the head group of PIP_2, and through a secondary, electrostatic interaction via the regulatory domain. There is still more work needed to be done to understand what role the myosin-I motors play as a link between the cytoskeleton and the plasma membrane. A full length construct containing the motor and tail domains of myo1c is essential to properly answer this question, as is a crystal structure of the PIP_2 binding region to better understand the specific binding site for PIP_2.

4.5.1 Myosin-I Isoform Phosphatidylinositol Binding Specificity

The characterization of the binding specificities of all of the myosin-I isoforms will lead to a greater understanding of their non-redundant localization and function in the cell. All of the short-tail isoforms contain the PH domain signature motif and are therefore predicted to bind to phosphatidylinositols. Long-tail isoforms have been shown to bind to the membrane, but do not contain the PH domain signature motif. Differences in non-conserved residues may lead to stereo-specificity of head group binding like that seen in PH domains. This would lead to subcellular localization of different myosin-I isoforms to membranes enriched in specific phosphatidylinositols. Regulation of phosphatidylinositols through kinases and phosphatases would also regulate the localization and activity of the myosin-Is that bind to them. Differentiating the specific phosphatidylinositol binding of the myosin-I isoforms as well as obtaining

crystal structures of their membrane binding sites will lead to a better understanding of their specific and non-redundant biological roles.

4.5.2 Forces

Determining the forces that myo1c can apply to the membrane during a powerstroke will define the functions that it can perform while bound to the membrane. Binding forces and lateral diffusion coefficients are needed to define these functions, and knowing these will allow us to better postulate whether or not myo1c will be able to translocate an actin filament relative to the membrane or deform the membrane. If myo1c cannot perform either of these functions, it is more likely that it acts as a tether or tension sensor rather than a motor while bound to the membrane. Finally, a full length construct is required to determine the possibilities and limitations of a myosin-I acting as a motor while bound to the membrane.

4.5.3 Regulation

How the interactions of myosin-Is with the membrane are regulated remains unknown. Many lipid binding proteins are regulated by the lipids themselves. Phosphatidylinositol levels at the membrane are highly dynamic and are controlled by many signaling cascades in the cell. However, this would require binding specifity of the different myosin-I isoforms. Other modes of regulation involve other proteins binding to the lipid binding site. One possibility is a protein sterically blocking the lipid

binding site with binding of another protein to inhibit membrane localization. Also, binding partners that are themselves membrane bound could enhance the association of a myosin-I with the membrane. In the case of myo1c, cadherin 23 is a transmembrane protein that could form a complex with myo1c and the transduction apparatus in the stereocilia of hair cells. Phosphorylation could also regulate the interactions of a myosin-I with the anionic membrane by neutralizing the basic charge of its binding site. Finally, one must consider Ca^{2+} regulation on the conformation and dissociation of one or more CaM from the regulatory domain. We have shown that Ca^{2+} increases the affinity of the regulatory domain for anionic lipids *in vitro*. Whether this increased affinity is physiologically relevant remains to be seen.

4.5.4 Binding Partners

The tail domains of the different short-tailed myosin-Is is the proposed region responsible for membrane association. However, this does not imply that their only function is to bind to lipids. The tail domains of myosin are generally thought of as a cargo binding domain. The tail domains of myosin-Is could have unique binding partners depending on the isoform. This would explain why there are multiple isoforms expressed in the same cell and their differing functions. Myo1c has been shown to bind to PHR1, NEMO, and cadherin 23; however, the function of each of these interactions is not clear. Determining the binding partners for all of the myosin-I isoforms is an

important step to complete their characterization and uncover what their biological roles are at the membrane.

5 Abbreviations

1. ADP adenosine diphosphate
2. ATP adenosine triphosphate
3. BSA, bovine serum albumin
4. Ca^{2+}, calcium ion
5. CaM, calmodulin
6. CHO, Chinese hamster ovary
7. COS-7, African green monkey cells
8. DAG, diacylglycerol
9. DEAE, Diethylaminoethyl
10. DLS, dynamic light scattering
11. DMEM, Dulbecco's Modification of Eagle's Medium
12. DNTB, 5,5´-dithiobis-(2-nitrobenzoic acid)
13. DTT, dithiothreitol
14. ECL, enzymatic chemilumenscence
15. ED, effector domain
16. EDTA, ethylenediamine tetraacetic acid
17. EF-hand, helix-turn-helix motif
18. EGTA, ethylene glycol tetraacidic acid
19. FBS, fetal bovine serum
20. FL, fluorescein
21. FLAG, polypeptide protein tag (N-DYKDDDDK-C)
22. FPLC, fast performance liquid chromatography

23. FRAP, fluorescence recovery after photobleaching

24. FRET, fluorescence resonance energy transfer

25. GFP, green fluorescence protein

26. GST, glutathione-S-transferase

27. ^{3}[H]Ins(1, 4,5)P_3, tritiated Ins(1,4,5)P_3

28. HEK 293T, human embryonic kidney

29. HEPES, 4-(2-hydroxyethyl)-1-piperazineethanesulfonic acid

30. HNa100, 10 mM HEPES, pH 7.0, 100 mM NaCl, 1 mM EGTA, 1 mM DTT

31. IgG, immunoglobulin G

32. Ins(1,2,3,5,6)P5, d-*myo*-inositol-1,2,3,5,6-pentakisphosphate

33. Ins(1,2,5,6)P4, d-*myo*-inositol-1,2,5,6-tetrakisphosphate

34. Ins(1,2,6)P3, d-*myo*-inositol-1,2,6-trisphosphate

35. Ins(1,3,4)P3, d-*myo*-inositol-1,3,4-trisphosphate

36. Ins(1,3,4,5)P4, d-*myo*-inositol-1,3,4,5-tetrakisphosphate

37. Ins(1,3,4,6)P4, d-*myo*-inositol-1,3,4,6-tetrakisphosphate

38. Ins(1,4,5)P3, d-*myo*inositol-1,4,5-trisphosphate

39. Ins(3)P1, d-*myo*-inositol-3-monophosphate

40. InsP6, d-*myo*-inositol hexakisphosphate

41. IPTG, isopropyl β-D-1-thiogalactopyranoside

42. K^+, potassium ion

43. LUV, large unilamellar vesicle

44. MARCKS, myristoylated alanine rich C kinase substrate

45. MES, 2-(N-morpholino)ethanesulfonic acid

46. Mg^{2+}, magnesium ion

47. N_2, nitrogen

48. NEMO, nuclear factor κB essential modulator

49. NRK, normal rat kidney

50. N-WASP, Neural Wiskott-Aldrich syndrome protein

51. OD, optical density

52. PA, phospatidic acid

53. PBS, phosphate buffered solution

54. PC, phosphatidylcholine

55. PDB, protein data bank

56. PDK1, 3-phosphatidylinositol-dependent protein kinase 1

57. PE, phosphatidyl ethanolamine

58. PG, phosphatidylglycine

59. PH, pleckstrin homology

60. PI, phospophoinositol

61. PI3K, phosphoinositol-3 kinase

62. PIP_2, phosphatidyl inositol-4,5-bisphosphate

63. PKC, protein kinase C

64. PLC, phospholipase C

65. PMSF, phenylmethylsulphonyl fluoride

66. PPB poly-phosphatidylinositol binding

67. PPD, p-phenylenediamine

68. PS, phosphatidylserine

69. RPMI, Roswell Park Memorial Institute medium

70. SDS-PAGE, sodium dodecyl sulfate polyacylamide gel electrophoresis ^{3}H-Ins(1,4,5,)P_3, Tritium labeled Ins(1,4,5,)P_3

71. SH3,src homology 3

72. SI, soybean inhibitor

73. TIRF, total internal reflection fluorescence

74. TMR, tetramethylrhodamine

6 Bibliography

Adam, G., Delbruck, M. (1968). Reduction of Dimensonality in biological diffusion procsses. San Francisco, Freeman.

Adams, R. J. and T. D. Pollard (1989). "Binding of myosin I to membrane lipids." Nature **340**(6234): 565-8.

Arbuzova, A., A. A. Schmitz, et al. (2002). "Cross-talk unfolded: MARCKS proteins." Biochem J **362**(Pt 1): 1-12.

Arbuzova, A., L. Wang, et al. (2000). "Membrane binding of peptides containing both basic and aromatic residues. Experimental studies with peptides corresponding to the scaffolding region of caveolin and the effector region of MARCKS." Biochemistry **39**(33): 10330-9.

Axelrod, D. (2001). "Total internal reflection fluorescence microscopy in cell biology." Traffic **2**(11): 764-74.

Axelrod, D., N. L. Thompson, et al. (1983). "Total internal inflection fluorescent microscopy." J Microsc **129**(Pt 1): 19-28.

Bahler, M. and A. Rhoads (2002). "Calmodulin signaling via the IQ motif." FEBS Lett **513**(1): 107-13.

Baraldi, E., K. D. Carugo, et al. (1999). "Structure of the PH domain from Bruton's tyrosine kinase in complex with inositol 1,3,4,5-tetrakisphosphate." Structure **7**(4): 449-60.

Barylko, B., M. C. Wagner, et al. (1992). "Purification and characterization of a mammalian myosin I." Proc Natl Acad Sci U S A **89**(2): 490-4.

Bateman, A., L. Coin, et al. (2004). "The Pfam protein families database." Nucleic Acids Res **32**(Database issue): D138-41.

Batters, C., C. P. Arthur, et al. (2004). "Myo1c is designed for the adaptation response in the inner ear." Embo J **23**(7): 1433-40.

Bentz, J. and N. Duzgunes (1985). "Fusogenic capacities of divalent cations and effect of liposome size." Biochemistry **24**(20): 5436-43.

Berg, J. S., B. C. Powell, et al. (2001). "A millennial myosin census." Mol Biol Cell **12**(4): 780-94.

Bonneau, R., C. E. Strauss, et al. (2002). "De novo prediction of three-dimensional structures for major protein families." J Mol Biol **322**(1): 65-78.

Bose, A., A. Guilherme, et al. (2002). "Glucose transporter recycling in response to insulin is facilitated by myosin Myo1c." Nature **420**(6917): 821-4.

Brough, D., F. Bhatti, et al. (2005). "Mobility of proteins associated with the plasma membrane by interaction with inositol lipids." J Cell Sci **118**(Pt 14): 3019-25.

Buser, C. A. and S. McLaughlin (1998). "Ultracentrifugation technique for measuring the binding of peptides and proteins to sucrose-loaded phospholipid vesicles." Methods Mol Biol **84**: 267-81.

Cho, H., Y. A. Kim, et al. (2005). "Low mobility of phosphatidylinositol 4,5-bisphosphate underlies receptor specificity of Gq-mediated ion channel regulation in atrial myocytes." Proc Natl Acad Sci U S A **102**(42): 15241-6.

Collins, J. H. and H. Swanljung-Collins (1992). "Calcium regulation of myosin I--a motor for membrane movement." Adv Exp Med Biol **321**: 159-63.

Coluccio, L. M. (1997). "Myosin I." Am J Physiol **273**(2 Pt 1): C347-59.

Cronin, T. C., J. P. DiNitto, et al. (2004). "Structural determinants of phosphatidylinositol selectivity in splice variants of Grp1 family PH domains." Embo J **23**(19): 3711-20.

Cullen, P. J., G. E. Cozier, et al. (2001). "Modular phosphatidylinositol-binding domains--their role in signalling and membrane trafficking." Curr Biol **11**(21): R882-93.

Cyr, J. L., R. A. Dumont, et al. (2002). "Myosin-1c interacts with hair-cell receptors through its calmodulin-binding IQ domains." J Neurosci **22**(7): 2487-95.

Dantzig, J. A., Y. E. Goldman, et al. (1992). "Reversal of the cross-bridge force-generating transition by photogeneration of phosphate in rabbit psoas muscle fibres." J Physiol **451**: 247-78.

Diefenbach, T. J., V. M. Latham, et al. (2002). "Myosin 1c and myosin IIB serve opposing roles in lamellipodial dynamics of the neuronal growth cone." J Cell Biol **158**(7): 1207-17.

DiNitto, J. P., T. C. Cronin, et al. (2003). "Membrane recognition and targeting by lipid-binding domains." Sci STKE **2003**(213): re16.

Doberstein, S. K. and T. D. Pollard (1992). "Localization and specificity of the phospholipid and actin binding sites on the tail of Acanthamoeba myosin IC." J Cell Biol **117**(6): 1241-9.

Dormann, D., G. Weijer, et al. (2002). "Visualizing PI3 kinase-mediated cell-cell signaling during Dictyostelium development." Curr Biol **12**(14): 1178-88.

El Mezgueldi, M., N. Tang, et al. (2002). "The kinetic mechanism of Myo1e (human myosin-IC)." J Biol Chem **277**(24): 21514-21.

Etournay, R., A. El-Amraoui, et al. (2005). "PHR1, an integral membrane protein of the inner ear sensory cells, directly interacts with myosin 1c and myosin VIIa." J Cell Sci **118**(Pt 13): 2891-9.

Ferguson, K. M., M. A. Lemmon, et al. (1994). "Crystal structure at 2.2 A resolution of the pleckstrin homology domain from human dynamin." Cell **79**(2): 199-209.

Fiske and Subbarow (1925). "Phosphorous assay." *J. Biol. Chem.* **66**: 374-389.

Footer, M. J., J. W. Kerssemakers, et al. (2007). "Direct measurement of force generation by actin filament polymerization using an optical trap." Proc Natl Acad Sci U S A **104**(7): 2181-6.

Foth, B. J., M. C. Goedecke, et al. (2006). "New insights into myosin evolution and classification." Proc Natl Acad Sci U S A **103**(10): 3681-6.

Funaki, M., L. DiFransico, et al. (2006). "PI 4,5-P2 stimulates glucose transport activity of GLUT4 in the plasma membrane of 3T3-L1 adipocytes." Biochim Biophys Acta **1763**(8): 889-99.

Gambhir, A., G. Hangyas-Mihalyne, et al. (2004). "Electrostatic sequestration of PIP2 on phospholipid membranes by basic/aromatic regions of proteins." Biophys J **86**(4): 2188-207.

Geleoc, G. S. and J. R. Holt (2003). "Developmental acquisition of sensory transduction in hair cells of the mouse inner ear." Nat Neurosci **6**(10): 1019-20.

Gillespie, P. G. (2004). "Myosin I and adaptation of mechanical transduction by the inner ear." Philos Trans R Soc Lond B Biol Sci **359**(1452): 1945-51.

Gillespie, P. G. and J. L. Cyr (2004). "Myosin-1c, the hair cell's adaptation motor." Annu Rev Physiol **66**: 521-45.

Gillespie, P. G., S. K. Gillespie, et al. (1999). "Engineering of the myosin-ibeta nucleotide-binding pocket to create selective sensitivity to N(6)-modified ADP analogs." J Biol Chem **274**(44): 31373-81.

Glaser, M., S. Wanaski, et al. (1996). "Myristoylated alanine-rich C kinase substrate (MARCKS) produces reversible inhibition of phospholipase C by sequestering phosphatidylinositol 4,5-bisphosphate in lateral domains." J Biol Chem **271**(42): 26187-93.

Golub, T., S. Wacha, et al. (2004). "Spatial and temporal control of signaling through lipid rafts." Curr Opin Neurobiol **14**(5): 542-50.

Hayden, S. M., J. S. Wolenski, et al. (1990). "Binding of brush border myosin I to phospholipid vesicles." J Cell Biol **111**(2): 443-51.

Hirono, M., C. S. Denis, et al. (2004). "Hair cells require phosphatidylinositol 4,5-bisphosphate for mechanical transduction and adaptation." Neuron **44**(2): 309-20.

Hokanson, D. E., J. M. Laakso, et al. (2006). "Myo1c binds phosphatidylinositols through a putative pleckstrin homology domain." Mol Biol Cell **17**(11): 4856-65.

Hokanson, D. E. and E. M. Ostap (2006). "Myo1c binds tightly and specifically to phosphatidylinositol 4,5-bisphosphate and inositol 1,4,5-trisphosphate." Proc Natl Acad Sci U S A **103**(9): 3118-23.

Holmes, K. C., R. R. Schroder, et al. (2004). "The structure of the rigor complex and its implications for the power stroke." Philos Trans R Soc Lond B Biol Sci **359**(1452): 1819-28.

Holt, J. R., S. K. Gillespie, et al. (2002). "A chemical-genetic strategy implicates myosin-1c in adaptation by hair cells." Cell **108**(3): 371-81.

Howard, J. and A. J. Hudspeth (1987). "Mechanical relaxation of the hair bundle mediates adaptation in mechanoelectrical transduction by the bullfrog's saccular hair cell." Proc Natl Acad Sci U S A **84**(9): 3064-8.

Hozumi, S., R. Maeda, et al. (2006). "An unconventional myosin in Drosophila reverses the default handedness in visceral organs." Nature **440**(7085): 798-802.

Huang, S., L. Lifshitz, et al. (2004). "Phosphatidylinositol-4,5-bisphosphate-rich plasma membrane patches organize active zones of endocytosis and ruffling in cultured adipocytes." Mol Cell Biol **24**(20): 9102-23.

Hudspeth, A. J. and P. G. Gillespie (1994). "Pulling springs to tune transduction: adaptation by hair cells." Neuron **12**(1): 1-9.

Insall, R. H. and O. D. Weiner (2001). "PIP3, PIP2, and cell movement--similar messages, different meanings?" Dev Cell **1**(6): 743-7.

Isakoff, S. J., T. Cardozo, et al. (1998). "Identification and analysis of PH domain-containing targets of phosphatidylinositol 3-kinase using a novel in vivo assay in yeast." Embo J **17**(18): 5374-87.

Jacobson, M. P., D. L. Pincus, et al. (2004). "A hierarchical approach to all-atom protein loop prediction." Proteins **55**(2): 351-67.

Jontes, J. D. and R. A. Milligan (1997). "Three-dimensional structure of Brush Border Myosin-I at approximately 20 A resolution by electron microscopy and image analysis." J Mol Biol **266**(2): 331-42.

Jung, G., K. Remmert, et al. (2001). "The Dictyostelium CARMIL protein links capping protein and the Arp2/3 complex to type I myosins through their SH3 domains." J Cell Biol **153**(7): 1479-97.

Jung, G., X. Wu, et al. (1996). "Dictyostelium mutants lacking multiple classic myosin I isoforms reveal combinations of shared and distinct functions." J Cell Biol **133**(2): 305-23.

Kelley, L. A., R. M. MacCallum, et al. (2000). "Enhanced genome annotation using structural profiles in the program 3D-PSSM." J Mol Biol **299**(2): 499-520.

Komander, D., A. Fairservice, et al. (2004). "Structural insights into the regulation of PDK1 by phosphatidylinositols and inositol phosphates." Embo J **23**(20): 3918-28.

Kubala, M., J. Plasek, et al. (2004). "Fluorescence competition assay for the assessment of ATP binding to an isolated domain of Na+, K(+)-ATPase." Physiol Res **53**(1): 109-13.

Lankiewicz, L., J. Malicka, et al. (1997). "Fluorescence resonance energy transfer in studies of inter-chromophoric distances in biomolecules." Acta Biochim Pol **44**(3): 477-89.

Leduc, C., O. Campas, et al. (2004). "Cooperative extraction of membrane nanotubes by molecular motors." Proc Natl Acad Sci U S A **101**(49): 17096-101.

Lemmon, M. A. (2007). "Pleckstrin homology (PH) domains and phosphatidylinositols." Biochem Soc Symp(74): 81-93.

Lemmon, M. A. and K. M. Ferguson (2001). "Molecular determinants in pleckstrin homology domains that allow specific recognition of phosphatidylinositols." Biochem Soc Trans **29**(Pt 4): 377-84.

Lemmon, M. A., K. M. Ferguson, et al. (1995). "Specific and high-affinity binding of inositol phosphates to an isolated pleckstrin homology domain." Proc Natl Acad Sci U S A **92**(23): 10472-6.

Lindahl, E., Hess, B., and van der Spoel, D. (2001). "GROMACS 3.0: A package for molecular simulation and trajectory analysis." Journal of Molecular Modeling **7**(8): 306-317.

Marguet, D., P. F. Lenne, et al. (2006). "Dynamics in the plasma membrane: how to combine fluidity and order." EMBO J **25**(15): 3446-57.

Mashanov, G. I., D. Tacon, et al. (2004). "The Spatial and Temporal Dynamics of Pleckstrin Homology Domain Binding at the Plasma Membrane Measured by Imaging Single Molecules in Live Mouse Myoblasts." J. Biol. Chem. **279**(15): 15274-15280.

McLaughlin, S. and D. Murray (2005). "Plasma membrane phosphatidylinositol organization by protein electrostatics." Nature **438**(7068): 605-11.

McLaughlin, S., J. Wang, et al. (2002). "PIP(2) and proteins: interactions, organization, and information flow." Annu Rev Biophys Biomol Struct **31**: 151-75.

Meltzer, R. H., M. M. Lurtz, et al. (2006). "Nicotinic acetylcholine receptor channel electrostatics determined by diffusion-enhanced luminescence energy transfer." Biophys J **91**(4): 1315-24.

Miyata, H., B. Bowers, et al. (1989). "Plasma membrane association of Acanthamoeba myosin I." J Cell Biol **109**(4 Pt 1): 1519-28.

Mooseker, M. S. and R. E. Cheney (1995). "Unconventional myosins." Annu Rev Cell Dev Biol **11**: 633-75.

Morone, N., T. Fujiwara, et al. (2006). "Three-dimensional reconstruction of the membrane skeleton at the plasma membrane interface by electron tomography." J. Cell Biol. **174**(6): 851-862.

Mueller, H., H. J. Butt, et al. (1999). "Force measurements on myelin basic protein adsorbed to mica and lipid bilayer surfaces done with the atomic force microscope." Biophys J **76**(2): 1072-9.

Murphy, C. T., R. S. Rock, et al. (2001). "A myosin II mutation uncouples ATPase activity from motility and shortens step size." Nat Cell Biol **3**(3): 311-5.

Murray, D., A. Arbuzova, et al. (1999). "Electrostatic properties of membranes containing acidic lipids and adsorbed basic peptides: theory and experiment." Biophys J **77**(6): 3176-88.

Nakamori, Y., M. Emoto, et al. (2006). "Myosin motor Myo1c and its receptor NEMO/IKK-gamma promote TNF-alpha-induced serine307 phosphorylation of IRS-1." J Cell Biol **173**(5): 665-71.

Novak, K. D., M. D. Peterson, et al. (1995). "Dictyostelium myosin I double mutants exhibit conditional defects in pinocytosis." J Cell Biol **131**(5): 1205-21.

Ostap, E. M., P. Maupin, et al. (2003). "Dynamic localization of myosin-I to endocytic structures in Acanthamoeba." Cell Motil Cytoskeleton **54**(1): 29-40.

Papayannopoulos, V., C. Co, et al. (2005). "A polybasic motif allows N-WASP to act as a sensor of PIP(2) density." Mol Cell **17**(2): 181-91.

Peitzsch, R. M. and S. McLaughlin (1993). "Binding of acylated peptides and fatty acids to phospholipid vesicles: pertinence to myristoylated proteins." Biochemistry **32**(39): 10436-43.

Phillips, K. R., S. Tong, et al. (2006). "Stereociliary myosin-1c receptors are sensitive to calcium chelation and absent from cadherin 23 mutant mice." J Neurosci **26**(42): 10777-88.

Pollard, T. D. and E. D. Korn (1973). "Acanthamoeba myosin. I. Isolation from Acanthamoeba castellanii of an enzyme similar to muscle myosin." J Biol Chem **248**(13): 4682-90.

Putkey, J. A., G. R. Slaughter, et al. (1985). "Bacterial expression and characterization of proteins derived from the chicken calmodulin cDNA and a calmodulin processed gene." J Biol Chem **260**(8): 4704-12.

Raucher, D., T. Stauffer, et al. (2000). "Phosphatidylinositol 4,5-bisphosphate functions as a second messenger that regulates cytoskeleton-plasma membrane adhesion." Cell **100**(2): 221-8.

Ruppert, C., J. Godel, et al. (1995). "Localization of the rat myosin I molecules myr 1 and myr 2 and in vivo targeting of their tail domains." J Cell Sci **108 (Pt 12)**: 3775-86.

Rusten, T. E. and H. Stenmark (2006). "Analyzing phosphatidylinositols and their interacting proteins." Nat Methods **3**(4): 251-8.

Ryu, S. H., P. G. Suh, et al. (1987). "Bovine brain cytosol contains three immunologically distinct forms of inositolphospholipid-specific phospholipase C." Proc Natl Acad Sci U S A **84**(19): 6649-53.

Saeki, K., Y. Miura, et al. (2003). "The B cell-specific major raft protein, Raftlin, is necessary for the integrity of lipid raft and BCR signal transduction." EMBO J **22**(12): 3015-26.

Sakamoto, T., F. Wang, et al. (2003). "Neck length and processivity of myosin V." J Biol Chem **278**(31): 29201-7.

Sako, Y. and A. Kusumi (1995). "Barriers for lateral diffusion of transferrin receptor in the plasma membrane as characterized by receptor dragging by laser tweezers: fence versus tether." J Cell Biol **129**(6): 1559-74.

Scandella, C. J., P. Devaux, et al. (1972). "Rapid lateral diffusion of phospholipids in rabbit sarcoplasmic reticulum." Proc Natl Acad Sci U S A **69**(8): 2056-60.

Schatz, P. J. (1993). Biotechnology (NY) **11**(10): 1138-1143.

Schietroma, C., H. Y. Yu, et al. (2007). "A role for myosin 1E in cortical granule exocytosis in Xenopus oocytes." J Biol Chem.

Siemens, J., C. Lillo, et al. (2004). "Cadherin 23 is a component of the tip link in hair-cell stereocilia." Nature **428**(6986): 950-5.

Simonsen, A., A. E. Wurmser, et al. (2001). "The role of phosphatidylinositols in membrane transport." Curr Opin Cell Biol **13**(4): 485-92.

Snapp, E., Altan, N. and Lippincott-Schwartz, J. (2003). Measuring protein mobility by photobleaching GFP-chimeras in living cells. New York, John Wiley & Sons.

Sokac, A. M. and W. M. Bement (2000). "Regulation and expression of metazoan unconventional myosins." Int Rev Cytol **200**: 197-304.

Sokac, A. M., C. Schietroma, et al. (2006). "Myosin-1c couples assembling actin to membranes to drive compensatory endocytosis." Dev Cell **11**(5): 629-40.

Speder, P., G. Adam, et al. (2006). "Type ID unconventional myosin controls left-right asymmetry in Drosophila." Nature **440**(7085): 803-7.

Stephens, L. R., T. R. Jackson, et al. (1993). "Agonist-stimulated synthesis of phosphatidylinositol(3,4,5)-trisphosphate: a new intracellular signalling system?" Biochim Biophys Acta **1179**(1): 27-75.

Stoffler, H. E., C. Ruppert, et al. (1995). "A novel mammalian myosin I from rat with an SH3 domain localizes to Con A-inducible, F-actin-rich structures at cell-cell contacts." J Cell Biol **129**(3): 819-30.

Swanljung-Collins, H. and J. H. Collins (1992). "Phosphorylation of brush border myosin I by protein kinase C is regulated by Ca(2+)-stimulated binding of myosin I to phosphatidylserine concerted with calmodulin dissociation." J Biol Chem **267**(5): 3445-54.

Swanson, J. A., M. T. Johnson, et al. (1999). "A contractile activity that closes phagosomes in macrophages." J Cell Sci **112 (Pt 3)**: 307-16.

Takagi, Y., E. E. Homsher, et al. (2006). "Force generation in single conventional actomyosin complexes under high dynamic load." Biophys J **90**(4): 1295-307.

Tang, N., T. Lin, et al. (2002). "Dynamics of myo1c (myosin-Iβ) lipid binding and dissociation." J Biol Chem **277**(45): 42763-8.

Tang, N. and E. M. Ostap (2001). "Motor domain-dependent localization of myo1b (myr-1)." Curr Biol **11**(14): 1131-5.

Tyska, M. J., A. T. Mackey, et al. (2005). "Myosin-1a is critical for normal brush border structure and composition." Mol Biol Cell **16**(5): 2443-57.

Verkleij, A. J., R. F. Zwaal, et al. (1973). "The asymmetric distribution of phospholipids in the human red cell membrane. A combined study using

phospholipases and freeze-etch electron microscopy." Biochim Biophys Acta **323**(2): 178-93.

Wang, F. S., C. W. Liu, et al. (2003). "Modeling the role of myosin 1c in neuronal growth cone turning." Biophys J **85**(5): 3319-28.

Wang, F. S., J. S. Wolenski, et al. (1996). "Function of myosin-V in filopodial extension of neuronal growth cones." Science **273**(5275): 660-3.

Wang, J., A. Arbuzova, et al. (2001). "The effector domain of myristoylated alanine-rich C kinase substrate binds strongly to phosphatidylinositol 4,5-bisphosphate." J Biol Chem **276**(7): 5012-9.

Wang, J., A. Gambhir, et al. (2002). "Lateral sequestration of phosphatidylinositol 4,5-bisphosphate by the basic effector domain of myristoylated alanine-rich C kinase substrate is due to nonspecific electrostatic interactions." J Biol Chem **277**(37): 34401-12.

Wylie, S. R., P. J. Wu, et al. (1998). "A conventional myosin motor drives neurite outgrowth." Proc Natl Acad Sci U S A **95**(22): 12967-72.

Yin, H. L. and P. A. Janmey (2003). "Phosphatidylinositol regulation of the actin cytoskeleton." Annu Rev Physiol **65**: 761-89.

Zhu, T., K. Beckingham, et al. (1998). "High affinity Ca2+ binding sites of calmodulin are critical for the regulation of myosin Ibeta motor function." J Biol Chem **273**(32): 20481-6.